Microwave-assisted Heterogeneous Catalysis of Propene Selective Oxidation

JIA SUN

School of Chemistry

Cardiff University

2022

ABSTRACT

Compared with traditional heating methods, microwave heating has the advantages of uniform and fast heating of substrates, selective heating of components in a mixture, easily switching on and off, and a sensitive response to changes in input power. As an energy source, it has been widely used in chemistry, especially in organic synthesis and material processing. However, the application of microwaves in gas-phase heterogeneous catalysis is somewhat limited because microwaves are not sufficient to break chemical bonds to initiate chemical reactions, and gases cannot be heated by microwaves. In this doctoral thesis, the selective oxidation of propene was selected as the target reaction to investigate the feasibility and potential of microwave-assisted gas-phase catalysis. Bismuth molybdate, a material that performs well for this reaction in traditional catalysis, was selected as the main catalyst in this study. Different synthesis methods such as hydrothermal synthesis, sol-gel synthesis, and a sol-gel deposition method were used to synthesize and modify the supported bismuth molybdate samples.

Whether a material can be heated in a microwave electric field is governed by their dielectric properties. The dielectric properties of a range of materials were analysed and the results compared to their performance as catalysts for propene oxidation. It has been proposed that bismuth-based composite metal oxides have good dielectric properties and can be heated to suitable temperatures under microwave conditions.

The results of these studies found that bismuth molybdate samples synthesized under certain conditions also showed good performance in microwave-assisted heterogeneous catalysis. The dielectric loss factor of the material will vary depending on the synthesis method and it was found that catalysts synthesized by a hydrothermal method had a higher dielectric loss factor

than materials prepared using a sol-gel method, so they were easier to heat in the microwave, and performed better in the microwave-assisted catalysis process.

Modifying standard bismuth molybdate materials was also investigated. Replacing molybdenum with vanadium in bismuth molybdate increases defects in the material, making it more easily heated by microwave radiation. The use of silicon carbide as a support was also found to improve the microwave-absorbing ability of the catalyst, giving a uniform catalyst bed temperature, and increasing the conversion rate of propene, the yield of acrolein and the stability of the catalyst.

The chemical and physical properties of the catalysts used in this work were characterized by several different techniques including X-ray diffraction (XRD), Raman spectroscopy (Raman), Inductively coupled plasma mass spectrometry (ICP-MS), X-ray photoelectron spectroscopy (XPS) , dielectric perturbations, to elucidate structure activity relationships for the different catalysts.

Insights gained in this study provide new information on the role of catalysts in microwave assisted catalysis for gas-phase selective oxidation with potential applications in greenhouse gas conversion.

ACKNOWLEDGEMENTS

This thesis would not be accomplished without the support and assistance that I received from many people. It is a great honour to be PhD student of Cardiff University (Prifysgol Caerdydd). Firstly, I would like to express my sincere thanks to my supervisor Dr Jonathan Bartley for his guidance and encouragement. In this period of study and research, he provided me with lots of suggestions and help. He taught me how to work efficiently and gave me the authority to develop my ideas. I was lucky and happy to work with him. I would also like to acknowledge my co-supervisors Dr Daniel Slocombe and my colleague Dr Micheal Barter in the School of Engineering. I was always inspired by their ideas on the engineering side.

I would like to express my sincerest thanks to Dr James Hayward and Dr William Wallace. Before joining Cardiff Catalysis Institution (CCI), I didn't have enough chemistry background, they patiently taught me all the chemistry experiment skills needed to complete this work, more importantly, they give me plenty of useful suggestions and advice in all aspects.

Special thanks go to Dr Greg Shaw, Dr Michal Perdjon, Dr Nia Richards, Dr David Morgan and Dr Simon Waller for their kind help in materials characterization. Special thanks also go to Prof. Songmei Sun, Dr Samual Pattisson, Dr Mark Douthwaite, Dr James Carter, Dr Xiaoyang Huang, and Dr Tao Tong for their kind help on my lab works.

My deep appreciation goes to my friends: Mr Kai Wang, Mr Muhao Du, Mr Kang Wang, and Miss Mengxi Li provide me with strong support and continuous encouragement to help me through tough times.

I can't adequately express my gratitude to, Prof. Xiaoliang Li, Dr Tongqi Ye, Dr Rong Wang, Dr Run Zhao, Dr Jiayu Chan, Dr Nating Yang and Dr Jingyun Zhao during their academic visit to CCI, spending numerous happy times with me.

Last but not the least, my family has been all my support to carry out and complete my PhD work. They encouraged me to pursue my dreams and the life I wanted. I am so proud of them, and they are the most precious treasure in my life.

Jia Sun

March 2022

Abbreviations and Units

% - Percent

°C – Degrees Celsius

Å – Angstrom (10^{-10} m)

a.u. – Arbitrary units

BET – Brunauer, Emmet and Teller

cm – Centimetre

cm^{-1} – Reciprocal centimetre

CO_x – Carbon oxides (CO/CO_2)

EM – Electromagnetic wave

EMR – Electromagnetic wave radiation

FID – Flame ionization detector

g – Gram

GC – Gas chromatography

h – Hours

ICP – Inductively coupled plasma

J – Joule

K – Kelvin

M – Molar (mol dm^{-3})

m – Metre

m^2 – Square metre

m^{-2} – Reciprocal square metre

mg – Milligram (10^{-3} g)

min – Minutes

min^{-1} – Reciprocal minute

mL – Millilitre (10^{-3} L)

µm – Micrometre (10^{-6} m)

mol – Moles

mol^{-1} – Reciprocal moles

MS – Mass spectrometry

nm – Nanometre (10^{-9} m)

s – Second

s^{-1} – Reciprocal second

SEM – Scanning electron microscopy

TCD – Thermal conductivity detector

TGA – Thermogravimetric analysis

wt. - % Weight percent

W – Watt

XPS – X-ray photoelectron spectroscopy

XRD –X-ray diffraction

Table of Contents

1 Motivation and Background

This project aims to develop new catalysts for use in microwave-assisted processes for the selective oxidising propene to acrolein. In this chapter, all the essential background of microwave-assisted propene selective oxidation to acrolein will be introduced. The first part of this chapter will be an introduction to electromagnetic waves. The second part will be an introduction to heterogeneous catalysis. In the third part, the introduction of microwave-assisted catalysis will be presented, and the fourth part will be the introduction and review of propene selective oxidation to produce acrolein.

1.1 Introduction to Electromagnetic Waves

1.1.1 Electromagnetic Basis of EM Waves

An electromagnetic (EM) wave consists of an electric field, defined in terms of the force per charge on a stationary charge, and a magnetic field, defined in terms of the force per charge on a moving charge. EM waves travelling in space without obstruction, and the behaviour of their transmission can be approximately simplified as plane waves. Electromagnetic waves have an electric (**E**) field component and a magnetic (**H**) field component that oscillate in phase and in directions perpendicular to each other, and both **E** and **H** components are perpendicular to the travelling direction of the electromagnetic wave.

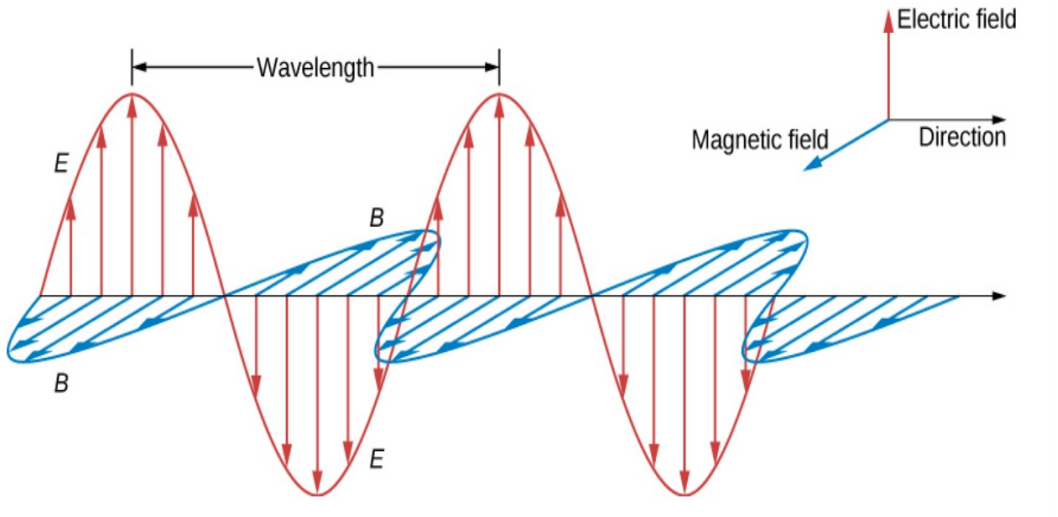

1.1 Direction of EM Wave Propagation[1]

1.1.2 Wave-particle Duality of EM Waves and Interactions Between Matter and Electromagnetic Waves

In 1807, English physicist Thomas Young's double-slit interference experiment[2] confirmed that light has the nature of a wave. But almost one century later, in 1905, Albert Einstein explained[3] the photoelectric effect, an experiment that the wave theory of light failed to explain. Now, on account of the progress of quantum mechanics, we know that light has wave-particle duality. In quantum mechanics, EM radiation consists of photons, which are responsible for all electromagnetic interactions. When EM radiation interacts with single atoms or molecules, its behaviour also depends on the amount of energy per quantum (photon) it carries.

The matter is any substance that has mass and takes up space by having volume[4]. These include classical everyday phases such as solid, liquid, and gas, but other states are possible, including plasma, Bose-Einstein condensates, fermionic condensates, and quark-gluon

plasma[5]. EM radiation is emitted by electrically charged particles undergoing acceleration, and these waves can subsequently interact with other charged particles, exerting force on them[6]. Also, in the quantum mechanical view, the interactions between EM radiation and single atoms or molecules depend on the amount of energy per photon. Both theories make it clear that to understand how the EM radiation interacts with matter, the atomic and molecular level needs to be considered. Molecules in gases possess three types of internal energy states: rotational, vibrational and electronic. For any electronic state, a variety of vibrational states is possible, and for any vibrational state, a variety of rotational states is possible. The total internal energy of the molecules at any time is the sum of the energy of the three states. However, for liquid and solid, the atoms or molecules are in continual motion, which precludes the rotational energy states. Therefore, only vibrational, and electronic states remain in liquid and solid[7].

1.1.3 Electromagnetic Waves and Chemistry

Microwave assisted chemistry is based on the EM radiation-matter interaction. The EM spectrum in Table 1.1 provides the energy carried by the photon in different EM waves. The corresponding interaction behaviors are given in Table 1.1.

When considering the connection between the EM energy and chemistry, spectroscopy, the study of the interaction between matter and EM radiation, would be the most familiar form for chemists. Spectroscopy is a fundamental exploratory tool in the field of chemistry and material science research. By using spectroscopy with EM radiation of different power and frequencies, the composition, physical structure, and electronic structure of matter can be investigated at the atomic, molecular and macro scale.

Table 1.1 EMW-matter interaction

Category	Form of excitation
Gamma rays	Ionization excitation
Hard X-rays	
Soft X-rays	
Extreme ultraviolet	Electronic excitation
Near ultraviolet	
Visible (blue and green)	
Visible (yellow to red)	Vibrational excitation
Near infrared	
Mid infrared	
Far infrared	Rotational excitation
Microwave	

Spectroscopy for chemical analysis can be regarded as a physical process applied to chemistry research. The close relationship between EM waves and modern chemistry can be highlighted by EM energy initiated chemical processes, in which, microwave chemistr[8] and photochemistry[9] are two fields that have attracted attention from chemists. Photochemistry is not the main topic for this project, therefore this introduction will focus on microwave chemistry and microwave-assisted heterogeneous catalysis in particular.

Table 1.2 Types of spectroscopies

Type of spectroscopy	**Techniques**	
Atom spectroscopy	Atom absorption spectroscopy (AAS), Inductively coupled plasma atomic emission spectroscopy (ICP), X-ray fluorescence (XRF), X-ray photoelectron spectroscopy (XPS)	
Molecule spectroscopy	Electron spin	Electron paramagnetic resonance (EPR)
	Electron excitation	Visible/UV fluorescence spectroscopy
	Molecular rotation spectroscopy	Microwave spectroscopy
	Molecular vibration spectroscopy	Infrared spectroscopy (IR), Raman spectroscopy
Nuclei spectroscopy		Nuclear magnetic resonance spectroscopy (NMR)

1.2 Introduction to Heterogeneous Catalysis

1.2.1 Thermodynamics and Kinetics of Chemical Reactions

A chemical reaction is a process that leads to the chemical transformation of one set of chemical substances to another. Chemical reactions are determined by the laws of thermodynamics. The thermodynamics of the system determines the maximum attainable yield of products under specified conditions. Reactions can proceed by themselves if they release energy. The associated free energy, G, of the reaction is composed of two different thermodynamic quantities, enthalpy, H, and entropy, S

$$\Delta G = \Delta H - T\Delta S$$

T: absolute temperature, Δ: difference (change between original and product).

The change of G, H and S depends only upon the initial and final states of the system and not upon the path taken to move from one to another.

1.2.2 Catalysis

The phenomenon of catalysis has been known for many years, and now, is a vital part of chemistry[10]. For the last 100 years, research into catalysis has developed rapidly, and it is now widely applied in the chemical industry.

Catalysis is the process of increasing the rate of a chemical reaction by adding a substance known as a catalyst. In a general catalytic reaction, a catalyst increases the rate of a chemical reaction by forming bonds with the adsorbents (A and B in Figure 1.2) and allowing them react to make products (P in Figure 1.2). Then, the products can desorb from the catalyst and it is recovered in its original form at the end of the reaction cycle. Apart from the process shown in Figure 1.2, there are alternatives such as Eley-Rideal and Mars-van Krevelen mechanisms where only one of the reactants (A) adsorbs to the catalyst surface, and the second reactant reacts with the activated catalyst.

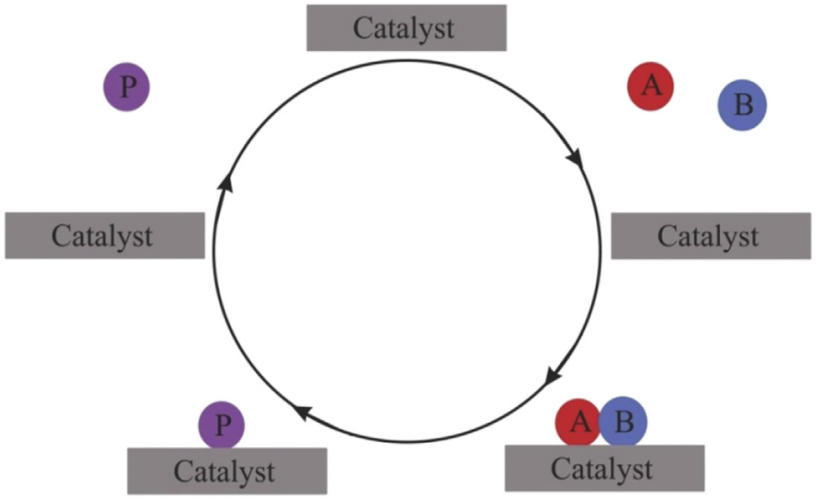

1.2 Flowchart of a catalytic reaction[11]

.

The accepted definition of a catalyst is that it is a substance that increases the rate at which a chemical system approaches equilibrium, without being consumed in the process. Catalysts may not always maintain good activity. During a chemical reaction, the production of side reactions or changes in the catalyst's structure can lead to the deactivation of the catalyst. Turnover number (TON) is a measure of catalyst stability. It is defined as the maximum number of times the catalyst can be used in a certain reaction under specified reaction conditions. It is represented by the number of molecular reactions or by the number of reaction cycles occurring at the reactive centre before complete deactivation. In addition, Turnover frequency (TOF) is an indicator for the intrinsic activity of a catalyst. The TOF value measures the rate of the catalytic reaction that occurs on a catalyst and can well reflect the catalytic performance of the catalyst.

A catalyst offers an alternative reaction pathway with much lower activation energy than the uncatalyzed reaction. A potential energy diagram is presented in Figure 1.3 to show the differences between a catalysed and uncatalyzed reaction.

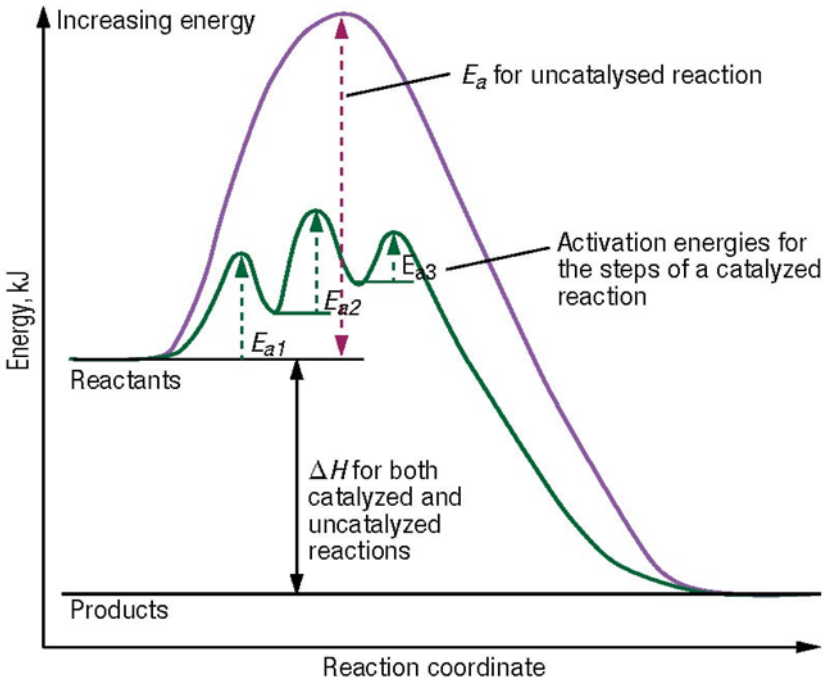

Figure 1.3 Potential energy diagram of uncatalyzed reaction and catalyzed reaction[12]

As can be seen from Figure 1.3, the catalysed reaction may involve several intermediate and transition-state complexes, which are completely different from the one-step mechanism for the reaction that occurs without any catalyst. The catalysts can form fleeting intermediate chemical complexes with reactants, allowing the reaction to follow a different mechanistic pathway that requires a lower activation energy (E_a) than the corresponding uncatalyzed reaction. E_a is often thought of as an energy barrier over which the reactants must pass to form products. Catalysts do not affect the equilibrium state of a reaction. In the presence of a catalyst, the same amounts of reactants and products will be present at equilibrium as there would be in the uncatalyzed reaction. To state this in chemical terms, catalysts affect the kinetics, but not the thermodynamics, of a reaction.

1.2.3 Kinetics of Catalysed Reactions

Unlike thermodynamics, which deals with the direction in which a process occurs but gives no information on its rate, kinetics is concerned with the rate of a chemical reaction. The primary effect of a catalyst on a chemical reaction is to increase the reaction rate. This means that the rate coefficient is increased when catalysts are involved in the chemical reaction. According to the absolute rate theory[13], the rate coefficient k is given by

$$k = \frac{\boldsymbol{k}T}{h} e^{\frac{-\Delta G^a}{RT}}$$

Where $\boldsymbol{k}$ is the Boltzmann constant, h is the Plank's constant, $-\Delta G^a$ is the Gibbs free energy of activation. The effect of catalysts in a reaction must be decrease the free energy of activation, which is composed of an entropy and an enthalpy of activation. As the entropy of a catalysed reaction is usually less than in the corresponding uncatalyzed reaction (because the transition state is immobilized on the catalyst surface), there must be a decrease in the enthalpy of activation. The Arrhenius diagram of uncatalyzed and catalysed gas-phase reaction is shown in the Figure 1.4. It reveals that the effect of a catalyst is either to increase the rate coefficient at a given temperature or to decrease the temperature at which it achieves a given value[14].

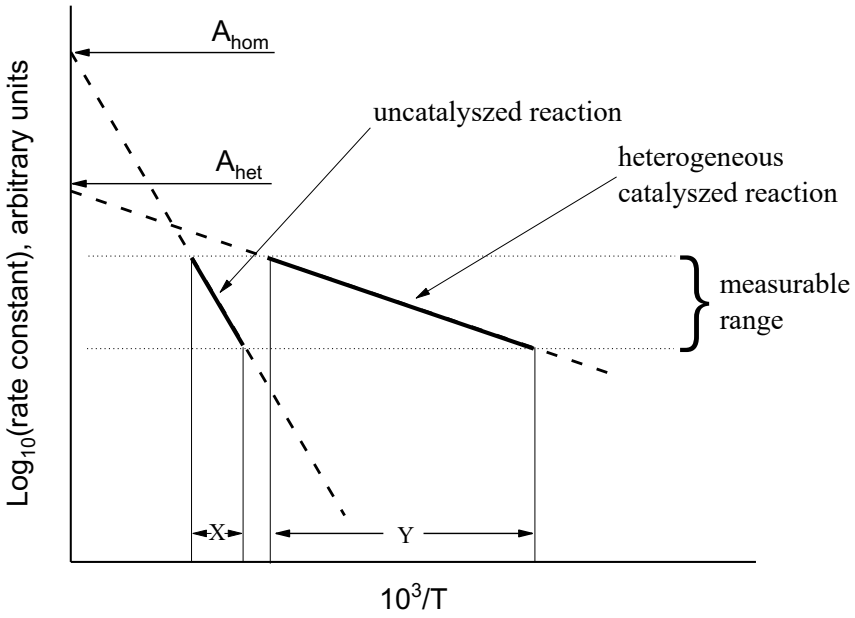

Figure 1.4 Arrhenius diagram of uncatalyzed reaction and catalysed reaction[14]

1.2.4 Heterogeneous catalysis

Catalysis is commonly categorized as homogeneous catalysis or heterogeneous catalysis. Homogeneous refers to the catalytic reactions in which the catalysts are in a single phase. By contrast, in heterogeneous catalysis, the catalyst occupies a different phase from the reactants and products. Here are some evaluation criteria for a good heterogeneous catalyst:

1. Inexpensive.

(e.g. easy to synthesis, and does not contain rare or expensive elements)

2. Stable during reaction.

(e.g. does not significantly change during the reaction, and iss not severely poisoned)

3. Enables high rates of chemical production.

To be successful the catalyst must allow the reaction to proceed at a suitable rate under conditions that are economically desirable.

4. High surface area

This is perhaps the most common property shared by effective heterogeneous catalysts, as those intermediate reactions usually happen on the surface.

1.3 Microwave-assisted Heterogeneous Catalysis

1.3.1 Introduction

Quantum mechanics has clearly indicated that microwave irradiation does not have sufficient energy to trigger any major chemical processes such as breaking bonds and transferring electrons[15]. However, microwave heating effects makes the integration of microwave radiation and chemistry possible[16]. The first chemical applications of microwave heating were at the start at 1970s in the field of sample pretreatment[17–19], and the technique has now become routine and provides simple, fast procedures. Later, in 1986, two papers published in Tetrahedron Letters are thought to be the real birth of organic microwave synthetic chemistry[20,21]. Nowadays, "Microwave-assisted" processes are an active topic in chemistry research, including organic chemistry[22], analytical chemistry[23], biochemistry[24], polymer chemistry[25], and the inorganic chemistry of materials processing[26]. The use of microwave irradiation in chemistry has become a popular technique, and in the near future, the use of microwave energy to heat chemical reactions on a laboratory scale will be widespread. In past research, microwave-assisted heterogeneous catalysis has been shown to give different results from conventional catalysis due to the different mechanisms of the heating present in microwave radiation[27,28].

Studies of microwave dielectric heating of high loss inorganic materials[29] make the application of microwave into heterogeneous catalysis possible. Materials with high loss factor can

efficiently convert the electromagnetic energy from microwave radiation into heat to break the energy barrier of the reaction. The principles of microwave heating will be introduced in detail in Chapter 3.

1.3.2 Review of Microwave-assisted Heterogeneous Catalytic Processes

Previous studies on microwave-assisted heterogeneous catalysis in the gas phase have focused on several reactions, including the oxidative coupling of methane[30], CO_2 reforming of methane[31], partial oxidation of hydrocarbons[32], water-gas shift[33] and hydrocarbon fuel dehydrogenation[34].

The oxidative coupling of methane was one of the active topics in microwave-assisted heterogeneous process, and several studies have dealt with evaluating the microwave feasibility of this reaction since the 1990s[30,35,36]. Chen and coworkers use a $SrBaO_3$ based mixed metal oxide material as the catalyst and found that when compared to conventional heating, a change in both product species and product selectivity was found. The products shown in the conventional tests are CO, CO_2, C_2H_4 and C_2H_6, in addition to the products obtained with conventional heating, the presence of C_2H_2 was observed[30]. They explained that the change of selectivity and product species was caused by the hot spots generated by localized coupling of microwave energy to point defects or a weak surface bond. Similar findings were also reported by Roussy and coworkers[35]. In their study, a significant change in product selectivity in methane coupling was also observed. Under microwave irradiation, a C_2 selectivity of 100% was found for CH_4 at low conversion, while with conventional heating, characterized by 0% C2 selectivity. They suggested that this difference on selectivity could arise from that under microwave irradiation.

CO_2 reforming of methane into syngas is also another highly interesting topic for microwave-assisted heterogeneous catalytic processes studies. Zhang and coworkers studied the CO_2 reforming of methane with γ-Al_2O_3 supported Pt catalysts both with microwave-assisted and conventional heating[37]. They reported that H_2/CO ratio at low temperatures was lower than the equilibrium for conventional heating, while it was higher for microwave-assisted heating, this should because of the "hotspot" effect. While at high temperatures, the H_2/CO ratio approached the thermodynamic equilibrium for both the heating systems. The effect of the microwave was attributed to hot-spot formation on the catalyst. When microwave heating was employed, there are some zones in the catalytic bed where the reaction occurs at higher temperatures than those measured. Fidalgo and coworkers investigated mixtures of carbon materials and Ni/Al_2O_3 for the CO_2 reforming of methane[31,38]. Ni/Al_2O_3 is not heated by microwave radiation as for its physical property, so it must be mixed with a microwave receptor, such as carbonaceous material. They studied the effect of the addition of a commercial activated carbon, FY5, metallurgical coke, and rich potassium char obtained from biomass pyrolysis. They found that microwave heating can enhance the conversion of both methane and carbon dioxide. They pointed out that the hot spots generated by the microwave contributed to the removal of the carbon deposits, which can be understood as an in situ regeneration of the catalyst[38].

For the topic of microwave-assisted heterogeneous catalysis, some research groups have reported their ongoing research. For example, since 2000, Zhang and coworkers studied the application of microwave dielectric heating in environmental-related heterogeneous catalytic reaction systems and reviewed them in 2006[39]. Their works include the decomposition of hydrogen sulfide[40], the reduction of sulfur dioxide with methane[41], the reforming of methane by carbon dioxide[37], the hydrodesulfurization of thiophene[42], and the oxidative coupling of methane[43]. Results of their studies showed that when compared to conventional heating

reactions at the same temperature, significant increases in reaction rates were observed by using microwave heating, and changes of product selectivity were also reported in the carbon dioxide reforming of methane and the oxidative coupling of methane. Additionally, in some reactions, like the decomposition of hydrogen sulfide, the carbon dioxide reforming of methane, and the hydrodesulfurization of thiophene, obvious shifts in the position of equilibrium had been obtained under microwave heating, and the equilibrium shifts were in opposite directions for endothermic and exothermic reactions. Zhang points out that the large difference between the hot-spot temperature and the average temperature measured is responsible for the acceleration of reaction rates, changes in product selectivity, and the apparent equilibrium shifts.

The group of Edwards at Oxford University have investigated the field of microwave-assisted catalytic processes and have studied the production of highly pure hydrogen from hydrocarbon fuels[34,44–47] and the destruction of plastic waste[48]. In 2016, they used the heavy hydrocarbon paraffin waxes as potential hydrogen production and storage materials and rapidly released large amounts of hydrogen through microwave-assisted catalytic decomposition by using a carbon-supported ruthenium catalyst[40]. In 2017, they illustrated a microwave-initiated catalytic process on dehydrogenation of crude oils fuel consisting of mainly n-alkanes from C_{12} to C_{21}, and the resulting hydrocarbon fossil fuels allow for the rapid production of large volumes of hydrogen using silicon carbide supported iron catalysts. In this process, alkanes were rapidly dehydrogenated over the Fe/SiC catalyst, with a hydrogen selectivity of 91%, which is much higher than the hydrogen selectivity of the equivalent conventional process (65%)[46]. In 2018, their team prepared a series of supported catalysts with varying iron content and evaluated the resulting H_2 production from hexadecane. Under microwave activation, most of the catalysts exhibited high selectivity for H_2 in the effluent gas. Fe (<10 wt.%) catalysts supported on SiC are found to be the most effective catalysts for producing high-purity H_2 from hexadecane[41].

In 2020, their group explored a new route to convert coal tar into hydrogen-rich gases and carbonaceous materials through microwave-initiated deep dehydrogenation[49]. Also in 2020, they established the one-step microwave-assisted deconstruction process for breaking down various plastic feedstocks into hydrogen and high-value carbons over $FeAlO_x$ catalysts[48]. A high hydrogen yield of 55.6 mmol g^{-1} is achieved, with over 97 % of the theoretical mass of hydrogen being extracted from the deconstructed plastic. Similar to the conclusions of Zhang and coworkers[27], the studies of Edwards' group showed that the heterogeneous system (hydrocarbon fuel/plastic & catalyst) under microwave initiation can not only lead to the conversion enhancement and selectivity change compared with conventional heating processes, but also lead to non-equilibrium conditions, and appear to accelerate specific endothermic reactions due to the difference in heat transfer between the microwave and thermal heating. Under microwave irradiation, the microwave absorbing metallic particle (iron) itself heats rapidly and transfers the generated heat to the surrounding support and host reactant medium. In contrast, in a conventional thermal process, heat transfer to the catalyst particle must first be transported through the surrounding reactant fluid, with heat finally arriving at metal catalyst particle. Therefore, in the convection/thermal heating processes, the temperature of the hydrocarbon surroundings is higher than the catalyst as the process begins and develops. Thus, the host substance could either self-decompose or decompose over the catalyst/support and this leads to different products selectivity in the catalytic process. In the microwave heating processes, the incident microwave electromagnetic energy was selectively, effectively, and preferentially absorbed by the metallic fine particles as the active catalytic centre, with only modest heating of the surrounding bulk reactants by the incoming microwaves. This could potentially "protect" products from subsequent post-catalyst reactions. Thus, pure hydrogen is rapidly extracted from the reactant hydrocarbon fuel or plastic through the microwave-initiated catalytic reaction at the active site on the catalyst surface.

Research on microwave-assisted heterogeneous catalysis has been carried out for decades and in general, microwaves can provide a faster heating rate for the reaction and have a significant effect on improving reaction rate and conversion, as well as changing selectivity compared with conventional heating processes. The increase in reaction rate and the change in selectivity are mainly due to the different heat transfer methods from traditional catalysis, and the presence of hot spots in the catalyst bed.

1.4 Introduction of Propene Selective Oxidation to Acrolein

1.4.1 Propene and Acrolein

Propene, also known as propylene, is an unsaturated organic compound with the chemical formula $CH_3CH=CH_2$. It has one double bond and is the second simplest member of the alkene class of hydrocarbons.

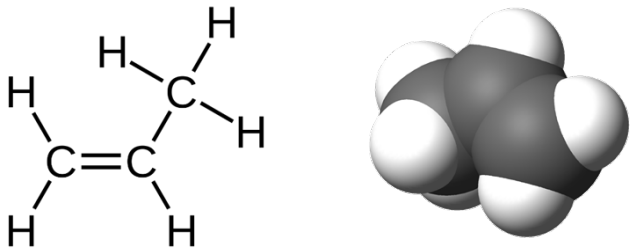

Figure 1.5 Molecular structure of propene

The main technologies for producing propene are steam cracking[32] of naphtha and catalytic cracking of gas or oil. Propene is the second most important starting product in the petrochemical industry after ethylene. It is the raw material for a wide variety of products. The main use for propene is the manufacturer of polypropylene, which consumes nearly two-thirds

of global production. Propene is also used to produce important chemicals such as propylene oxide, acrolein, acrylonitrile, cumene, butyraldehyde, and acrylic acid.

Acrolein is the simplest unsaturated aldehyde. The molecular structure of acrolein is shown in Figure 1.6. It is a colourless liquid with an acrid smell, and usually evaporates quickly and burns easily. It is produced industrially from propene and is mainly used as a biocide and a building block to other chemical compounds, such as acrylic acid and amino acid methionine. Acrolein has two conjugative unsaturated carbon bonding, one from the vinyl group and the other from the aldehyde group. Due to the existence of these groups, acrolein undergoes reactions characteristic of both an unsaturated and an aldehyde compound.

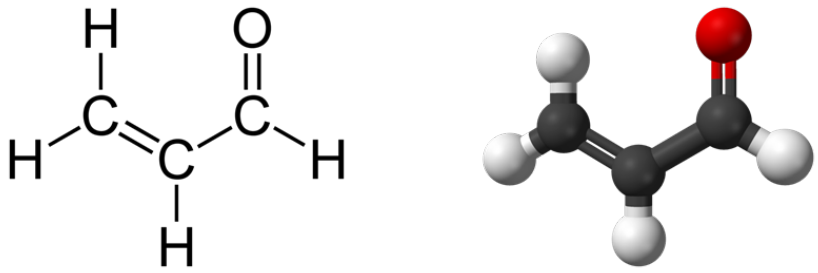

Figure 1.6 Molecular structure of acrolein

Acrolein is mainly produced by the selective oxidation of propene. The industrial process uses air as the source of oxygen and requires metal oxides as heterogeneous catalysts[51]. Acrolein, as an intermediate for the synthesis of acrylic acid and the starting substrate to produce the important amino acid methionine, is always in high demand, which makes the selective oxidation of propene to acrolein received much attention. Meanwhile, it is anticipated that the supply of propene may be under pressure. This situation will drive the propene prices up and even further motivating the research on optimizing the catalytic process of propene to acrolein.

1.4.2 Propene Selective Oxidation to Acrolein

The catalytic selective oxidation of propene to acrolein follows the reaction equation below.

$CH_2=CH-CH_3+O_2 \rightarrow CH_2=CH-CHO+H_2O$

The reaction is exothermic and reaction enthalpy is -340.8 kJ mol^{-1}. The Gibbs free energy (ΔG) is -180.19 kJ mol^{-1}, which shows that the reaction will spontaneously occur, once the reaction is initiated[34]. Acrolein is not the only product when propene is reacted with oxygen. Several other products such as CO_2, CO, acetaldehyde, formaldehyde, carboxylic acids etc. can also form.

The oxidation of propene is crucial in the chemical industry. Copper oxide was firstly found to be efficient in propene oxidation to acrolein by Shell[53]. Acrolein and propene oxide are the typical products of the oxidation of propylene over Cu-containing catalysts. The selectivity is determined by the Cu oxidation state. Cu^0 strongly adsorbs propene and is therefore active for the epoxidation of propene to propene oxide.

The industrial catalytic process for propene oxidation to acrolein are based on multicomponent metal oxides containing mainly Bi-Mo-O phases modified by various metal elements such as Fe, Co, Ni[54]. In 1962, Callahan and coworkers reported that bismuth and molybdenum catalysts produced acrolein from propylene in higher yields than that obtained in the cuprous oxide system[55]. The authors also found that the bismuth/molybdenum catalysts produced butadiene from butene and, probably more importantly, observed that a mixture of propylene, ammonia, and air yielded acrylonitrile[56]. The bismuth/molybdenum catalysts now more commonly known as bismuth molybdate catalysts were brought to commercial realization by the Standard Oil of Ohio Company (SOHIO), and the vapor-phase oxidation and ammoxidation processes which they developed are now utilized worldwide. Shortly after the introduction of the bismuth

molybdate catalysts, SOHIO developed and commercialized an even more selective catalyst, the uranium antimonate system[57]. At about the same time, Distillers Company, Ltd. developed an oxidation catalyst which was a combination of tin and antimony oxides[58]. These earlier catalyst systems have essentially been replaced on a commercial scale by multi-component catalysts which were introduced in 1970 by SOHIO. As their name implies, these catalysts contain a number of elements, the most commonly reported being nickel, cobalt, iron, bismuth, molybdenum, potassium, manganese, and silica[59–63].

1.4.3 Propene Selective Oxidation over Bismuth Molybdate

Bismuth molybdate was first reported as a good catalyst for propene selective oxidation in 1957[64]. In the past 60 years, a large number of studies have been carried out on bismuth molybdate to improve its catalytic performance, including the combination of different catalyst preparation[65–68]. Characterization[69] and theory modelling [70,71] are also widely used to understand the catalytic process of propene selective oxidation over the bismuth molybdate catalysts. Three bismuth molybdate materials (α-$Bi_2Mo_3O_{12}$, β-$Bi_2Mo_2O_9$, and γ-Bi_2MoO_6) are well-known due to their excellent activity for one of the most important industrial processes: the oxidation/ammoxidation of lower olefins[72]. The three phases of bismuth molybdate show different crystal structures. While γ-Bi_2MoO_6 is an aurivillius-type phase, β-$Bi_2Mo_2O_9$ and α-$Bi_2Mo_3O_{12}$ have a scheelite structure. The metastable β-$Bi_2Mo_2O_9$ phase generally requires high calcination temperatures (560 °C) for its formation, which usually leads to low surface areas, whereas the α and γ phases are readily accessible at lower temperatures.

As the production of one-quarter of the most important industrial organic chemicals and intermediates (such as acrolein, acrylic acid, propene oxide) is from selective oxidation of propene, the oxidation/ammoxidation over bismuth molybdate plays an important role in the

chemical industry[73]. Early studies had found that both pure phase MoO_3 and pure Bi_2O_3 have activity for propene selective oxidation to produce acrolein, but their mixture as bismuth molybdate perform much better[74 75]. The good performance of bismuth molybdate in the field of propene selective oxidation to acrolein, in modern chemical industries, relevant catalysts for propene to acrolein are usually based on bismuth molybdates[76].

A large number of investigations for identifying the order of relative activity of the three bismuth molybdate phases had been published in the past few decades, however, there is still a debate in the literature about the relative activity of these bismuth molybdate phases[44]. Some early studies made by Batist et al.[77], Grasselli et al.[78], and Keulks et al.[79] had reported β-$Bi_2Mo_2O_9$ to be more active than the other two bismuth molybdate phases, while other researchers such as Krenzke et al.[80] stated that the γ-Bi_2MoO_6 has the best catalytic activity for propylene oxidation. Carson et al.[81] stated that the catalytic activity for propylene oxidation decreases in the following order: $\alpha > \gamma > \beta$. For bismuth molybdates catalysts, the lattice oxygen plays the key role in the catalytic activity for propene selective oxidation over bismuth molybdate. The role of lattice oxygen has been proven by several researchers by using ^{18}O labelled oxygen and catalysts[82], and photoelectron characterization of the catalyst surface[83].

1.4.4 Mechanism Oxidation of Propene to Acrolein on Bismuth Molybdate Catalysts

A great deal of research on investigating the mechanism of propene selective oxidation over bismuth molybdate was performed during the 1970s and 1990s [84–87].

In 2002, Grasselli set up a series of guidelines[61], which is based on 30 years of experience and discussions with pioneering scientists, to describe influencing factors for various selective oxidation reactions. The propene selective oxidation on bismuth molybdate also met most aspects of these 'seven pillars', including highly active lattice oxygen, appropriate metal-

oxygen bond strength, stable host structure, feasible redox behaviour, and multifunctionality of active sites [89].

It is generally accepted that the selective oxidation of propene follows a Mars-van Krevelen mechanism with lattice oxygen as the oxidizing agent[69]. Grasselli and co-workers recommended a mechanism for propene selective oxidation with molecular oxygen over bismuth molybdate, by reviewing the previous studies:

1. Propene is first adsorbed and an α-H abstraction of a hydrogen atom from a methyl group gives a symmetric π-allyl intermediate. This activation occurs via a bismuth site, and the α-H abstraction is the rate-determining step.
2. The π-allyl radical is then coordinated to a molybdenum ion, bridged by an oxygen atom (Bi−O−Mo).
3. Mo-bound lattice oxygen (Mo=O) is then inserted, introducing a C−O bond by forming a Mo-bound allyl alkoxide.
4. A second hydrogen abstraction step followed by desorption of the product acrolein leaves the reduced molybdenum site.
5. Molybdenum site re-oxidized by the gas phase oxygen O_2, molybdenyl oxygen regenerated.

In this mechanism, there are four electrons taking part in the catalytic reaction, in which Bi^{3+} and Mo^{6+} sites are both reduced to Bi^{2+} and Mo^{5+}/Mo^{4+}, respectively [69,90].

However, there was some disagreement in the literature as to which metal centres contribute to the redox cycle[70,91] and recently, Bell and co-workers proposed a new mechanism in remarkable studies utilizing advanced spectroscopic and modelling tools. By using DFT and XAS in combination with kinetic studies, they concluded that bismuth is neither oxidized nor reduced at any point during the oxidation of propene to acrolein, but remains Bi^{3+} throughout

and only Mo sites undergo a redox cycle during the reaction[92]. Their proposed mechanism is summarized as below:

1. The α-H abstraction occurs at a molybdenyl oxygen, and it is stabilized by the orbitals of a neighbouring bismuth cation.
2. The propene activation occurs via a spin-coupled singlet to triplet transition.
3. An immediate O insertion of a molybdenyl oxo group (Mo=O), giving an allyl alkoxide bond to Mo, a symmetric π-allyl radical intermediate is formed.
4. The second hydrogen abstraction, produces acrolein.
5. Desorption of acrolein and water, two reduced Mo^{4+} centres are present.
6. Mo^{4+} centres are reoxidized by molecular oxygen from the gas phase.

The mechanism proposed by Bell and co-workers only includes the reduction of two Mo^{6+} centres to Mo^{4+}. However, they explained that bismuth is needed to provide a suitable electronic and structural environment for propene oxidation. Licht et al. also tried to identify the influence of $Bi_2Mo_3O_{12}$ structure on the activation of propene, and they held a similar view to Bell's. The presence of bismuth in $Bi_2Mo_3O_{12}$ enables a certain five-coordinate Mo geometry, which is significantly more active for hydrogen abstraction[93].

1.5 Summary

In this project, we aim to develop new catalysts and processes to upgrade propene to more valuable products acrolein and to investigate the effects of microwave irradiation upon heterogeneous catalytic processes.

In Chapter 2, details of catalysts preparation; catalysts testing procedures and reaction conditions for propene selective oxidation are described. Meanwhile, product analysis and

quantification using gas chromatography (GC) and several catalyst characterization techniques are introduced.

Detailed experimental evidence is given and discussed in following Chapters 3, 4, 5 and 6. A summary of each results chapter is given below.

In Chapter 3, the principle of microwave-assisted catalysis will be introduced, some results of the initial screening tests will be presented. In this chapter, all samples will be tested under the same reaction conditions, and the samples with better performance will be screened for in-depth study in the following chapters.

In Chapter 4, a group of γ-Bi_2MoO_6 catalysts made using a hydrothermal method will be investigated in both conventional and microwave conditions. In this chapter, various catalyst characterization methods are used to investigate the structural differences between hydrothermally synthesized samples under different conditions (precursor solution pH and calcination step). The dielectric properties of samples are also measured to investigate the catalysts' potential to interact with the microwave field. Their performance under microwave and conventional heating will also be compared.

In Chapter 5, a group of bismuth molybdate vanadate catalysts made using a sol-gel method will be investigated in both conventional and microwave conditions. Catalyst characterization and dielectric measurements will also be described. The effects of vanadium contents are studied, and the optimized vanadium content for the catalyst used in the microwave-assisted process will be confirmed. The performances of the optimized sample under microwave and conventional conditions will also be compared.

In Chapter 6, silicon carbide will be chosen to use as a microwave absorber to activated $Bi_2Mo_3O_{12}$ catalysts, therefore SiC supported $Bi_2Mo_3O_{12}$ catalysts will be investigated in both conventional and microwave conditions. Catalyst characterizations and dielectric

measurements will also be done. The effect of several factors include combining method, loading amount and the ratio of Mo/Bi in the solution when loading will be evaluated.

1.6 References

1. Tang, J. & Resurreccion, F. P. Electromagnetic basis of microwave heating. *Development of Packaging and Products for Use in Microwave Ovens* 3–38e (2009) doi:10.1533/9781845696573.1.3.

2. Greenberger, D. M., Hentschel, K. & Weinert, F. Compendium of quantum physics : concepts, experiments, history and philosophy. 901 (Springer, 2009).

3. Feynman, R. P. 2. Photons: Particles of Light. *QED* 36–76 (2019) doi:10.1515/9781400847464-007.

4. Saunders, Simon. & Brown, H. R. *The Philosophy of vacuum*. (Clarendon Press, 1991).

5. *RHIC Scientists Serve Up "Perfect" Liquid*. (Brookhaven National Laboratory, 2005).

6. Longair, M. S. Maxwell (1865): A Dynamical Theory of the Electromagnetic Field. *Theoretical Concepts in Physics* 107–122 (2020) doi:10.1017/9781108613927.009.

7. Interaction of Electromagnetic Radiation with Matter. *Developments in Soil Science* 12–54 https://doi.org/10.1016/S0166-2481(08)70028-X (1987).

8. Galema, S. A. Microwave chemistry. *Chemical Society Reviews* **26**, 233 (1997).

9. Marco Montalti, Alberto Credi, Luca Prodi, M. Teresa Gandolfi. Handbook of Photochemistry. (Boca Raton, 2006)

10. Wisniak, J. The History of Catalysis. From the Beginning to Nobel Prizes. *Educación Química* **21**, 60–69 (2010).

11. Kakaei, K., Esrafili, M. D. & Ehsani, A. Introduction to Catalysis. *Interface Science and Technology* **27**, 1–21 (2019).

12. Catalysis Fundamentals - Chemical Engineering | Page1. https://www.chemengonline.com/catalysis-fundamentals/.

13. Hyle 18-2 (2012): The Unity of Chemistry and Physics: Absolute Reaction Rate Theory. http://www.hyle.org/journal/issues/18-2/hettema.htm.

14. Bond, G. *Heterogeneous catalysis : principles and applications*. (Clarendon Press, 1987).

15. Sun, J., Wang, W. & Yue, Q. Review on microwave-matter interaction fundamentals and efficient microwave-associated heating strategies. *Materials* **9**, (2016).

16. Mello, P. A., Barin, J. S. & Guarnieri, R. A. *Microwave Heating*. *Microwave-Assisted Sample Preparation for Trace Element Determination* (Elsevier, 2014). doi:10.1016/B978-0-444-59420-4.00002-7.

17. Jones, D. I. H. & Griffith, G. Microwave Drying Of Herbage. *Grass and Forage Science* **23**, 202–205 (1968).

18. Microwave Pretreatment of Coal Prior to Magnetic Separation. (1995) https://www.hindawi.com/journals/psse/1995/090127/.

19. Vanderhoff, J. W. Method For Carrying Out Chemical Reactions Using Microwave Energy. US Patent no. 3432413 (1969).

20. Giguere, R. J., Bray, T. L., Duncan, S. M. & Majetich, G. Application of commercial microwave ovens to organic synthesis. *Tetrahedron Letters* **27**, 4945–4948 (1986).

21. Gedye, R. *et al.* The use of microwave ovens for rapid organic synthesis. *Tetrahedron Letters* **27**, 279–282 (1986).

22. Kappe, C. O. Microwave dielectric heating in synthetic organic chemistry. *Chemical Society Reviews* **37**, 1127–1139 (2008).

23. Green, J. J. & Sandy, F. Microwave Characterization of Partially Magnetized Ferrites. *IEEE Transactions on Microwave Theory and Techniques* **22**, 641–645 (1974).

24. Pan, X., Liu, H., Jia, G. & Shu, Y. Y. Microwave-assisted extraction of glycyrrhizic acid from licorice root. *Biochemical Engineering Journal* **5**, 173–177 (2000).

25. Zong, L., Zhou, S., Sgriccia, N., Hawley, M. C. & Kempel, L. C. A Review of Microwave-Assisted Polymer Chemistry (MAPC). *Journal of Microwave Power and Electromagnetic Energy* vol. 38 49–74 (2003).

26. Mishra, R. R. & Sharma, A. K. Microwave-material interaction phenomena: Heating mechanisms, challenges and opportunities in material processing. *Composites Part A: Applied Science and Manufacturing* **81**, 78–97 (2016).

27. Chemat-Djenni, Z., Hamada, B. & Chemat, F. Atmospheric pressure microwave assisted heterogeneous catalytic reactions. *Molecules* **12**, 1399–1409 (2007).

28. Bag, S., Dasgupta, S. & Torok, B. Microwave-Assisted Heterogeneous Catalysis: An Environmentally Benign Tool for Contemporary Organic Synthesis. *Current Organic Synthesis* **8**, 237–261 (2011).

29. Tousey, R. F., Rajan, S. & Pekrul, E. Lossy material. (Institute of Electrical and Electronics Engineers (IEEE), 2002).

30. Chen, C., Hong, P., Dai, S. & Kan, J. Microwave effects on the oxidative coupling of methane over proton conductive catalysts. *Journal of the Chemical Society, Faraday Transactions* **91**, 1179–1180 (1995).

31. Fidalgo, B., Arenillas, A. & Menéndez, J. A. Mixtures of carbon and Ni/Al_2O_3 as catalysts for the microwave-assisted CO_2 reforming of CH_4. *Fuel Processing Technology* **92**, 1531–1536 (2011).

32. Tsai, C. H., Hsieh, T. H., Shih, M., Huang, Y. J. & Wei, T. C. Partial oxidation of methane to synthesis gas by a microwave plasma torch. *AIChE Journal* **51**, 2853–2858 (2005).

33. Chen, W. H., Cheng, T. C., Hung, C. I. & Lin, B. J. Chemical reactions and kinetics of a low-temperature water gas shift reaction heated by microwaves. *International Journal of Hydrogen Energy* **37**, 276–289 (2012).

34. Jie, X. *et al.* The decarbonisation of petroleum and other fossil hydrocarbon fuels for the facile production and safe storage of hydrogen. *Energy & Environmental Science* **12**, 238–249 (2019).

35. Roussy, G. *et al.* Controlled oxidation of methane doped catalysts irradiated by microwaves. *Catalysis Today* **21**, 349–355 (1994).

36. Wan, J., Tse, M., Husby, H. & Depew, M. High – Power Pulsed Micro – Wave Catalytic Processes: Decomposition of Methane. *http://dx.doi.org/10.1080/08327823.1990.11688107* **25**, 32–38 (2016).

37. Zhang, X., Lee, C. S. M., Mingos, D. M. P. & Hayward, D. O. Carbon Dioxide Reforming of Methane with Pt Catalysts Using Microwave Dielectric Heating. *Catalysis Letters 2003 88:3* **88**, 129–139 (2003).

38. Domínguez, A., Fernández, Y., Fidalgo, B., Pis, J. J. & Menéndez, J. A. Biogas to Syngas by Microwave-Assisted Dry Reforming in the Presence of Char. *Energy and Fuels* **21**, 2066–2071 (2007).

39. Zhang, X. & Hayward, D. O. Applications of microwave dielectric heating in environment-related heterogeneous gas-phase catalytic systems. *Inorganica Chimica Acta* (2006)

40. Zhang, X., Hayward, D. O. & Mingos, D. M. P. Dielectric Properties of MoS_2 and Pt Catalysts: Effects of Temperature and Microwave Frequency. *Catalysis Letters 2002 84:3* **84**, 225–233 (2002).

41. Zhang, X., Hayward, D. O., Lee, C. & Mingos, D. M. P. Microwave assisted catalytic reduction of sulfur dioxide with methane over MoS2 catalysts. *Applied Catalysis B: Environmental* **33**, 137–148 (2001).

42. Zhang, X., Hayward, D. O. & Mingos, D. M. P. Effects of Microwave Dielectric Heating on Heterogeneous Catalysis. *Catalysis Letters 2003 88:1* **88**, 33–38 (2003).

43. Zhang, X., Lee, C. S. M., Mingos, D. M. P. & Hayward, D. O. Oxidative coupling of methane using microwave dielectric heating. *Applied Catalysis A: General* **249**, 151–164 (2003).

44. Gonzalez-Cortes, S. *et al.* Wax: A benign hydrogen-storage material that rapidly releases H_2-rich gases through microwave-assisted catalytic decomposition. *Scientific Reports 2016 6:1* **6**, 1–11 (2016).

45. Jie, X. *et al.* On the performance optimisation of Fe catalysts in the microwave - assisted H_2 production by the dehydrogenation of hexadecane. *Catalysis Today* **317**, 29–35 (2018).

46. Jie, X. *et al.* Rapid Production of High-Purity Hydrogen Fuel through Microwave-Promoted Deep Catalytic Dehydrogenation of Liquid Alkanes with Abundant Metals. *Angewandte Chemie* **129**, 10304–10307 (2017).

47. Jie, X. *et al.* The decarbonisation of petroleum and other fossil hydrocarbon fuels for the facile production and safe storage of hydrogen. *Energy & Environmental Science* **12**, 238–249 (2019).

48. Jie, X. *et al.* Microwave-initiated catalytic deconstruction of plastic waste into hydrogen and high-value carbons. *Nature Catalysis* **3**, 902–912 (2020).

49. Yan, Y. *et al.* The decarbonization of coal tar via microwave-initiated catalytic deep dehydrogenation. *Fuel* **268**, 117332 (2020).

50. Technology Economics: Propylene via Propane Dehydrogenation, Part 3. https://www.slideshare.net/intratec/technology-economics-propylene-via-propane-dehydrogenation-part-3.

51. 4.1 Selective Hydrocarbon Oxidation Reactions, *Ullmann's Encyclopedia of Industrial Chemistry* (2000) doi:10.1002/14356007

52. Grasselli, R. K. Selective oxidation and ammoxidation catalysis: history of catalyst design. *nato asi Series, Series C: Mathematical and Physical Sciences* 273–288 (1983)

53. Preparation Of Olefinic Compounds. Patents No：US 3161670A. (1964).

54. Bettahar, M. M., Costentin, G., Savary, L. & Lavalley, J. C. On the partial oxidation of propane and propylene on mixed metal oxide catalysts. *Applied Catalysis A: General* **145**, 1–48 (1996).

55. Veatch, F., et al. New data on Sohio's acrylo process. *Hydrocarbon Processing & Petroleum Refinery* **41**, 187–190 (1962).

56. Callahan, J. L., Grasselli, R. K., Milberger, E. C. & Strecker, H. A. Oxidation and Ammoxidation of Propylene over Bismuth Molybdate Catalyst. *Industrial and Engineering Chemistry Product Research and Development* **9**, 134–142 (1970).

57. Mixed antimony oxide-uranium oxide oxidation catalyst. Patents No：US3198750A. (1962).

58. Distillers Company, Ltd. developed an oxidation catalyst which was a combination of tin and antimony oxides

59. Grasselli, R. K. *et al.* Catalyst for the manufacture of acrylonitrile and methacrylonitrile. **863**, 11 (1988).

60. Process for the catalytical preparation of acrylonitrile. No：US4097518A. (1979).

61. Reactivation of molybdenum containing oxidation catalysts in fluid bed reactors. Patents No:US2963443A. (1973).

62. Iron-modified bismuth phosphomolybdate catalyst. Patents No:US3629148A. (1969).

63. James Gassen, E. & owns, E. Preparation of an antimony oxide-tin oxide catalyst composition. Patents No:US3309325A (1964).

64. Process for the manufacture of acrylonitrile. Patents No: US3200141A(1957).

65. Farin, B., Monteverde Videla, A. H. A., Specchia, S. & Gaigneaux, E. M. Bismuth molybdates prepared by solution combustion synthesis for the partial oxidation of propene. *Catalysis Today* **257**, 11–17 (2015).

66. Le, M. T., Do, V. H., Truong, D. D. & Pham, N. N. Sol-Gel Synthesis of Bismuth Molybdate Catalysts for the Selective Oxidation of Propylene to Acrolein: Influence of pH Value and Theoretical Molar Atomic Ratio. *Journal of the Chinese Chemical Society* **64**, 1326–1332 (2017).

67. Schuh, K. *et al.* One-step synthesis of bismuth molybdate catalysts via flame spray pyrolysis for the selective oxidation of propylene to acrolein. *Chemical Communications* **50**, 15404–15406 (2014).

68. Zhai, Z., Wütschert, M., Licht, R. B. & Bell, A. T. Effects of catalyst crystal structure on the oxidation of propene to acrolein. *Catalysis Today* **261**, 146–153 (2016).

69. Sprenger, P., Kleist, W. & Grunwaldt, J.-D. Recent Advances in Selective Propylene Oxidation over Bismuth Molybdate Based Catalysts: Synthetic, Spectroscopic, and Theoretical Approaches. (2017) doi:10.1021/acscatal.7b01149.

70. Getsoian, A., Shapovalov, V. & Bell, A. T. DFT+U investigation of propene oxidation over bismuth molybdate: Active sites, reaction intermediates, and the role of bismuth. *Journal of Physical Chemistry C* **117**, 7123–7137 (2013).

71. Pudar, S., Oxgaard, J., Chenoweth, K., van Duin, A. C. T. & Goddard, W. A. Mechanism of selective oxidation of propene to acrolein on bismuth molybdates from quantum mechanical calculations. *Journal of Physical Chemistry C* **111**, 16405–16415 (2007).

72. Le, M. T. Bismuth Molybdate-Based Catalysts for Selective Oxidation of Hydrocarbons. in *Bismuth - Advanced Applications and Defects Characterization* (InTech, 2018).

73. Energy-Related Catalysis, Handbook of Heterogeneous Catalysis. (Wiley, 2008) doi:10.1002/9783527610044.

74. Swift, H. E., Bozik, J. E. & Ondrey, J. A. Dehydrodimerization of propylene using bismuth oxide as the oxidant. *Journal of Catalysis* **21**, 212–224 (1971).

75. Peacock, J. M., Parker, A. J., Ashmore, P. G. & Hockey, J. A. The oxidation of propene over bismuth oxide, molybdenum oxide, and bismuth molybdate catalysts. I. The preparation and testing of the catalysts. *Journal of Catalysis* **15**, 373–378 (1969).

76. Millet, J. M. M., Ponceblanc, H., Coudurier, G., Herrmann, J. M. & Védrine, J. C. Study of multiphasic molybdate-based catalysts. II. Synergy effect between bismuth molybdates and

mixed iron and cobalt molybdates in mild oxidation of propene. *Journal of Catalysis* **142**, 381–391 (1993).

77. Batist, P., Kinderen, A. der, … Y. L.-J. of & 1968, undefined. The catalytic oxidation of 1-butene over bismuth molybdate catalysts: IV. Dependence of activity on the structures of the catalysts. *Journal of Catalysis* **12**, 45-60 (1968).

78. Grasselli, R., Catalysis, J. B.-A. in & 1981, undefined. Selective oxidation and ammoxidation of propylene by heterogeneous catalysis. *Advanced Catalysis* **30**, 133 – 163 (1981).

79. Keulks, G., Krenzke, L., Catalysis, T. N.-A. in & 1979, undefined. Selective oxidation of propylene. *Academic Press* **27,**183-225 (1979).

80. Krenzke, L., Catalysis, G. K.-J. of & 1980, undefined. The catalytic oxidation of propylene: VI. Mechanistic studies utilizing isotopic tracers. *Journal of Catalysis* **61.2,** 316-325 (1980).

81. Carson, D., Forissier, M. & Vedrine, J. C. Kinetic study of the partial oxidation of propene and 2-methylpropene on different phases of bismuth molybdate and on a bismuth iron molybdate phase. *Journal of the Chemical Society, Faraday Transactions 1: Physical Chemistry in Condensed Phases* **80**, 1017–1028 (1984).

82. Wragg, R. D., Ashmore, P. G. & Hockey, J. A. Selective oxidation of propene over bismuth molybdate catalysts: The oxidation of propene using ^{18}O labeled oxygen and catalyst. *Journal of Catalysis* **22**, 49–53 (1971).

83. Ayame, A., Uchida, K., Iwataya, M. & Miyamoto, M. X-ray photoelectron spectroscopic study on α- and γ-bismuth molybdate surfaces exposed to hydrogen, propene and oxygen. *Applied Catalysis A: General* **227**, 7–17 (2002).

84. Martir, W. & Lunsford, J. H. The Formation of Gas-Phase π-Allyl Radicals from Propylene over Bismuth Oxide and γ-Bismuth Molybdate Catalysts. *Journal of the American Chemical Society* **103**, 3728–3732 (1981).

85. Matsuura, I., Schut, R. & Hirakawa, K. The surface structure of the active bismuth molybdate catalyst. *Journal of Catalysis* **63**, 152–166 (1980).

86. Keulks, G. W., Rosynek, M. P. & Daniel, C. Bismuth Molybdate Catalysts Kinetics and Mechanism of Propylene Oxidation. *Industrial and Engineering Chemistry Product Research and Development* **10**, 138–142 (1971).

87. Wragg, R. D., Ashmore, P. G. & Hockey, J. A. Selective oxidation of propene over bismuth molybdate catalysts: The oxidation of propene using ^{18}O labeled oxygen and catalyst. *Journal of Catalysis* **22**, 49–53 (1971).

88. Védrine, J. C. & Fechete, I. Heterogeneous partial oxidation catalysis on metal oxides. *Comptes Rendus Chimie* vol. 19 1203–1225 (2016).

89. Grasselli, R. K. Fundamental principles of selective heterogeneous oxidation catalysis. *Topics in Catalysis* **21**, 79–88 (2002).

90. Grasselli, R. K. *et al.* Active centers, catalytic behavior, symbiosis and redox properties of MoV(Nb,Ta)TeO ammoxidation catalysts. *Topics in Catalysis* **38**, 7–16 (2006).

91. Arora, N., Deo, G., Wachs, I. E. & Hirt, A. M. Surface Aspects of Bismuth–Metal Oxide Catalysts. *Journal of Catalysis* **159**, 1–13 (1996).

92. Getsoian, A. "Bean" & Bell, A. T. The Influence of Functionals on Density Functional Theory Calculations of the Properties of Reducible Transition Metal Oxide Catalysts. *Journal of Physical Chemistry C* **117**, 25562–25578 (2013).

93. Licht, R. B., Getsoian, A. & Bell, A. T. Identifying the Unique Properties of α-$Bi_2Mo_3O_{12}$ for the Activation of Propene. *Journal of Physical Chemistry C* **120**, 29233–29247 (2016).

2 Experimental

2.1 Introduction

In this chapter, details of catalysts preparation; catalysts testing procedures and reaction conditions for propene selective oxidation in both conventional and microwave-assisted processes are described. Product analysis and quantification using gas chromatography (GC) and several catalyst characterization techniques are introduced.

2.2 Reagents and materials

The following chemicals and materials have been used for the purposes of catalyst preparation, catalytic testing, and data analysis:

TiO_2 (P25, Aeroxide®, Evonik);

SiO_2 (P432, Camlab);

γ-Al_2O_3 (Nanopowder, Sigma–Aldrich);

Carbon (G60, NORIT);

$BaTiO_3$(99%, Sigma–Aldrich);

SiC (98%, Sigma–Aldrich);

$Ni(NO_3)_2$ (98%, Sigma–Aldrich);

$Bi(NO_3)_3{\cdot}5H_2O$ (98%, Sigma–Aldrich);

$(NH_4)_6Mo_7O_{24}{\cdot}4H_2O$ (99.98%, Sigma–Aldrich);

$Na_2MoO_4 \cdot 2H_2O$ (98%, Sigma–Aldrich);

Na_3VO_4 (98%, Sigma–Aldrich);

Titanium(IV) isopropoxide (97%, Sigma–Aldrich);

$Fe(NO_3)_3.9H_2O$ (98%, Sigma–Aldrich);

NaOH (Fisher Scientific, >98.5 %);

Molecular O_2 (BOC. > 99.95%);

Molecular N_2 (BOC. > 99.95%);

Molecular C_3H_6 (BOC. > 99.95%);

Molecular H_2 (Peak Sentific, Hydrogen generator);

Distilled water millipore (18.2 MΩ.cm at 25°C);

2.3 Catalyst preparation

2.3.1 Supported Nickel Catalysts Made by Impregnation Method

A series of nickel supported catalysts were made by an impregnation method. Support materials including titanium oxide, silicon oxide, aluminium oxide, activated carbon, silicon carbide and barium titanate. The procedure of making a 5 wt.% mass ratio Ni/TiO_2 catalyst is introduced as an example.

0.247g $Ni(NO_3)_2 \cdot 6H_2O$ was dissolved into 2.5 mL of deionized water, and then 1.0 g of support material powder was added into the solution to form a paste-like mixture. The paste-like mixture was dried at 110 ˚C overnight. Then the resulting powder was calcined by heating from room temperature to 500 °C with a ramping rate of 2 °C/min and then kept at 500 °C for

2 h in static air. The resultant supported nickel oxide precursors were reduced to the corresponding nickel catalysts by heating in a gas flow of 5% hydrogen in argon with a flow rate of 50 mL/min from room temperature to 500 °C with a ramping rate of 2 °C/min and then held at 500 °C for 2 h.

The only difference of making supported nickel catalysts with other support material is different amounts of deionized water was used to dissolve the 0.247g $Ni(NO_3)_2 \cdot 6H_2O$. The amount of water was determined by the pore volume of the support materials, which was determined by water absorption.

Table 2.1 Water absorption of support materials

Support material	Water absorption (mL g^{-1})
TiO_2	2.5
SiO_2	3.6
Al_2O_3	1.7
Activated carbon	4.8
SiC	0.3
$BaTiO_3$	0.5

(The water absorption of the support materials were tested by adding water dropwise to the powder until the mixture is toothpaste-like)

2.3.2 Bismuth-based Mixed Metal Oxide Made by Sol-gel Method

A group of bismuth-based Bi–Me–O oxides, where the Me is V, Mo or Fe were prepared using a sol-gel method[1]. Bismuth nitrate was used as the bismuth source.

$Bi_2Mo_3O_{12}$ catalyst

4.85 g of $Bi(NO_3)_3 \cdot 5H_2O$, 0.264 g of $(NH_4)_6Mo_7O_{24} \cdot 4H_2O$ and 10 g of citric acid were dissolved in 50 mL of water. The obtained solution was held at 60 °C under stirring conditions in an open container for 24 h to remove water. The gel formed was dried at 110 °C overnight. The resulting powder was calcined by heating in static air from room temperature to 500 °C with a ramping rate of 2 °C/min and then held at 500 °C for 2 h.

$Bi_2Mo_2O_9$ catalyst

4.85 g of $Bi(NO_3)_3 \cdot 5H_2O$, 0.176 g of $(NH_4)_2MoO_4$ and 8 g of citric acid were dissolved in 50 mL of water. The obtained solution was held at 60 °C under stirring conditions in an open container for 24 h to remove water. The gel formed was dried at 110 °C overnight. The resulting powder was calcined by heating from room temperature in static air to 500 °C with a ramping rate of 2 °C/min and then held at 500 °C for 2 h.

Bi_2MoO_6 catalyst

4.85 g of $Bi(NO_3)_3 \cdot 5H_2O$, 0.088 g of $(NH_4)_2MoO_4$ and 6 g of citric acid were dissolved in 50 mL of water. The obtained solution was held at 60 °C under stirring conditions in an open container for 24 h to remove water. The gel formed was dried at 110 °C overnight. The resulting powder was calcined by heating in static air from room temperature to 500 °C with a ramping rate of 2 °C/min and then held at 500 °C for 2 h.

$BiVO_4$ catalyst

2.43 g of $Bi(NO_3)_3 \cdot 5H_2O$, 0.059 g of NH_4VO_3 and 4 g of citric acid were dissolved in 50 mL of water. The obtained solution was held at 60 °C under stirring conditions in an open container for 24 h to remove water. The gel formed was dried at 110 °C overnight. The resulting powder

was calcined by heating in static air from room temperature to 500 °C with a ramping rate of 2 °C/min and then held at 500 °C for 2 h.

$BiFeO_3$ catalyst

2.43 g of $Bi(NO_3)_3 \cdot 5H_2O$, 2.02 g of $Fe(NO_3)_3 \cdot 9H_2O$ and 4 g of citric acid were dissolved in 50 mL of water. The obtained solution was held at 60 °C under stirring conditions in an open container for 24 h to remove water. The gel formed was dried at 110 °C overnight. The resulting powder was calcined by heating in static air from room temperature to 500 °C with a ramping rate of 2 °C/min and then held at 500 °C for 2 h.

2.3.3 Bismuth-based Mix Metal Oxide Made by Hydrothermal Method

Another group of bismuth-based Bi–Me–O oxides, where the Me is V, Mo, Fe or Ti were prepared using a hydrothermal method[2].

Bi_2MoO_6 catalyst

2.425 g of $Bi(NO_3)_3 \cdot 5H_2O$, and 0.606 g of $Na_2MoO_4 \cdot 2H_2O$ were dissolved into 5 mL of HNO_3 (4 M). Then a concentrated aqueous solution of NaOH (2 M) was added dropwise into the solution until the target pH value was reached (4, 6 or 8). After being stirred for 2 h, the suspension was transferred into a 100 mL Teflon-lined stainless-steel autoclave to 70% of the total volume. The autoclave was heated at 160 °C for 24 h at autogenous pressure and then cooled to room temperature naturally. The resulting samples were separated by filtration, washed with 100 ml deionized water and 100 ml absolute alcohol several times, and then dried at 110 °C overnight. A group of calcined samples were also made by calcining samples under static air at 500 °C with a ramping rate of 5 °C min^{-1}.

$BiVO_4$ catalyst

2.425 g of $Bi(NO_3)_3 \cdot 5H_2O$, and 1.83g of Na_3VO_4 were dissolved into 5 mL of HNO_3 (4 M). Then a concentrated aqueous solution of NaOH (2 M) was added dropwise into the solution until the target pH value was reached 4. After being stirred for 2 h, the suspension was transferred into a 100 mL Teflon-lined stainless-steel autoclave to 70% of the total volume. The autoclave was heated at 100 °C for 12 h at autogenous pressure and then cooled to room temperature naturally. The resulting samples were separated by filtration, washed with 100 ml deionized water and 100 ml absolute alcohol several times, and then dried at 110 °C overnight.

$BiFeO_3$ catalyst

2.425 g of $Bi(NO_3)_3 \cdot 5H_2O$, and 2.02 g of $Fe(NO_3)_3 \cdot 9H_2O$ were dissolved into 5 mL of HNO_3 (4 M). Then a concentrated aqueous solution of NaOH (2 M) was added dropwise into the solution until the target pH value was reached 12. After being stirred for 2 h, the suspension was transferred into a 100 mL Teflon-lined stainless-steel autoclave to 70% of the total volume. The autoclave was heated at 200 °C for 24 h at autogenous pressure and then cooled to room temperature naturally. The resulting samples were separated by filtration, washed with 100 ml deionized water and 100 ml absolute alcohol several times, and then dried at 110 °C overnight.

$Bi_4Ti_3O_{12}$ catalyst

2.425 g of $Bi(NO_3)_3 \cdot 5H_2O$, and 1.06 g of titanium-isopropanol were dissolved into 5 mL of HNO_3 (4 M). Then a concentrated aqueous solution of NaOH (2 M) was added dropwise into the solution until the target pH value was reached 12. After being stirred for 2 h, the suspension was transferred into a 100 mL Teflon-lined stainless-steel autoclave to 70% of the total volume. The autoclave was heated at 200 °C for 24 h at autogenous pressure and then cooled to room temperature naturally. The resulting samples were separated by filtration, washed with 100 ml deionized water and 100 ml absolute alcohol several times, and then dried at 110 °C overnight.

2.3.5 Bismuth Vanadate Molybdate Made by Sol-gel Method

A group of bismuth vanadate molybdate catalysts were made by the sol-gel method[3], the detailed making procedure is introduced below.

Bismuth molybdate

The metal precursors were added to the preparation solutions at the atomic ratios of Bi:Mo = 2:1, to produce materials with the stoichiometry Bi_2MoO_6. Solution A contained $Bi(NO_3)_3 \cdot 5H_2O$ and citric acid with the molar ratio of 1:1 dissolved in 2 M HNO_3. HNO_3 was used in place of water in solution A to prevent precipitation of bismuth hydroxides. Solution B contained ($(NH_4)_6Mo_7O_{24} \cdot 4H_2O$) and citric acid prepared with the molar ratio of 0.142:1 dissolved in deionized water. Solution B was slowly added to solution A. The resulting mixture was placed in an oven at 65 °C for about 24 h in the air until it formed a gel. The gel was then dried at 110 °C overnight and then calcined in air at 500 °C for 2 h.

Bismuth vanadate molybdate and bismuth vanadate

For the samples containing both vanadium and molybdenum, NH_4VO_3 was used as the vanadium source. The metal precursors were added to the preparation solutions at the atomic ratios of Bi:(Mo+V) = 2:1. The procedure used was similar to the synthesis of Bi_2MoO_6. Solution A contained $Bi(NO_3)_3 \cdot 5H_2O$ and citric acid with the molar ratio of 1:1 dissolved in 2 M HNO_3. Solution B contained $(NH_4)_6Mo_7O_{24} \cdot 4H_2O$ and citric acid prepared with the molar ratio of 0.142:1 dissolved in deionized water. Solution C contained NH_4VO_3 and citric acid prepared with the molar ratio of 1:1 dissolved in deionized water. Solution B was slowly added to solution A, and then solution C was slowly added to the mixture. The resulting mixture was placed in an oven at 65 °C for about 24 h in the air until it formed a gel. The gel was then dried at 110 °C overnight and then calcined in air at 500 °C for 2 h. For pure $BiVO_4$, the metal

precursors were added to the preparation solutions at the atomic ratios of Bi:V = 1:1. The procedure was similar to that described for the mixed Mo/V materials without solution B, where solution C was slowly added to solution A. The resulting mixture was placed in an oven at 65 °C for about 24 h in the air until it formed a gel. The gel was then dried at 110 °C overnight.

2.3.6 SiC Supported Bismuth Molybdate

Two groups of SiC supported bismuth molybdate catalyst were made by a sol-gel deposition method, the detailed making procedure is introduced below.

SiC Supported $Bi_2Mo_3O_{12}$ made with the solution with Bi:Mo = 1:1

$Bi(NO_3)_3 \cdot 5H_2O$, $(NH_4)_6Mo_7O_{24} \cdot 4H_2O$ and citric acid were dissolved in 50 mL of water with the molar ratio of 7:1:14. The obtained solution was held at 60 °C under stirring conditions in an open container for 2 h. Then .1.00 g of SiC was added to the container and the mixture was kept at 60 °C under stirring conditions overnight to remove water. The resulting materials were dried at 110 °C overnight. The resulting powder was calcined by heating in static air from room temperature to 500 °C with a ramping rate of 2 °C/min and then held at 500 °C for 2 h.

SiC Supported $Bi_2Mo_3O_{12}$ made with the solution with Bi:Mo = 2:3

$Bi(NO_3)_3 \cdot 5H_2O$, $(NH_4)_6Mo_7O_{24} \cdot 4H_2O$ and citric acid were dissolved in 50 mL of water with the molar ratio of 14:3:28. The obtained solution was held at 60 °C under stirring conditions in an open container for 2 h. Then 1.00 g of SiC was added to the container and the mixture was kept at 60 °C under stirring conditions overnight to remove water. The resulting materials were dried at 110 °C overnight. The resulting powder was calcined by heating in static air from room temperature to 500 °C with a ramping rate of 2 °C/min and then held at 500 °C for 2 h.

2.4 Catalyst testing

2.4.1 Testing Protocols

2.4.1.1 Conventional Testing

The catalytic performance of the prepared catalysts was evaluated for the selective oxidation of propene to acrolein at atmospheric pressure in a laboratory fixed bed reactor. Typically, 0.2 g of the catalyst was placed in a quartz reactor tube (7 mm internal diameter) held between plugs of quartz wool. The reactor was placed in a tubular furnace (ε-lements) and the temperature was monitored using a thermocouple at the centre of the catalyst bed. The propene, nitrogen and oxygen were introduced using mass flow controllers (Bronkhorst) to give a total flow rate of 50 ml min^{-1} (propene:O_2:He = 5:10:85). The outlet lines were heated to 140 °C to prevent condensation of the products.

2.4.1.2 Microwave-assisted Testing

For the experiments carried out in this study, microwave-assisted catalytic reactions are based on a single-mode microwave cavity designed by colleagues in the School of Engineering[4]. The single-mode microwave heating cavity cut-away diagram is shown in Figure 2.1.

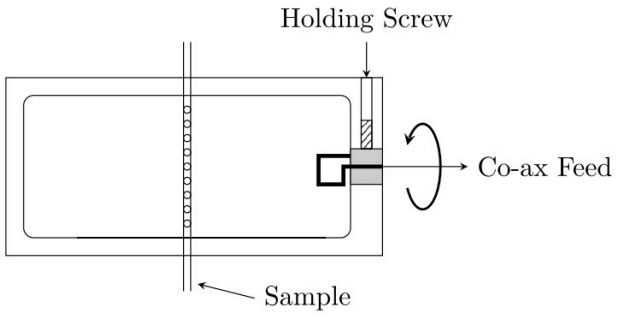

Figure 2.2 Single-mode microwave heating cavity cut-away diagram[4].

The sample is positioned to maximize exposure to the electric or magnetic field as required. In the typical TM_{010} setup, and for electric field heating, the sample is placed axially and coupling is provided by a short-circuit circuit loop. The loop is held by a screw but can be rotated to modify the coupling co-efficient (g) and achieve critical coupling. All microwave tests were carried out using the experimental setup shown in Figure 2.2.

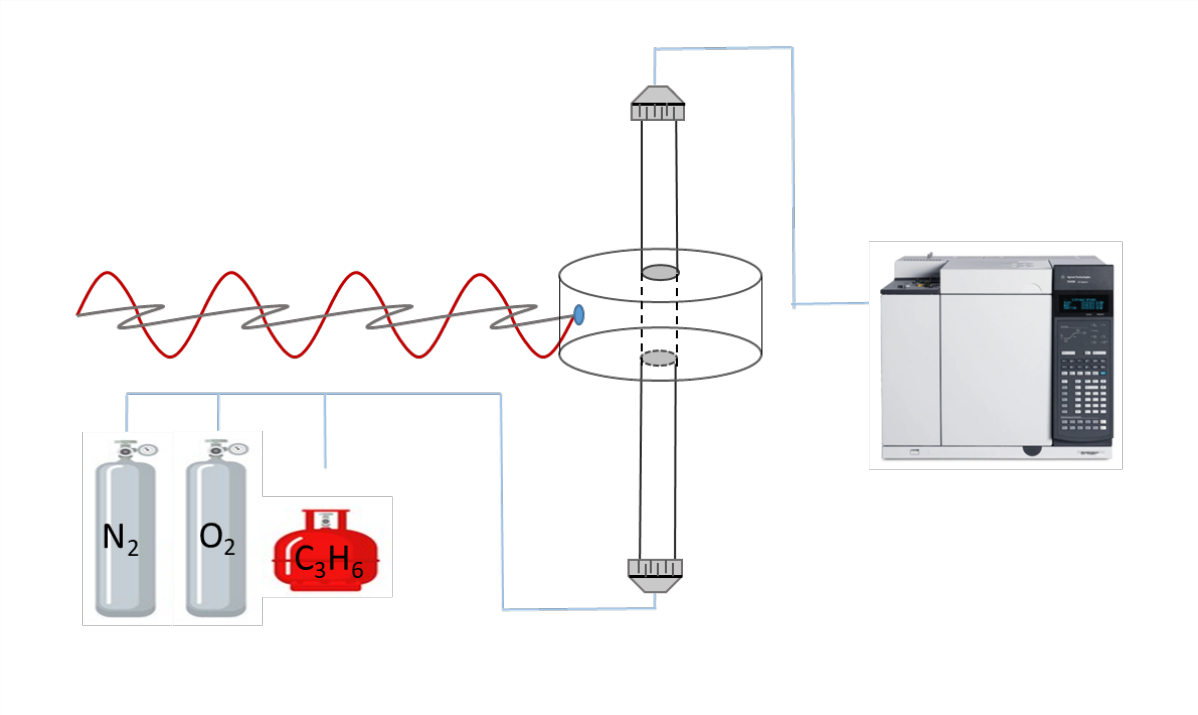

Figure 2.3 Experiment setup for Microwave-assisted gas-phase heterogeneous catalysis

In microwave tests, the candidate catalysts were packed in the tube and located in the middle of the cavity. Typically, 0.2 g of the catalyst was placed in a quartz reactor tube (7 mm internal diameter) held between plugs of quartz wool. 2.5 GHz microwave radiation with a power of 0-30 W irradiated the catalyst bed through a hole in the side of the cavity perpendicular to the catalyst bed. On the opposite side of the cavity, an infrared camera was mounted to detect the temperature of the catalyst bed when steady state was achieved. To maintain the same

conditions with conventional tests, catalyst mass, gas composition and flow rate remained the same as the conditions described in Section 2.4.1.1.

2.4.2 Products Analysis

All the products were collected and analyzed using an online gas chromatograph (Agilent 7680A) equipped with an HP-PlotQ (30 m * 0.530 mm) column and a Porapak Q (80-100 Mesh, 1.8 m * 2.0 mm) column for separation of the products, and flame ionization detector (FID) and thermal conductivity detector (TCD) for analyzing the products.

Gas chromatography (GC) is an analytical technique extensively used to separate and analyze mixtures of chemical compounds[5]. Both liquid and gas phase samples can be analyzed, with liquid samples initially vaporized at the sample injector; samples are then transported through the instrument via a carrier gas to a column where compounds are separated before the analytes are subsequently detected. The column can be a capillary column with a thin layer of nonvolatile chemicals coated onto the walls of a hollow column or a packed column containing inert solids, coated with a thin layer of nonvolatile chemicals. The nonvolatile chemicals are known as the stationary phase. The nature of the stationary phase will vary depending on the polarity of the analytes and the separation required. The different chemicals compounds present in a sample will interact with the stationary phase to differing extents, leading to their elution from the column at different times (retention time). This allows for the separation and detection of the products formed. Separations can also be achieved through a temperature gradient whereby the temperature is increased to allow the elution of more strongly retained compounds. The carrier gas is known as the mobile phase and is an inert gas, typically He Ar or N_2. It is important that the carrier gas has no interaction with the stationary phase.

FID is extensively used in the analysis of hydrocarbons. The effluent stream enters the detector where it is mixed with H_2/air and burnt, leading to the formation of ions and electrons, which flow between two electrodes present in the detector resulting in a current flow, which is amplified to generate a signal. FIDs typically provide high linearity over a wide concentration range, although low/no response is observed for several products including CO and CO_2. TCD is a universal detector, suitable for analytes that cannot be detected using an FID.

Table 2.1 Full products list with retention times

Product name	Retention time (min)	
	FID	TCD
CH_4	2.2	-
C_2H_4	2.8	-
C_2H_6	3.8	-
C_3H_8	11.2	-
Acetaldehyde	14.8	-
Propene oxide	19.9	-
Acrolein	20.7	-
Acetone	21.3	-
Isopropanol	21.6	-
CO	-	0.99
CO_2	-	2.22

2.4.3 Calculations for substrate conversion, product selectivity and yield, carbon balance

1. Propene conversion (%) = (moles of propene before reaction – moles of propene after reaction)/ moles of propene before reaction × 100 %.

2. Product selectivity (%) = moles of the product after reaction/moles of total products after reaction × 100%.

3. Product yield (%) = propene conversion × product selectivity / 100 %

4. Carbon balance (%) = total moles of carbon in products after reaction / (total moles of carbon in propene before reaction – total moles of carbon in propene after reaction) × 100 %.

2.5 Characterization techniques

2.5.1 Powder X-ray diffraction (XRD)

Theory

X-ray diffraction (XRD) is based on the elastic scattering of monochromatic X-ray photons by atoms ordered in a crystalline structure[6]. Thus, it is often used to estimate crystallite size. X-rays are used as they have sufficient energy to penetrate solids and have wavelengths in the angstrom range. When scattered, if the monochromatic X-rays are in phase a diffraction pattern is observed. This pattern corresponds to the lattice spacings of crystal planes which can be calculated based on Bragg's equation (see Figure 2.3)[6]:

$$n\lambda = 2d\sin\theta$$

Where

n = the order of the reflection (an integer),

λ = the X-ray wavelength,

d = the distance between two lattice planes

θ = the angle between the incoming X-rays and the normal to the reflecting lattice plane.

The crystalline phases present in the sample can be identified through a comparison of the collected diffraction pattern with a database of diffraction patterns. However, it is worth noting that the analyzed sample must have sufficient long-range lattice order (typically 5 nm or above) in order for peaks to be observed, and therefore is not suitable for the detailed study of amorphous materials.

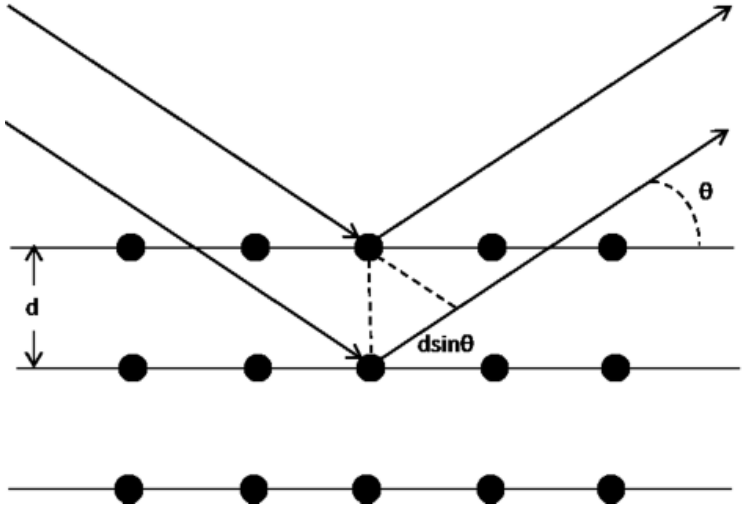

Figure 2.4 In phase x-rays scattered in an ordered lattice resulting in constructive interference

The XRD pattern is measured for a powdered sample with a stationary X-ray source and a moveable detector. The intensity of the diffracted radiation was scanned as a function of the angle (2θ) between the incoming and diffracted beams. Usually, the rotation of a sample can be carried out to enhance the number of particles that contribute to the diffraction.

The XRD diffraction patterns could also be used to evaluate the crystallite size according to the Scherrer equation[7]:

$$L = \frac{K\lambda}{\beta \cos\theta}$$

Where

L = is a measure of the crystallite size in the direction perpendicular to the reflecting plane

K = a constant (taken as 1)

λ = the X-ray wavelength

β = the peak width

θ = the angle between the beam and the normal on the reflecting plane

For example, with the decrease of crystalline size, the peaks broaden due to incomplete destructive interference in scattering directions where the X-rays are out of phase. However, it should be noted that the error resulting from the measurement would be significantly increased as the peaks become ill-defined. Generally, the particles with a size of < 5 nm cannot be analyzed and measured as the peaks are so broad that they merge into the background signal.

Experiment

In this work, the XRD technique was used to identify the crystal phases of all samples prepared by various methods and calculate crystallite sizes of selected matrials. Analysis was carried out using a PANalytical X'pert Pro powder diffractometer with a Cu $K_{\alpha 1}$ X-ray radiation (λ =0.154098 nm) sourc at ambient temperature. Samples were typically scanned in the range of 10-80 degrees at 40 kV and 40 mA. Samples were ground and place into a backfilled sample holder for analysis. Crystal structures were assigned to diffractograms using MDI/Jade software with databases from the Powder Diffraction File (PDF).

2.5.2 Raman spectroscopy

Theory

Raman spectroscopy is based on the Raman effect, specifically, the inelastic scattering of photons[8,9]. A sample is irradiated with monochromatic light of frequency, ν_0 whereby the majority of the photons undergo Rayleigh (elastic) scattering. The molecule is activated to an

excited state with energy, $h\nu_0$ above the ground state, then it decays back down to the ground state. Thus, no energy is exchanged between the molecule and the photon. However, when the excited molecule decays to the first vibrational energy level with frequency, ν_{vib} it removes an amount of energy equal to $h\nu_{vib}$ away from the photon. Thus, the scattered light exhibits intensity at the frequency ν_0-ν_{vib}. This Raman peak is called the Stokes band which is usually the side recorded for Raman scattering.

Experiment

Raman spectroscopy was performed using a Renishaw inVia microscope with a green argon-ion laser (λ = 514 nm). Samples were prepared by pressing onto a Raman inactive aluminium plate. Before sample analysis, the laser was calibrated using an internal Si reference and focused with an Olympus BH2-UMA microscope. 10 seconds of laser exposure and 30 accumulations were used in each scan, with the laser operating at a power of 0.1 %. Automatic cosmic ray removal was performed on all samples.

2.5.3 BET

Theory

BET (Brunauer, Emmett and Teller)[10] is commonly used in catalysis for the measurement of the surface area of a given catalyst. The BET equation can be explained as an adaption of the Langmuir isotherm which states that:

$$\theta = \frac{K_p}{1 + K_p}, K = \frac{k_a}{k_d}$$

Where:

K_p is the equilibrium constant of the adsorption process.

k_a and k_d are the rate constants for adsorption and desorption repectively.

The Langmuir isotherm only considers monolayer formation *ie*, θ <1 however the BET equation expands on this to multilayer formation *ie*, θ>1. A full monolayer does not need to be formed before multilayer formation can proceed. So the BET equation, as an expansion of the Langmuir isotherm is:

$$v = \frac{\left(\frac{v_m c}{p_0} p\right)}{\left(1 + \frac{c}{p_0} p\right)}$$

The rearranged form can be used to form straight line a plot of $\frac{p}{v(v_0 - p)}$ against $\left(\frac{p}{p_0}\right)$ with intercept $\frac{1}{v_m c}$ and a gradient of $\left(\frac{c-1}{v_m c}\right)$.

$$\frac{p}{v(v_0 - p)} = \frac{1}{v_m c} + \left(\frac{c-1}{v_m c}\right)\left(\frac{p}{p_0}\right) \; and \; c = exp\left(\frac{E_1 - E_L}{RT}\right)$$

Where:

p = pressure of adsorbate gas in pascals

v = volume of adsorbed gas at standard temperature and pressure

p_0 = saturation pressure in pascals

v_m = molar volume of gas to form the monolayer

E_1 = heat of adsorption for monolayer formation

E_2 = heat of adsorption for multilayer formation

R = gas constant

T = Temperature in K

Through obtaining v_m it is plausible to calculate the specific surface area using the following equation:

$$S = (N_a)(v_m)(A)$$

Where

S = specific surface area

N_a= Avogadro's number

v_m = molar volume of gas to form a complete monolayer

A = cross sectional area of adsorbent gas. For nitrogen, this is 16 Å^2

Experiment

Nitrogen adsorption isotherms were collected using a Quantachrome Quadrasorb evo™ surface area analyser at -196 °C. A 5-point plot was performed using N_2 as the adsorbate gas. Samples were degassed under vacuum at 150 °C for 3 hours before analysis. Surface areas were calculated following the BET method over the $\frac{p}{p_0}$ range of 0.05–0.3, using QuadraWin™ software.

2.5.4 X-Ray Photoelectron Spectroscopy (XPS)

Theory

X-Ray photoelectron spectroscopy (XPS) is commonly used in the field of material characterization for the determination of the elemental composition of samples and the oxidation state of the elements observed. XPS is based on the photoelectric effect: while an atom in the sample is irradiated with light, the atom will absorb photons of energy causing core

or valence electrons to be ejected with a specific kinetic energy that can be used to calculate its binding energy.

During XPS analysis a sample is irradiated with a single wavelength of X-ray radiation causing core or valence electrons to be ejected with specific kinetic energy (E_k). The frequency of radiation is kept constant. Thus, the binding energy of the photoelectrons can be determined by the equation below, where the kinetic energy of the ejected photoelectron can be measured.

$$E_k = h\nu - E_b$$

E_k = kinetic energy of the ejected photoelectron

h = Planck's constant (6.63 x 10^{-34} J·s)

ν = frequency of radiation

E_b = binding energy of the photoelectron or ionisation energy

It is worth noting that XPS is a surface-specific technique, i.e. it can only be used to probe a short distance into the surface, as photoelectrons have a limited escape depth (1-12 nm)[11].

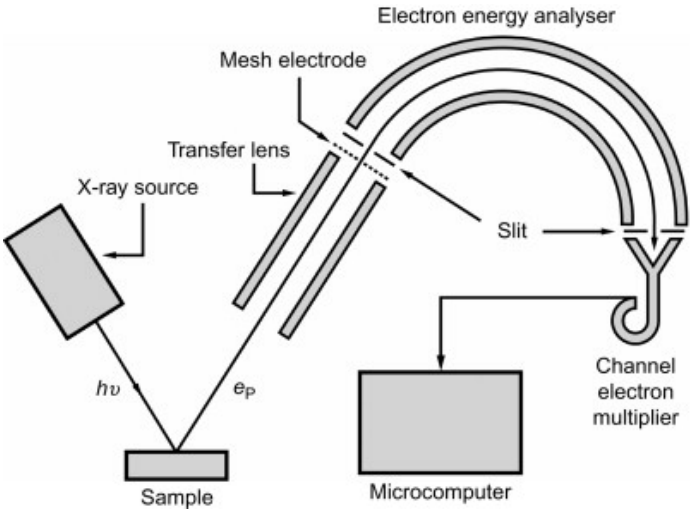

Figure 2.5 Schematic of an X-ray photoelectron spectrometer[12]

Furthermore, binding energies are not only element-specific but also change depending on if a withdrawal (oxidation) or addition (reduction) of valence electron charge is taking place, reflecting in an increase or decrease in binding energy, respectively. These small changes in the binding energies of core electrons allow for the determination of oxidation states of surface atoms[6].

Experiment

In this work, XPS analyses were carried out on a Kratos Axis Ultra-DLD spectrometer, utilizing a micro-focused monochromatic Al K_α X-ray source (hv=1486.6 eV) operating at 72 W power. Samples were analysed at pass energies of 40 and 150 eV for high-resolution and survey scans, respectively. A C_{1s} reference (284.5 eV) was used to correct the charge effect. Data analysis was performed in CasaXPS software using a Shirley-type background and Scofield cross-sections.

2.5.5 Inductively coupled plasma mass spectrometry (ICP-MS)

Theory

Inductively coupled plasma mass spectrometry (ICP-MS) is a state-of-the-art technique used for elemental analysis, especially for element determination at trace and ultra-trace levels[13]. It has excellent detection capability which could be used to simultaneously measure most elements in the periodic table. The basic principle of ICP-MS is that the ICP source converts the atoms in the sample into ions which are then separated and detected by the mass spectrometer. The sample is typically introduced into the plasma as an aerosol, where it is completely desolvated, and the elements are first converted into gaseous atoms and then ionized towards the end of the plasma. A plasma is generated by radiofrequency magnetic fields

induced by a coil wound around the end of a quartz torch through which argon flows. When a spark is applied to the argon flowing through the torch, the atoms become ions which get caught in the electromagnetic field to produce an argon plasma from colliding with other argon atoms. This energy transfer is called inductive coupling since it involves no electrodes[14].

Once the elements are converted into ions, they are then passed through a vacuum before entering the low-pressure region of the mass spectrometer ($< 1 \times 10^{-5}$ torr), since the ICP operates at atmospheric pressure while the mass spectrometer requires a vacuum condition. The ion source is collimated to an ion beam using a set of electrostatic lenses. Once the ions enter the mass spectrometer, the analytes are separated by their mass-to-charge ratio. Afterwards, they reach the detector which converts the ion current into electrical signals that are then counted by its integrated measurement circuitry. The magnitude of the electrical signals corresponds to the number of analyte ions present in the sample. Therefore, the element in an unknown sample could be detected and quantitively measured by comparing the ion signal with known calibration standards.

Experiment

In this work, selected samples were analysed using an Agilent 7900 ICP-MS instrument, equipped with a micro-mist nebuliser in organic phase mode. Quantification was carried out by comparison with a calibration curve.

2.5.6 Dielectric Measurement

Theory

Measurement of complex permittivity and permeability of dielectric and magnetic materials plays an important role in microwave technology. The cavity perturbation method was used for measuring the dielectric parameters in this work. When a small sample of material is inserted in a resonant cavity, it will cause a complex frequency shift. The amount of complex frequency shift is given by Waldron[15] as:

$$-\frac{\delta\omega}{\omega} = \frac{(\varepsilon_r - 1)\varepsilon_0 \int_{Vs} E \cdot E_0^* dv + (\mu_r - 1)\mu_0 \int_{Vs} H \cdot H_0^* \, dv}{\int_{Vc} D_0 \cdot E_0^* + B_0 \cdot H_0^* dv}$$

Where $\delta\omega$ is the complex frequency shift; E_0, D_0, B_0, H_0 are the unperturbed cavity fields, and E and H are the fields in the interior of the sample; ε_r, μ_r are the volumes of the cavity and the sample, respectively.

The fundamental idea of cavity perturbation is that the change in the overall geometrical configuration of the electromagnetic fields upon the introduction of a material sample should be small. This indicates that percentage change in the real part of resonant frequency must be small [4]. Therefore, the constraint on the above equation is that $\delta\omega << \omega$. For a sample placed at the electric field maximum position, the equation can be simplified to[16]:

$$-\frac{\delta\omega}{\omega} = \frac{(\varepsilon_r - 1) \int_{Vs} E \cdot E_{0\,max}^* \, dv}{2 \int_{Vc} |E_0 \cdot E_0| \, dv}$$

For a rectangular cavity operated at TE_{lOL} mode, the total fields can be written as[16]:

$$E_y = E_{0\,max} \sin\frac{\pi x}{a} \sin\frac{L\pi z}{d}$$

$$H_x = \frac{j\pi E_{0\,max}}{Z_{TE}} \sin\frac{\pi x}{a} \cos\frac{L\pi z}{d}$$

$$H_z = \frac{-j\pi E_{0\,max}}{K\eta a} \cos\frac{\pi x}{a} \cos\frac{L\pi z}{d}$$

Where a is the broader dimension of the waveguide, d is the length of the cavity, $Z_{TE} = (K\eta/\beta)$, is the wave impedance of transverse electromagnetic fields, η is the intrinsic impedance of the material filling the waveguide. For air filling, η equals 377 Q. K and β are the wavenumber and propagation constant of the waveguide. The complex frequency shift can separate into real and imaginary parts as[15]:

$$\frac{\delta\omega}{\omega} = -\frac{(f_s - f_0)}{f_s} + \frac{j}{2}\left[\frac{1}{Q_s} - \frac{1}{Q_0}\right]$$

Where f_0 and Q_0 are the resonance frequency and Q-factor of the cavity without sample inserted, and $f_s$and Q_s, are the resonance frequency and Q-factor of the cavity with sample inserted, respectively. If the perturbation condition is satisfied, we can assume $E = E_0$, $H = H_0$. After performing integration and rearranging, the real part and imaginary part of the complex permittivity can be calculated as[16]:

$$\varepsilon' = \frac{(f_0 - f_s)}{2f_s} + 1$$

$$\varepsilon'' = \frac{V_c}{4V_s}\left(\frac{1}{Q_s} - \frac{1}{Q_0}\right)$$

Experiment

In this work, dielectric properties analyses were carried out on a cyl-ε cavity[17] (See Figure 2.5). TM_{010} modes were used to measure the dielectric properties of a tube sample placed on the axis. f_0 and Q_0 were measured with an empty tube, and $f_s$and Q_s were recorded with samples

insert. The real part and imaginary part of the complex permittivity were calculated by the equations introduced in the theory part.

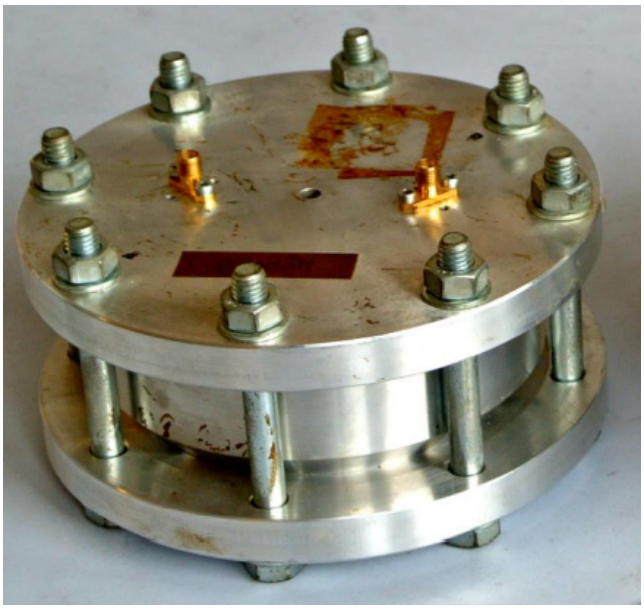

Figure 2.6 cyl-ε cavity used for microwave cavity perturbation analysis [17]

References

1. Wildberger, M. D., Grunwaldt, J. D., Maciejewski, M., Mallat, T. & Baiker, A. Sol-gel bismuth-molybdenum-titanium mixed oxides I. Preparation and structural properties. *Applied Catalysis A: General* **175**, 11–19 (1998).

2. Schuh, K. *et al.* Selective oxidation of propylene to acrolein by hydrothermally synthesized bismuth molybdates. *Applied Catalysis A: General* **482**, 145–156 (2014).

3. Zhai, Z., Wang, X., Licht, R. & Bell, A. T. Selective oxidation and oxidative dehydrogenation of hydrocarbons on bismuth vanadium molybdenum oxide. *Journal of Catalysis* **325**, 87–100 (2015).

4. Clark, N. *Microwave Methods for Additive Layer Manufacturing*. (2017).

5. Sparkman, O. D., Penton, Z. & Kitson, F. G. Gas Chromatography and Mass Spectrometry: A Practical Guide. *Gas Chromatography and Mass Spectrometry: A Practical Guide* (2011)

6. Niemantsverdriet, J. W. Spectroscopy in Catalysis: An Introduction: Third Edition. *Spectroscopy in Catalysis: An Introduction: Third Edition* 1–325 (2007)

7. Patterson, A. L. The Scherrer Formula for X-Ray Particle Size Determination. *Physical Review* **56**, 978 (1939).

8. Ferraro, J. R., Nakamoto, K. & Brown, C. W. Introductory Raman Spectroscopy: Second Edition. *Introductory Raman Spectroscopy: Second Edition* 1–434 (2003)

9. Vandenabeele, P. Practical Raman Spectroscopy - An Introduction. *Practical Raman Spectroscopy - An Introduction* (2013) doi:10.1002/9781119961284.

10. Naderi, M. Chapter Fourteen Surface Area Brunauer–Emmett–Teller (BET). *Progress in Filtration and Separation* 585–608 (2015) doi:10.1016/B978-0-12-384746-1.00014-8.

11. Hollander, J. M. *et al.* X-ray photoelectron spectroscopy. *Accounts of Chemical Research* **3**, 193–200 (2002).

12. Seyama, H., Soma, M. & Theng, B. K. G. X-Ray Photoelectron Spectroscopy. *Developments in Clay Science* **5**, 161–176 (2013).

13. Wilschefski, S. C. & Baxter, M. R. Inductively Coupled Plasma Mass Spectrometry: Introduction to Analytical Aspects. *The Clinical Biochemist Reviews* **40**, 115 (2019).

14. Nelms, S. M. Inductively Coupled Plasma Mass Spectrometry Handbook. *Inductively Coupled Plasma Mass Spectrometry Handbook* 1–485 (2009)

15. Waldron, R. A. Perturbation theory of resonant cavities. *Proceedings of the IEE Part C: Monographs* **107**, 272 (1960).

16. Cavity Perturbation Techniques for Measuring Dielectric Parameters of Water and Other Allied Liquids - Mathew - 2000 - Sensors Update - Wiley Online Library. https://onlinelibrary.wiley.com/doi/10.1002/1616-8984(200001)7:1%3C185::AID-SEUP185%3E3.0.CO;2-U.

17. Cuenca, J. A. Characterisation of Powders Using Microwave Cavity Perturbation. (2015).

3 Microwave-assisted Catalysis: A Feasibility Study on Propene Selective Oxidation

3.1 Aims

As mentioned in the introduction in Chapter 1, 'Microwave-assisted' is not a new research area, and it has been widely investigated in different fields of chemistry, especially organic synthesis using polar solvents [1] and solid material treatment [2–4]. In contrast, as the physical properties of gases are different from liquids and solids, gas-phase reactants are difficult to heat or activate directly using microwave radiation. Therefore, the research on microwave-assisted chemical processes in the gas phase is still rare. In this chapter, a feasibility study of microwave-assisted gas-solid phase heterogeneous catalysis will be introduced. This study is based on the selective oxidation of propene.

3.2 Microwave Heating

The energy conversion in the microwave cavity depends upon the type of interaction with the target materials. The processing of material using microwaves depends on its dielectric and magnetic properties as the electric field and magnetic field components interact with the media during irradiation. These mechanisms are responsible for the commonly known forms of heating such as dielectric, Joule, and induction heating, all of which are dependent on the electromagnetic field characteristics and the material's properties[5].

The power absorbed by a material is significantly influenced by the depth up to which the radiations penetrate it. If the size of a material is much higher than the penetration depth, only

surface will be heated by microwave and rest of the material will be heated by conduction. Thus, microwaves cannot penetrate inside in a similar fashion in all materials. Microwave penetration inside a non-metallic material is defined in terms of 'Penetration Depth' (the distance from the surface of the material at which the magnitude of field strength drops by a factor of $\frac{1}{e}$), which is expressed mathematically as [6]:

$$D_p = \frac{1}{\omega\sqrt{0.5\mu_0\mu''\varepsilon_0\varepsilon''[\sqrt{1+(\frac{\varepsilon''_{eff}}{\varepsilon'})^2}-]}}$$

Where ω =2 πf (Hz); f is frequency of the incident microwaves, μ_0 is the magnetic permeability of air, $\mu''$is the imaginary component of the magnetic permeability and is known as the magnetic loss factor. Similarly, ε_0 is the dielectric permittivity of air, $\varepsilon'$is the real component of the dielectric permittivity, ε'' is the imaginary component of the dielectric permittivity and is known as the dielectric loss factor, ε''_{eff} and is the effective dielectric loss factor.

In the case of metals, the microwave penetration inside the bulk is almost negligible in normal conditions. Consequently, the corresponding depth is termed as 'Skin Depth' and is defined as[6]:

$$D_s = \frac{1}{\sqrt{\pi f\mu\sigma}} = 0.029(\rho\lambda_0)^{0.5}$$

where σ is the electrical conductivity, ρ is electrical resistivity, f is frequency, and λ_0 is the incident wavelength. Although the skin depth is very small in metallic materials, most of the metallic particle dimensions in catalytic processes are comparable with skin depth. The

theoretical limitation on metallic powder size for uniform volumetric heating while processing with 2.45 GHz microwave radiation was found to be less than 100 μm[6].

It is thus imperative that the power absorbed during microwave irradiation depends on the electromagnetic characteristics and the thickness of the target material. In the case of thin sections of magnetic materials, the absorbed power, P, per unit volume (W m^3) of material can be estimated as [5]:

$$P = 2\pi f \varepsilon_0 \varepsilon'' E_{rms}^2 + 2\pi f \mu_0 \mu'' H_{rms}^2$$

where E_{rms} is the root mean square of the electric field and H_{rms} is the root mean square of the magnetic field.

As a single-mode cavity (which had been introduced in Chapter 2) is used in this project, the focus is on the heating mechanism of electric field components in microwaves. Power absorption from magnetic components can be neglected and absorbed power per unit volume can be reduced to a single term:

$$P = 2\pi f \varepsilon_0 \varepsilon'' E_{rms}^2$$

The loss tangent (tanδ) is frequently used in dielectric heating literature providing indications of how the material can be penetrated by an electric field and how it dissipates the energy in heat. Therefore, a material with a high loss factor is easily heated by microwave. The tanδ can be calculated as[7]:

$$tan\delta = \frac{\varepsilon''}{\varepsilon_0}$$

3.3 Heating Mechanism on Different Type of Media

To make the mechanism of microwave heating easier to understand, different media are firstly classified into four different general categories:

1. Free Space: Free space is defined as a perfect vacuum or, at microwave frequencies, air. No magnitude decreases on EM waves, in another words, there is no energy loss.
2. Lossless Dielectric: In a lossless dielectric medium the conductivity can be assumed approximately zero. No energy conversion when an EM wave passes through.
3. Lossy Dielectric: A lossy dielectric medium is defined as a medium in which the electric conductivity is not equal to zero, yet it is not a good conductor. If an EM wave penetrates the medium (whether the EM wave can penetrate depends on the frequency of the EM wave), there is reduction in EM intensity, and energy can be converted in to heat.
4. Good Conductor: Good conductors, such as metals, are characterized by extremely large electric conductivities. In this situation, EM wave is hard to penetrate the good conductor.

Only lossy dielectric materials can convert microwave radiation into heat, so these materials are needed to initiate a catalytic reaction. When the microwaves penetrate a lossy dielectric material, the electric and magnetic field components can interact with the material, agitating the orientation of the dipoles, causing free-electron movements, changing the position of domain walls and also causing electron spin. One or a combination of these phenomena occur during the interaction. However, if we are interested in the heating of the inorganic catalysts, the effective mechanisms are the changes in dipole orientation, free-electron movement and the position of electric domain walls.

3.3.1 Loss caused by dipole orientation (Dipolar Loss)

The dipolar loss is more effective in dielectric insulator materials in which dipoles are generated when exposed to an external electric field. These materials include water, ceramics, ceramic matrix composite (CMC), precious metal clay (PMC), food products.

The oscillating electric field creates agitation of the molecular dipoles during the processing of these materials as shown in Figure 3.1.

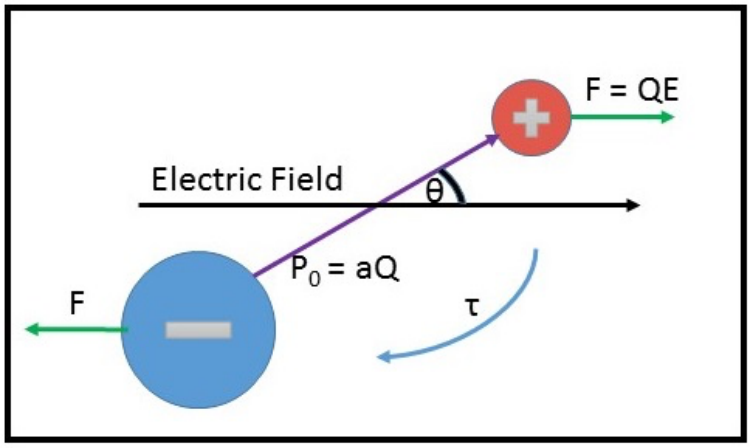

Figure 3.1 The effect of an electric field on a typical dipolar molecule[8]

P_0 symbolizes the dipole moment, a is the distance away from the body centre of the molecule, and F is the force, which is the charge, Q, multiplied by the electric field, E. Under a high-frequency electric field, the inertial, elastic, frictional and molecular interaction forces in the materials resist the frequent changes in orientation of the molecules. Thus, the dipoles do not have sufficient time to respond to the oscillating field, because of this phase lag, they collide with each other when they attempt to follow the field, and as a result, power is dissipated to cause the volumetric heating within a short time.

3.3.2 Loss caused by free electrons movement (Conduction Loss)

In the case of dielectric solid materials with charged particles that are free to move in a delimited region of the material, the mobile charge carriers (electrons, ions, etc.) will move back and forth in a delimited region of the material under the influence of the microwave E-field, creating an electric current. As the electrons cannot couple to the changes of the phase of the electric field, energy is dissipated in the form of heat due to the Interfacial or Maxwell-Wagner polarization effect.

For the pure metals, metallic based materials and semiconductors e.g. Cu, Al, Si, Fe, Ni, and metal matrix composites (MMC), the conductivity of these materials is high; consequently, the field gets attenuated rapidly inside the material which induces large current (I_i), the free electrons which starts movement in the direction of external electric field E with velocity v. Hence, an induced magnetic field (H_i) is developed in the opposite direction of external magnetic field inside the material. The induced magnetic field generates a force on moving electrons that pushes conducting electrons in reverse direction with velocity v_r. Therefore, a kinetic energy is imparted to the electrons and movement of the electron is restricted by the inertial, elastic, frictional and molecular interaction forces. The oscillating electric field repeats this phenomenon rapidly which generates volumetric and uniform heating inside the material[6].

3.4 Heat Transfer in Microwave-assisted Heterogeneous Catalytic Process

Unlike the conventional heating process which applies energy only to the outside of the material, microwaves work directly to heat a material from the inside out. The microwave heating occurs nearly instantaneously and so is very fast.

For a heterogeneous catalytic system, in a conventional heating process, thermal energy is transferred to the catalyst particles through convection, conduction and radiation of external heat from the outer surfaces of a container into the host material itself. In contrast, as discussed above, in a microwave heating process, microwave energy is delivered directly to the microwave-absorbing/microwave-receptive/component through molecular interactions or conduction–electron interactions with the electromagnetic field. Heat transfer by conventional heating is time-dependent, developing thermal gradients. However, in microwave heating, electromagnetic energy is directly transferred, and heat is instead generated, to microwave absorbing matter within the sample by electromagnetic coupling through a variety of charge-dynamical processes.

3.5 Screening Tests

3.5.1 What Kind of Materials can be Good Catalysts for Gas-Phase Microwave-assisted Heterogeneous Catalysis?

Before trying to answer the final question, we should first investigate some basic questions.

What is the Evaluation Criteria for Good Catalysts?

This question had been answered in the Section 1.2.4, which can be summarised into these 4 points:

1. Inexpensive.
2. Stable during reaction.
3. Enables high rates of chemical production.
4. High surface area

Will a good catalyst under conventional heating also be a good microwave-assisted catalyst?

Energy is indispensable in a catalytic process to drive the reactions. For a gas phase microwave-assisted heterogeneous reaction, the only way to obtain energy is the catalyst absorbing the energy in the microwave. As introduced in Section 2.2.1, not all kinds of materials can be easily heated by the microwave, and so not all conventional catalysts will work well under microwave heating.

What kinds of catalysts could be effective in our single-mode cavity?

As introduced in Section 2.2, the catalyst heated in the single-mode cavity is using the electric field part of the microwave radiation to gain energy. Therefore, the following 4 types of materials are promising to investigate.

1. Absorbing dielectric materials.
2. Carbon materials.
3. Supported metal catalyst.
4. Mixed metal oxide materials with an irregular electric domain.

A good catalyst for microwave-assisted heterogeneous should not only conform to the properties of being a good traditional catalyst but also have the ability to absorb and convert the microwave energy into heat. In the following section, some candidate catalysts will be introduced.

3.5.2 Screening Experiments

To gain a clearer and better understanding of the differences between the conventional and microwave-assisted heterogeneous catalysis in the gas phase, a series of comparison experiments were designed. In this stage, nickel-based supported catalysts and bismuth oxide-

based mixed metal oxide materials which are proved to have good dielectric properties, were chosen to be screened. Nickel-based supported catalysts were made by the impregnation method and the nickel loading is 5%. By this method, a larger nickel partial than the common conventional supported catalysts can be synthesized, which is comparable to the skin depth of the nickel partical[6] and can effectively absorb the microwave power. The bismuth-based mix metal oxide was made by hydrothermal method (HT) and sol-gel method based on the citric acid complexation (CA). These two method can produce pure phase of bismuth-based mix metal oxide. The detailed synthesised processes were introduced in Section 2.3.

In this section, two groups of catalysts will be tested under conventional heating and microwave-assisted conditions. At the same time, some of their properties and characteristics are also characterized.

Bismuth Based Mixed Metal Oxide

The bismuth-based metal oxides synthesized by two methods were used in the selective oxidation of propene under the traditional conditions of 400 °C and under the conditions of 25 W microwave, respectively. The experimental results, as well as the specific surface area and dielectric parameters of each sample are shown in Table 3.1.

Table 3.1 BET surface area, dielectric loss tangent and catalysts performance of bismuth mixed oxide catalysts under conventional and microwave heating. (Reaction conditions : 0.2 g of catalyst, propene:oxygen:nitrogen = 1:2:97, flow rate = 50 mL min^{-1})

Catalysts	BET Specific surface area /m^2 g^{-1})	Dielectric constant	Loss tangent	Conventional tests (400 ˚C)		Microwave test 25 W		
				Propene conversion	Acrolein selectivity	Temperature of catalyst at 25W /˚C (Measured separately)	Propene conversion	Acrolein selectivity
Bi_2MoO_6 HT	17	1.0012	0.0560	5%	24%	490	82%	1%
Bi_2MoO_6 CA	8	1.0013	0.0483	35%	61%	389	29%	69%
$Bi_2Mo_2O_9$ CA	6	1.0009	0.0174	11%	89%	120	3%	0%
$Bi_2Mo_3O_{12}$ CA	8	1.0001	0.0133	16%	87%	105	2%	0%
$BiVO_4$-HT	24	1.0010	0.0324	13%	24%	397	23%	49%
$BiVO_4$-CA	17	1.0013	0.0283	10%	21%	345	17%	45%
$Bi_4Ti_3O_{12}$-HT	9	1.0013	0.0494	20%	1%	377	86%	2%
$BiFeO_3$-HT	81	1.0011	0.1111	17%	1%	364	26%	0%

Based on the results, most of the bismuth-based mixed metal oxides (except the α-$Bi_2Mo_3O_{12}$ and β-$Bi_2Mo_2O_9$) have good ability to be heated and can convert propene under microwave-assisted conditions. Under conventional heating, among the 8 samples the bismuth molybdate catalysts led to both higher propene conversion and higher acrolein selectivity, while under the microwave condition, $Bi_2Mo_3O_{12}$ and $Bi_2Mo_2O_9$ cannot be well heated and Bi_2MoO_6 performed intermediately, and $BiVO_4$ samples also performed well in both propene conversion and acrolein selectivity.

According to the result of the conventional experiment, bismuth molybdate samples were better than other bismuth-based materials. The three bismuth molybdate samples synthesized by the citric acid complexation method all performed excellently in producing acrolein under conventional heating. However, under microwave-assisted conditions, only γ-Bi_2MoO_6 can be heated by the microwave and showed good catalytic activity in the microwave test among the three different phases of bismuth molybdate samples. Both α-$Bi_2Mo_3O_{12}$ and β-$Bi_2Mo_2O_9$ cannot be well heated and hence did not show good activity in the microwave as the temperature was not sufficient for them to be activated. This is due to the differences in the dielectric properties of the different bismuth molybdate samples. As had been introduced in Section 3.2, the loss tangent is an indicator of how efficient the material can convert the microwave energy into heat. Both α-$Bi_2Mo_3O_{12}$ and β-$Bi_2Mo_2O_9$ have very low loss tangents (3 times lower than γ-Bi_2MoO_6) and hance only have limited ability to convert the energy in the microwave to heat. The three samples are all bismuth molybdate materials and are prepared by the same synthesis method, but different molybdenum-bismuth ratios will lead to different structures of the materials, which will cause them to have different dielectric characters[9].

$BiFeO_3$ and $Bi_4Ti_3O_{12}$ are both have relatively high loss tangents, and can also be well heated by microwave, which means that they are both good candidates for microwave-assisted heterogeneous catalysis studies. However, as they are not selective to the acrolein in propene

oxidation even with low conversion in both conventional and microwave-assisted tests, they are not suitable for use in the selective oxidation of propene to acrolein, and cracking reaction is more favourable on these catalyst. It can be seen that in addition to the ability to be heated, a promising candidate must also have a good catalytic ability to the target products in terms of catalysis.

Among all candidates, $BiVO_4$ and γ-Bi_2MoO_6 are two of the best samples for investigating microwave-assisted selective oxidation, as they performed well in both heating ability and catalytic performance. The detailed studies based on these two materials will be introduced in Chapters 4 and 5. The hydrothermally synthesized samples seem to be better in the microwave tests. A more detailed explanation of hydrothermally synthesized samples will be shown in Chapter 4.

3.1.1 Nickel-Based Supported Catalyst

The nickel-based supported catalysts were used in the selective oxidation of propene under the traditional conditions of 400 °C and the conditions of 25 W microwave (under these conditions, the propene can be well converted), respectively. The experimental results as well as the specific surface area and dielectric parameters of each sample are shown in the Table 3.2.

As shown in Table 3.2, the common support materials TiO_2 SiO_2 and Al_2O_3 all have very low loss tangents, which indicated that they are not good at converting microwave energy into heat and the temperatures reached under 25 W microwave power were low, at 198 °C, 179 °C, 149 °C, respectively. Adding nickel nanoparticles to these materials can largely increase the loss tangent and improve their ability to be heated under microwave conditions. After loading nickel, a large enhancement of the catalyst bed temperature under 25 W microwave condition was observed, with 443 °C, 261 °C, and 295 °C reached by TiO_2 SiO_2 and Al_2O_3 supported

nickel catalysts, respectively. Here, two hypotheses can be made as to why the sample is more easily heated after addition of nickel. In the first case, nickel forms particles of suitable size comparable to the skin depth of nickel (see Section 3.2) on the surface of the support material. Usually for metallic nickel catalysts, an oxide layer will form on the surface of nickel particles, which hinders the conduction between particles. In this hypothesis, eddy currents form inside metal particles and cause thermoelectric losses. In this possible procedure only nickel particles will be heated, which is much more energy-efficient than the traditional catalytic process.

The second hypothesis is that nickel binds to the support surface to form new structures with different dielectric properties. Taking TiO_2 as an example, the process of loading nickel and reducing it involves high-temperature calcination and reduction. Under the flow of hydrogen, the surface of TiO_2 will form defects at high temperatures. At this point, nickel binds to its surface and $NiTiO_3$ can form[10], which has been shown to have good dielectric properties in the microwave[11–13]. Due to the constraints and lack of time caused by the impact of the Covid-19 epidemic, no further research has been carried out to investigate these hypotheses.

In terms of the catalytic performance, these three samples performed quite differently both under conventional heating and microwave heating. In the conventional heating test, the Ni-TiO_2 was more likely to crack the propene to produce CH_4 and C_2H_4 and C_6H_6. However, over the Ni-SiO_2 and Ni-Al_2O_3, the propene was more likely to be oxidized and the products include acetaldehyde, acrolein, acetone and carbon oxides. Although in the microwave test, the catalyst bed temperature of TiO_2 SiO_2 and Al_2O_3 supported nickel catalysts are lower than 400 °C, their performance, both in terms of propene conversion and selectivity to the products, was comparable with the conventional test at 400 °C.

Table 3.2 BET surface area, dielectric loss tangent and catalysts performance of nickel-based supported catalysts under conventional and microwave heating. (Reaction conditions： 0.2 g of catalyst, propene:oxygen:nitrogen = 1:2:97, flow rate = 50 mL min^{-1}).

Catalysts	Specific surface area (m^2/g)	Dielectric constant	Loss tangent (Catalyst)	Loss tangent (Support)	Conventional tests (400 ˚C)		Microwave tests (25 W)			
					Propene conversion	Acrolein selectivity	Temperature of support at 25 W /˚C(measured separately)	Temperature of catalyst at 25 W /˚C	Propene conversion	Acrolein selectivity
Ni/TiO_2	152	1.0015	0.0324	0.005	100%	0%	198	443	100%	0%
Ni/SiO_2	208	1.0007	0.0841	0.019	13%	15%	179	261	12%	10%
Ni/Al_2O_3	155	1.0008	0.0470	0.021	33%	3%	149	295	11%	4%
Ni/active carbon(Norit rox 0.8)	754	1.0004	7.1254	7.092	58%	5%	311	307	16%	8%
Ni/SiC	2	1.0003	0.2303	0.201	18%	0%	559	540	100%	0%
$Ni/BaTiO_3$	15	1.0002	0.0751	0.0780	22%	0%	540	535	100%	0%

Absorbing supports like activated carbon, SiC and $BaTiO_3$ usually have large values of loss tangent, and when applied for the microwave-assisted reactions, they all showed a very good heating effect. Nickel catalysts supported on SiC and $BaTiO_3$ are very active in microwave-assisted tests and give much higher conversion than conventional heating. This phenomenon provides insight for the subsequent design of catalysts. Combining the advantages of catalysts in traditional catalytic processes with these materials that heat well in microwave fields may yield promising results in microwave-assisted catalysis. The detailed studies based on this idea will be introduced in Chapter 6.

3.6 Conclusion

This Chapter focused on introducing the feasibility of microwave-assisted heterogeneous catalysis and screening potential catalysts for the selective oxidation of propene in a microwave-assisted heterogeneous catalytic process. Two groups of comparing experiments based on bismuth-based mix metal oxide and supported nickel catalysts were carried out.

Among the bismuth-based metal oxides, $BiVO_4$ and γ-Bi_2MoO_6 are two of the most promising samples for investigating microwave-assisted selective oxidation, and more detailed studies related to these two materials will be introduced in Chapter 4 and Chapter 5.

Loading metallic nickel on a common microwave-inert support material can improve the overall microwave usage capability of the samples. Also, the absorbing supports like SiC and $BaTiO_3$ can be effectively heated under microwave conditions, and it can be applied in the microwave-assisted processes by combining with various conventionally active components. The detailed studies based on this idea will be introduced in Chapter 6.

References

1. Kappe, C. O. Microwave dielectric heating in synthetic organic chemistry. *Chemical Society Reviews* **37**, 1127–1139 (2008).

2. Sutton, W. H. *Microwave processing of materials*. *MRS Bulletin* vol. 18 (National Academies Press, 1993).

3. Al-Harahsheh, M. & Kingman, S. W. Microwave-assisted leaching - A review. *Hydrometallurgy* **73**, 189–203 (2004).

4. Kingman, S. W. & Rowson, N. A. Microwave treatment of minerals - A review. *Minerals Engineering* **11**, 1081–1087 (1998).

5. Mello, P. A., Barin, J. S. & Guarnieri, R. A. *Microwave Heating*. *Microwave-Assisted Sample Preparation for Trace Element Determination* (Elsevier, 2014).

6. Mishra, R. R. & Sharma, A. K. Microwave-material interaction phenomena: Heating mechanisms, challenges and opportunities in material processing. *Composites Part A: Applied Science and Manufacturing* **81**, 78–97 (2016).

7. Barba, A. A. & d'Amore, M. Relevance of Dielectric Properties in Microwave Assisted Processes. *Microwave Materials Characterization* (2012)

8. Omran, A. Semiconductors and Dielectrics Introduced by : (2020).

9. Ohsato, H., Varghese, J. & Jantunen, H. Dielectric Losses of Microwave Ceramics Based on Crystal Structure. *Electromagnetic Materials and Devices* (2018)

10. Ganesh, I. *et al.* Preparation and Characterization of Ni-Doped TiO_2 Materials for Photocurrent and Photocatalytic Applications. *The Scientific World Journal* **2012**, (2012).

11. Anjana, P. S. & Sebastian, M. T. Synthesis, characterization, and microwave dielectric properties of $ATiO_3$ (A = Co, Mn, Ni) ceramics. *Journal of the American Ceramic Society* **89**, 2114–2117 (2006).

12. Pavithra, C. & Madhuri, W. Electrical and magnetic properties of $NiTiO_3$ nanoparticles synthesized by the sol–gel synthesis method and microwave sintering. *Journal of Materials Research and Technology* **8**, 3097–3101 (2019).

13. Anjana, P. S., Sebastian, M. T., Axelsson, A. K. & Alford, N. M. N. Microwave dielectric properties of CeO_2-0.5AO-0.5TiO_2 (A = Ca, Mg, Zn, Mn, Co, Ni, W) ceramics. *Journal of the European Ceramic Society* **27**, 3445–3452 (2007).

4 Microwave-assisted Catalysis: Propene Selective Oxidation by Hydrothermally Synthesized Bismuth Molybdate

4.1 Introduction

4.1.1 Aims

The aim of this chapter was to investigate the hydrothermally synthesized bismuth molybdate as a catalyst for the propene selective oxidation in the single-mode microwave cavity. In Chapter 3, gamma phase bismuth molybdate (γ-Bi_2MoO_6) was shown to be an effective catalyst under microwave heating, and hydrothermally synthesized samples performed better than other samples made by different procedures. Therefore, in this chapter, different γ-Bi_2MoO_6 catalysts made by hydrothermal method were investigated in both conventional and microwave conditions. The pH of precursor solution and calcination conditions were the two main factors that were investigated.

4.1.2 Introduction of Hydrothermal Synthesized Bismuth Molybdate

The most common method to prepare bismuth molybdate catalysts is co-precipitation[1], but also solid-state routes[2], sol-gel synthesis[3], and spray drying of aqueous solutions have been used. All these methods require heating or calcination of the precursor at temperatures over 500 °C, which may result in a decrease in the catalytic performance of the resulting phase due to bismuth enrichment of the catalyst surface[4]. Recently, mild hydrothermal techniques were applied to produce γ-Bi_2MoO_6 by Schuh and coworkers for the selective oxidation of propylene to acrolein [5] and reported that hydrothermally synthesized catalysts

were more selective at comparable propene conversions than co-precipitated γ-Bi_2MoO_6. Schuh and coworkers also found that the pH value of the precursor solution used in the synthesis had a strong influence on crystalline phases, specific surface area, bulk and surface composition, all of these factors can influence the catalytic performance [6]. Hydrothermal synthesis, which can produce advanced materials of high purity, controlled morphology, high crystallinity and good reproducibility can also be used to prepare α-$Bi_2Mo_3O_{12}$ and γ-Bi_2MoO_6, and most hydrothermally synthesized samples can reach a good specific surface area (>20 m^2/g)[7,8].

4.2 Characterization

4.2.1 XRD

The hydrothermal materials were synthesised by reacting aqueous solutions of bismuth nitrate and sodium molybdate in a stainless-steel autoclave at 160 °C at different pH. The XRD patterns of the materials before and after calcination is shown in Figure 4.1.

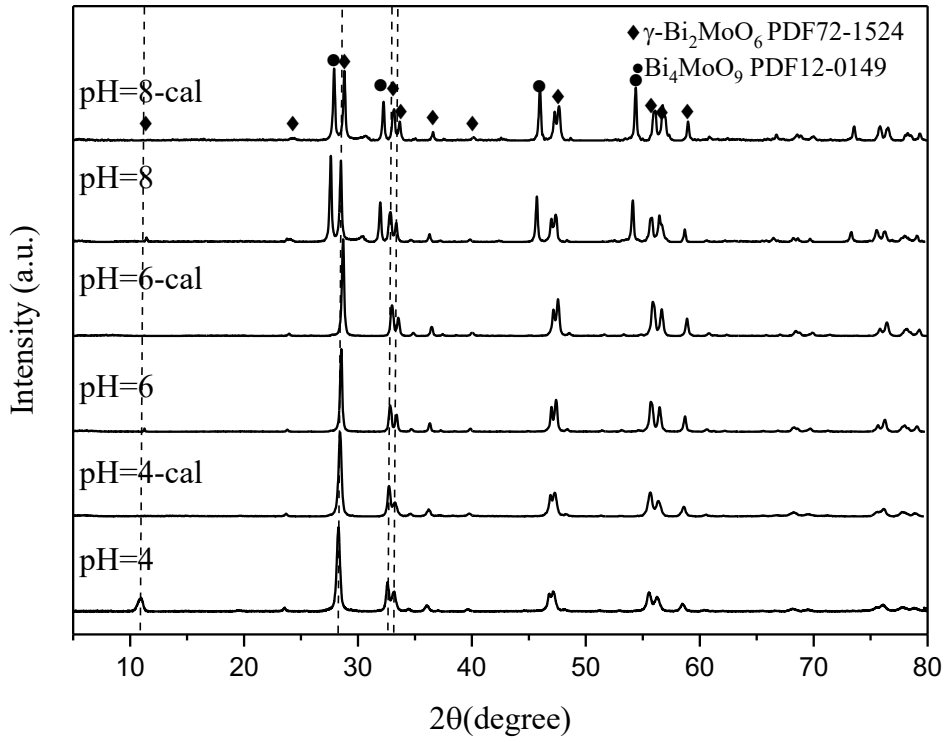

Figure 4.1 XRD patterns of bismuth molybdate materials hydrothermally synthesized at different pH

The XRD patterns revealed that a lower solution pH value contributes to the formation of orthorhombic Bi_2MoO_6 structure, while the higher pH value contributes to a mixed phase of orthorhombic Bi_2MoO_6 and cubic Bi_4MoO_9 structures. This result is similar to the findings of Phuruangrat and coworkers [7] who synthesized a group of Bi_2MoO_6 by a hydrothermal reaction and investigated the pH effect of the precursor solutions on the phases formed, morphologies, and photocatalytic activity. They illustrated that low pH (<7) contributes to the formation of orthorhombic Bi_2MoO_6 structure, medium pH (8-10) to mixed phase of orthorhombic Bi_2MoO_6 and cubic Bi_4MoO_9 structures and high pH (>10) to the formation of cubic Bi_4MoO_9.

Table 4.1 Relative intensities of Bi_2MoO_6 reflections of samples synthesised at different pH from the XRD patterns in Figure 4.1.

Sample	**(020)**	**(131)**	**(002)**	**(200)**
pH=4	12.8	100	35.1	23.8
pH=4-cal	0	100	36.6	16.5
pH=6	3.9	100	31.8	24
pH=6-cal	0	100	32.7	18.8
pH=8	3.16	100	34.7	25.8
pH=8-cal	0	100	39.2	22.3

XRD patterns also indicated that there were large differences in the relative intensities based on the (020), (131), (200), (002), and (060) peaks for the samples, indicating the possibility of different preferential orientation growth under different pH values. Intensities of the (020) refelection are much lower than those of the standard, indicating the inhibition of crystalline growth along the [010] direction with the formation of 2D plate-like materials. This result is in line with the characterization results reported by Phuruangrat and co-workers on the hydrothermally synthesized Bi_2MoO_6 in 2013 [7].

It should be noted that the XRD patterns of the sample pH=6 and pH=8 show shifts in the Bi_2MoO_6 characteristic peaks (See Figure 4.1) towards a higher scattering angle. Similar results were also reported by Bakiro and co-workers when synthesising $BiNbO_4$[9] by hydrothermal methods in different pH precursor solutions. They suggested that the shift in the peak can be attributed to the change in the phase composition associated with increasing the pH. According to their suggestion, the lower crystallite size of Bi_2MoO_6 at pH=4 may be attributed to the interactions between an acid and precursor solution that prevents coalescence of the nano-crystallites and inhibit particle growth. On the other hand, a different effect occurs when pH is

increased by introducing base in the precursor solution enhancing the formation of Bi_4MoO_9 which causes excess compressive stress on the crystalline lattice.

Table 4.2 Crystallite size and lattice constants for samples synthesised at different pH calculated from the (131) reflection of Bi_2MoO_6 and (111) reflection of Bi_4MoO_9 from the XRD patterns in Figure 4.1.

Samples	**Crystallite Size (Å)**	**Lattice Constants**							
			a	*b*	*c*	*α*	*β*	*γ*	Vol.
pH=4	226	Orthorhombic Bi_2MoO_6	5.54	16.23	5.50	90	90	90	494
pH=6	337	Orthorhombic Bi_2MoO_6	5.50	16.34	5.47	90	90	90	492
pH=8	456	Orthorhombic Bi_2MoO_6	5.49	16.20	5.48	90	90	90	488
		Cubic Bi_4MoO_9	5.63	5.63	5.63	90	90	90	179
pH=4-cal	251	Orthorhombic Bi_2MoO_6	5.50	16.20	5.46	90	90	90	488
pH=6-cal	366	Orthorhombic Bi_2MoO_6	5.50	16.29	5.47	90	90	90	491
pH=8-cal	467	Orthorhombic Bi_2MoO_6	5.48	16.20	5.46	90	90	90	487
		Cubic Bi_4MoO_9	5.63	5.63	5.63	90	90	90	179

The average crystallite size was calculated using Debye–Scherrer equation considering the broadening of the (131) reflection of Bi_2MoO_6 and (111) reflection of Bi_4MoO_9 from the XRD patterns and calculated results are tabulated in Table 4.2. The powders showed an increase in the crystallite size with an increase in the pH of the reaction mixture. Similar results were also found by Bakiro and co-workers when synthesising $BiNbO_4$[9]. They reported that high pH is

attributed to the increase crystallite size due to the agglomeration resulting in the preferred β-$BiNbO_4$ formation on the expense of stability of the α-$BiNbO_4$ at high pH. In Phuruangrat's studies of Bi_2MoO_6 synthesis, a similar conclusion was also reported, with acidic conditions favouring the formation of Bi_2MoO_6, and alkaline conditions leading to larger crystallite sizes of Bi_2MoO_6 and the formation of Bi_4MoO_9 [7].

4.2.2 Raman Spectroscopy

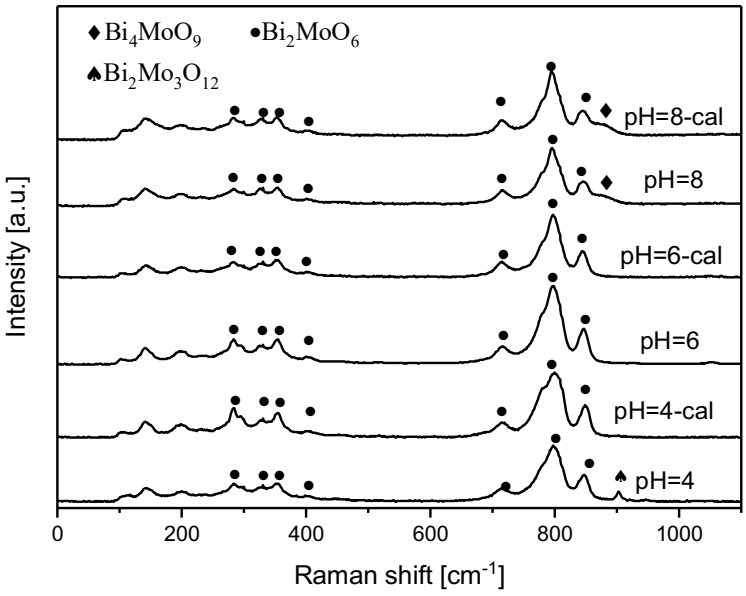

Figure 4.2 Raman spectra of bismuth molybdate materials hydrothermally synthesized at different pH

All spectra contain most of the characteristic bands of γ-Bi_2MoO_6. The modes below 180 cm^{-1} could be the translation of molybdenum and bismuth atoms. The vibration peak at 144 cm^{-1}, specified as the lattice model of Bi^{3+} atoms, was mainly in the direction normal to the layers. It is well known that the peaks in the 180–500 cm^{-1} range originated from bending modes of

the MoO_6 octahedrons coupled with stretching and bending modes of the bismuth-oxygen polyhedrons. The intense Raman modes near 290 cm^{-1} seemed to be from the E_g bending vibrations. Those at 325, 340, and 401 cm^{-1} corresponded to the E_u symmetric bending. The mode at 712 cm^{-1}, was specified as the asymmetric stretching vibration (E_u mode) of the MoO_6 octahedrons involving the motion of equatorial oxygen atoms joining the MoO_6 octahedrons within the layers. The Raman vibrations at 795 cm^{-1} (A_{1g} mode) and 849 cm^{-1} (A_{2u} mode) were, respectively, assigned to the symmetric and asymmetric stretching vibrations of the MoO_6 octahedrons involving the motion of apical oxygen atoms, normally directed to the $(Bi_2O_2)^{2+}$.[7,10,11].

Samples pH=6, pH=6-cal and pH=4-cal seemed to be in higher purity of γ-Bi_2MoO_6 than other samples, as their spectra do not contain other characteristic bands. The peak at 901 cm^{-1} in the spectra of pH=4 can be recognized as Mo-O vibration in $Bi_2Mo_3O_{12}$[8,12],which was not seen in XRD. The peak at around 880 in the spectra of pH=8 and pH=8-cal are the characteristic bands of Bi_4MoO_9[13], and this was consistent with the results of XRD.

4.2.3 BET, XPS and ICP-MS

BET surface areas were determined by N_2 adsorption, surface bismuth and molybdenum composition were conducted using X-ray photoelectron spectrometer (XPS) and the bulk composition of the catalysts was determined by optical emission spectrometry with inductively coupled plasma (ICP-MS). The specific surface area of samples and Bi/Mo ratios determined by ICP-OES and XPS are summarized in Table 4.3.

Table 4.3 Surface area and composition of the bismuth molybdate materials hydrothermally synthesized at different pH

Sample	BET surface area (m^2/g)	Bi/Mo ratio in bulk	Bi/Mo ratio on the surface
pH=4	16	2.1	2.1
pH=6	17	2.2	2.4
pH=8	25	3.2	3.8
pH=4-cal	14	2.1	2.4
pH=6-cal	14	2.2	2.5
pH=8-cal	19	3.3	4.0

According to the results in Table 4.3, samples that have not been calcined have a larger specific surface area compared with their calcined counterpart. The subsequent decline in the surface area upon thermal treatment at a higher temperature could be due to the increase in crystallite size, which is consistent with the XRD results (Table 3.1).

Samples synthesized in the solution with a higher pH value contains a larger amount of Bi both in the bulk and on the surface. This is in line with the XRD results in Section 3.2.1, which showed that large amounts of Bi rich phase Bi_4MoO_9 was produced by the higher pH value precursor solution. Further evidence was also provided by Raman results illustrated in Section 3.2.2. Higher pH value precursor solution enhances the formation of Bi_4MoO_9. A similar result was also reported by Schuh and co-workers, who synthesized a group of bismuth molybdate from solutions with various pH by hydrothermal method [6]. The calcination did not have a significant effect on the Bi/Mo ratio of the catalyst in the bulk, but the XPS results revealed that the calcination process increased the bismuth content on the catalyst surface, especially for samples made in solution with pH=4.

4.2.4 Dielectric properties

The dielectric properties were measured by a cyl-ε cavity operating at 2.5 GHz with TM_{010} mode. The detailed instruction of the cyl-ε cavity and calculating method were introduced in Section 2.3.4.

Table 4.4 Dielectric parameters for bismuth molybdate materials hydrothermally synthesized at different pH

Sample	Dielectric constant (ε')	Dielectric loss (ε'')
pH=4	1.0016	0.14135
pH=6	1.0014	0.12841
pH=8	1.0016	0.12691
pH=4-cal	1.0012	0.05607
pH=6-cal	1.0013	0.04210
pH=8-cal	1.0013	0.04194

The dielectric constant (ε') does not show a significant change for the different bismuth molybdate samples, while the calcination procedure seems to lead to a large drop in the dielectric loss (ε'') of the materials.

As had been mentioned in Section 3.1.2, in microwave heating systems, it is understood that the interaction of materials with microwaves and the heating behaviour of materials by microwave irradiation is strongly dependent on their dielectric properties. The most important property of heating processes is the complex permittivity (ε^*), and the ratio of the dielectric loss and the dielectric constant is commonly used to measure the ability of a material to convert electromagnetic energy into heat energy, which is referred to as the loss tangent ($\tan\delta$). The loss tangent of bismuth molybdate vanadate catalysts are shown in Figure 4.4.

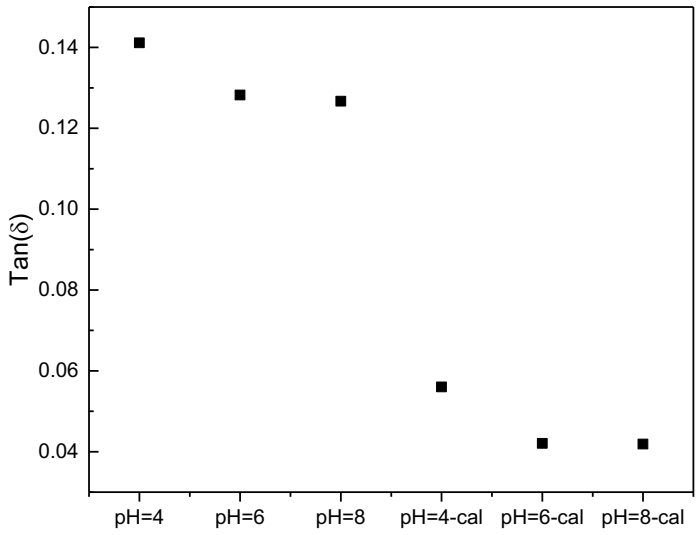

Figure 4.3 Loss tangent of the bismuth molybdate materials hydrothermally synthesized at different pH

It is interesting to observe that the non-calcined samples are more likely to reach higher temperatures than the calcined samples. This may be due to the presence of water of crystallinity or other impurities like NO_3^- in the sample structure that can facilitate microwave absorbing at the very beginning stage of microwave heating, as the water and NO_3^- usually have larger polarity than bismuth molybdate. The high polarity of nitrate salts with water of crystallinity means they are usually better at utilizing the microwave energy and become dielectric lossy. Due to the excellent dielectric property, bismuth nitrate salts have been used in microwave synthesis of naphthyridines[15], microwave-assisted synthesis of molecules of medicinal interest[16], and to catalyse a unique route toward 1,4-dihydropyridines[17]. Figure 3.3 shows the TGA results for the uncalcined pH=4 sample and calcined pH=4 sample which were carried out to identify any impurities to support the hypothesis.

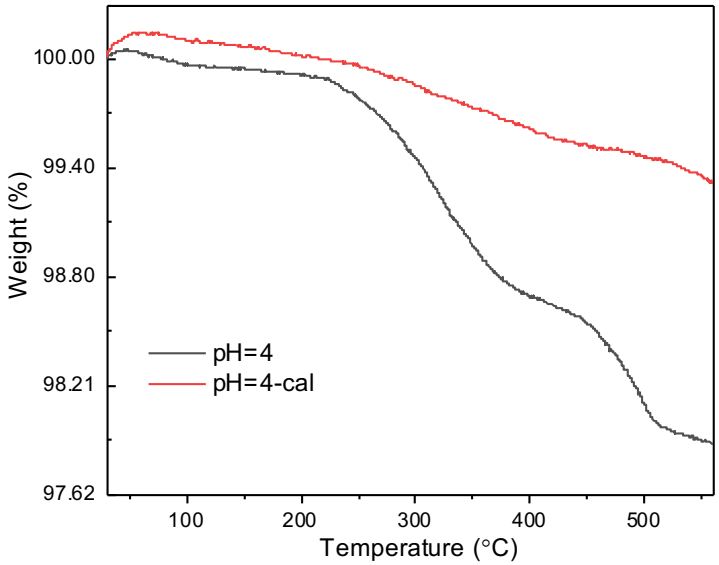

Figure 4.4 TGA for non-calcined and calcined bismuth molybdate materials hydrothermally synthesised at pH 4

Figure 4.4 shows the weight drop processes occurring when the two samples are heated from room temperature to 600 °C. The non-calcined sample shows a much larger weight drop than the calcined sample and has two clear weight-loss stages while the calcined sample only has one. The first loss of mass occurs from 300 °C corresponding to the removal of water of crystallinity. The second weight drop process in the range of temperature from 400-500 °C is related to the decomposition of the nitrate salts.

4.3 Catalyst Testing

The catalytic activity of bismuth molybdate samples for the selective oxidation of propene was tested under conventional and microwave heating.

4.3.1 Microwave Heating Performance

All samples were heated in the microwave cavity with power ranging from 2.5 W to 30 W. The temperature of the catalyst bed was measured by an infrared camera and shown in Figure 4.5.

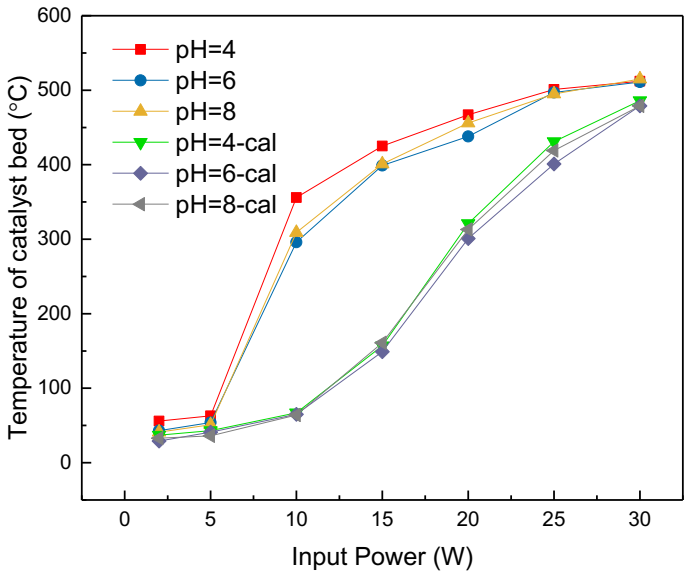

Figure 4.5 Temperature of the catalyst bed under microwave heating(every point in this graph is tested by an independent run with fresh catalysts)

All samples can be heated by microwave radiation and reached a desirable temperature (more than 360 °C), which indicated that γ-Bi_2MoO_6 is a good candidate for microwave-assisted heterogeneous catalysis.

As can be seen from the Figure 4.5, all the tested samples cannot be well heated when the input power is lower than 5 W. this is because that the microwave power is too low to induce

sufficient heat into the samples. When the input power became higher, the non-calcined samples seems to be more likely to reach higher temperatures than the calcined samples. This is because that comparing with the calcined samples (as can be seen from the Figure 4.3) the non-calcined samples have higher dielectric loss, which indicate that they have better ability to convert the microwave energy into heat.

When the microwave power was between 5 W and 15 W, the temperature of non-calcined sample increased dramatically, while when the power became even higher, the catalyst bed temperature did not increase so much. This is because when temperature is high, the heat dissipation rate will also increase, which limited the rate of temperature rise. At the same time, the structure of the catalyst itself will also change due to high temperature (for instance, removal of the water and NO_3^-), which will also reduce the ability to absorb microwave. The temperature of calcined catalyst increases rapidly in the whole power range, when the microwave power become even higher and comes to 30 W, all the calcined samples also reached a similar temperature with the non-calcined sample, at arround 450-500 °C.

Although both the water in the samples and NO_3^- impurity will be removed when the temperature reaches a high level (300 °C and 450 °C, respectively), their positive effects on improving the early-stage temperature are still very important to assist the bulk catalyst to reach a higher temperature. In the initial heating stage, the impurities like water and NO_3^- can absorb a large amount of microwave energy and transfer heat to the surrounding catalyst which result in a pre-heating effect on the catalyst bed. Zhang and co-workers demonstrated research on how the temperature affects the dielectric property of the solid catalyst in a heterogeneous catalytic process[18]. They pointed out that the dielectric loss is highly temperature dependent. In their studies, they firstly preheated the tested samples with conventional apparatus and then measured their dielectric properties at different temperatures. For all the samples they measured,

the energy dissipation factor, or loss tangent (which is an indicator of the ability of a material, to convert the energy in the microwave into heat (see Section 3.1), was found to increase with increasing temperature. Similar effects were also reported by other researchers[19]. At a higher temperature, the mobility of charge carriers in the solid solution materials will be higher, which increases the polarization of the materials and leads to high dielectric loss[20]. Therefore, pre-heating the catalyst in advance is beneficial for the catalyst to absorb more microwave energy.

4.3.2 Conventional Test

To check the catalytic performance of the prepared catalysts, conventional tests from 200 °C to 500 °C were carried out in a flow of propene, oxygen, and nitrogen. Results for conventional tests are shown in Figures 4.6 and 4.7, with the full product selectivity shown in Table 4.5.

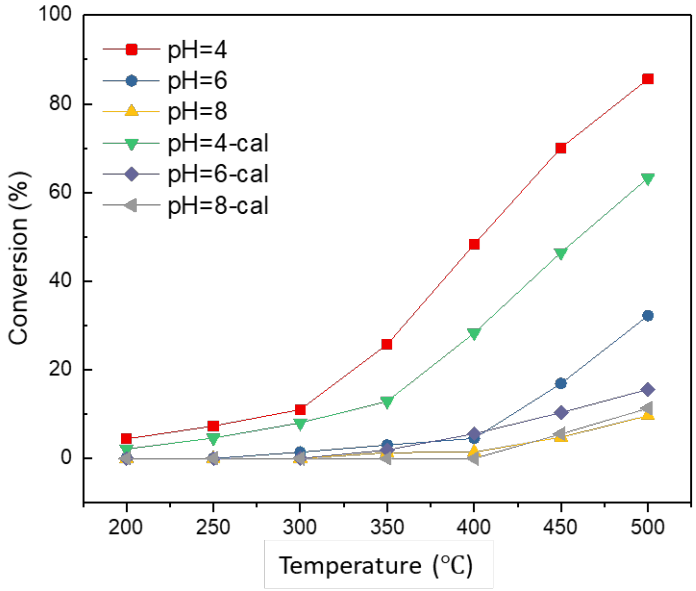

Figure 4.6 Propene conversion in conventional heating tests (0.2 g of catalyst, propene:oxygen:nitrogen = 1:2:97, flow rate = 50 mL min^{-1})

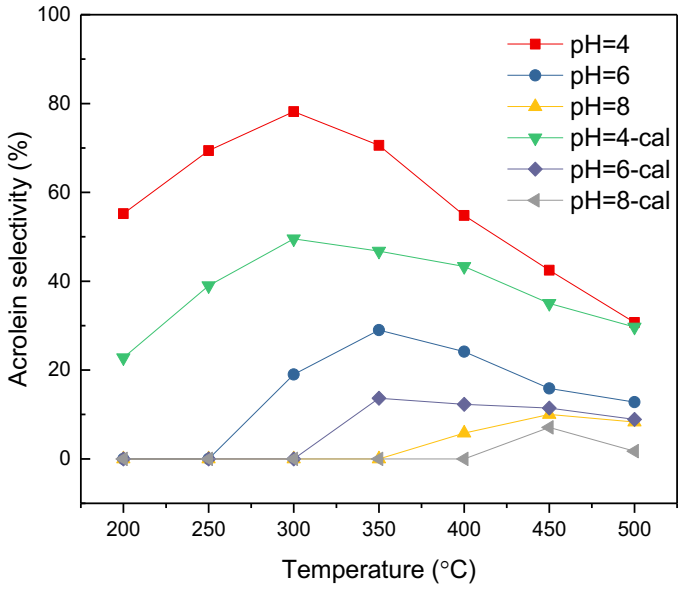

Figure 4.7 Acrolein selectivity in conventional tests (0.2 g of catalysts propene:oxygen:nitrogen = 1:2: 97, flow rate = 50 mL·min^{-1})

As shown in Figure 4.6, all the calcined samples performed worse than the corresponding non-calcined samples, with both propene conversion and acrolein selectivity lower. An explanation for the decrease of propene conversion could be the increase in crystallite size and the decrease of the surface area of samples, leading to low propene conversion (see Table 4.2 and 4.3). The decrease in acrolein selectivity suggests the active sites were also changed. According to the ICP-OES and XPS results (Table 4.3) samples synthesized in the solution with a higher pH value contains a larger amount of Bi both in the bulk and on the surface, and the calcination process increased the bismuth content on the catalyst surface. According to the proposed mechanism for propene selective oxidation, introduced in the Chapter 1, the absorption of both the first and second hydrogen of propene are on the Mo site, and only the Mo site will be reduced when acrolein is formed, implying the surface Mo concentration is crucial for bismuth molybdate to maintain high selectivity to acrolein. The increase in surface bismuth sites makes

the catalyst more inclined to produce carbon dioxide at higher temperature, which had been reported by previous researchers for propene selective oxidation over the bismuth molybdate catalysts[21–23].

Considering the conversion and acrolein selectivity results in Figure 4.6 and 4.7, the sample synthesised at pH=4 performed best in the conventional test at 350-400 °C and reached propene conversions of 28%–45%, with an acrolein selectivity of 82%–69%. The corresponding calcined sample, pH=4-cal, also performs better than other samples, which reached propene conversions of 16%–29% at acrolein selectivity of 48%–42%. The major by-products of both samples were CO_2 and CO (10%-30%), and acetaldehyde (5-8%). Ethylene and hexadiene were also detected in small amounts temperatures above 500 °C (See Table 4.5). The outstanding performance of sample pH=4 may be because of the catalytic synergy between α and γ phases of bismuth molybdate, which had been reported by early research[24]. Thang and co-workers tested the catalytic activity of three phases of bismuth molybdate prepared under different conditions for propene selective oxidation. They suggested that impurities from other phases is one reason differences in catalytic activity observed for bismuth molybdate. According to the Raman spectra of samples pH=4 and pH=4-cal, α-$Bi_2Mo_3O_{12}$ was contained in the samples and when α and γ phases are present together in a catalyst, the activity and selectivity are much higher than they are in each pure phase. Zhou and co-workers have carried out detailed research investigating the cooperative effects between α and γ phase bismuth molybdate in the selective oxidation of propene using various surface characterization techniques. They suggest that, in general, γ phase bismuth molybdate can facilitate the usage of gaseous oxygen, and this phase usually has a higher reaction rate[25]. However, γ phase bismuth molybdate is very active, and can easily combust the reactant into CO_2, and this would be the reason why the pure γ phase usually does not lead good acrolein selectivity compared with the mixed phase and pure α

phase. Additionally, having certain amount of α phase on the surface can increase the amount of propene absorption on the catalyst surface, as the propene absorption and its oxidation had been proposed to be taken place on an unsaturated Mo site on the surface[14,21,26]. The surface α phase can provide more Mo site on the surface (from XPS analysis, see Section 4.2.3), which leads to a higher acrolein selectivity.

Sample pH=8 and pH=8-cal showed much lower propene conversion and acrolein selectivity than other samples in the temperature region of 350-400 °C (only 2-3% conversion with less than 10% acrolein selectivity), This could be because it contained a bismuth rich phase of Bi_4MoO_9, and Bi_2O_3 (see XRD results in Section 4.2.1), which means it has much lower Mo surface concentration (see XPS results in Section 4.2.3). The early research by Wilson and co-workers indicated that over Bi_2O_3, the major reaction product is 1,5-hexadiene, as Bi_2O_3 usually has less ability to utilize the oxygen atom from the lattice than bismuth molybdate[27]. Schuh and co-workers also reported similar findings. In their study they tested a series of bismuth molybdate catalysts prepared by hydrothermal synthesis from solution with variations in the pH value and Bi/Mo ratio. They found that, compared to the sample containing only Bi_2MoO_6 under the same conditions, the selective oxidation of propene over a bismuth rich catalyst, a much lower propene conversion and very low acrolein selectivity were achieved[6].

Table 4.5 Selectivity of the main products from propene oxidation under conventional testing

Sample	Temperature (°C)	acrolein selectivity	acetaldehyde	CO_x	Higher Hydrocarbons	Lower Hydrocarbons
pH=4	200	65%	0%	0%	0%	0%
	250	76%	7%	0%	0%	0%
	300	89%	7%	0%	0%	3%
	350	81%	6%	0%	6%	3%
	400	46%	5%	9%	23%	10%
	450	42%	8%	11%	13%	23%
	500	31%	8%	13%	3%	41%
pH=4-cal	200	23%	0%	0%	0%	0%
	250	27%	7%	0%	0%	0%
	300	40%	7%	0%	0%	3%
	350	41%	5%	0%	6%	3%
	400	46%	5%	9%	23%	10%
	450	50%	8%	10%	13%	23%
	500	30%	7%	13%	3%	41%
pH=6	200	0%	0%	0%	0%	0%
	250	0%	0%	0%	0%	0%
	300	12%	13%	0%	0%	2%
	350	11%	19%	0%	0%	3%
	400	11%	33%	0%	0%	4%
	450	13%	36%	5%	5%	26%
	500	43%	2%	9%	3%	45%
pH=6-cal	200	0%	0%	0%	0%	0%
	250	0%	0%	0%	0%	0%
	300	0%	16%	0%	0%	3%
	350	14%	19%	0%	0%	3%
	400	12%	31%	0%	0%	4%
	450	14%	37%	4%	5%	27%
	500	39%	3%	8%	3%	45%
pH=8	200	0%	0%	0%	0%	0%
	250	0%	0%	0%	0%	0%
	300	0%	0%	0%	0%	0%
	350	0%	20%	0%	0%	20%
	400	6%	4%	0%	0%	27%
	450	10%	3%	10%	47%	21%
	500	8%	3%	5%	79%	2%
pH=8-cal	200	0%	0%	0%	0%	0%
	250	0%	0%	0%	0%	0%
	300	0%	0%	0%	0%	0%
	350	0%	22%	0%	0%	0%
	400	0%	2%	0%	0%	0%
	450	5%	1%	11%	10%	47%
	500	11%	2%	17%	5%	79%

(Lower hydrocarbons include CH_4 C_2H_4 and C_2H_6, higher hydrocarbons include benzene and hexene. Selectivity does not add up to 100% as other C_3 oxygenate include acetone, propanol, iso-propanol are not listed. No significant carbon deposit were found on the post-reaction catalyst)

4.3.3 Microwave Test

To check the feasibility of using hydrothermally made bismuth molybdate in the microwave cavity reactor, a set of tests were carried out in the flow of mixed gas made up with propene, oxygen, and nitrogen. The performance of different bismuth molybdate samples under microwave heating are shown in Figure 4.8 and 4.9. The full products distribution is shown in Table 4.6.

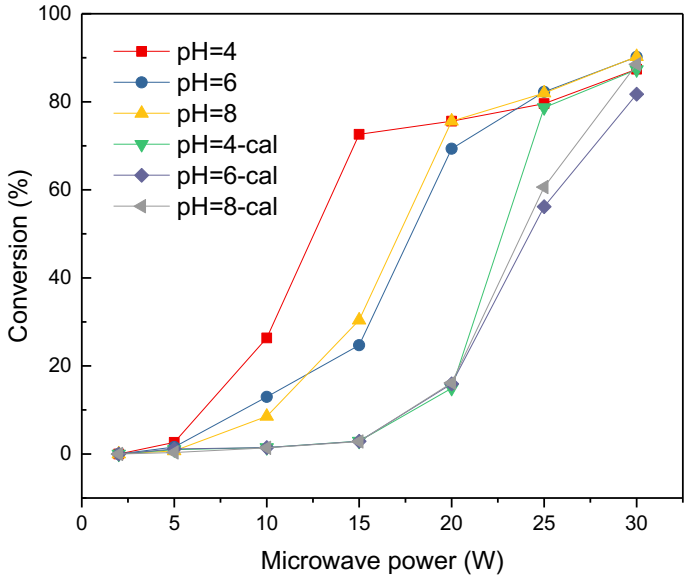

Figure 4.8 Propene conversion in microwave tests (0.2 g of catalyst, propene:oxygen:nitrogen = 1:2:97, flow rate = 50 mL min^{-1})

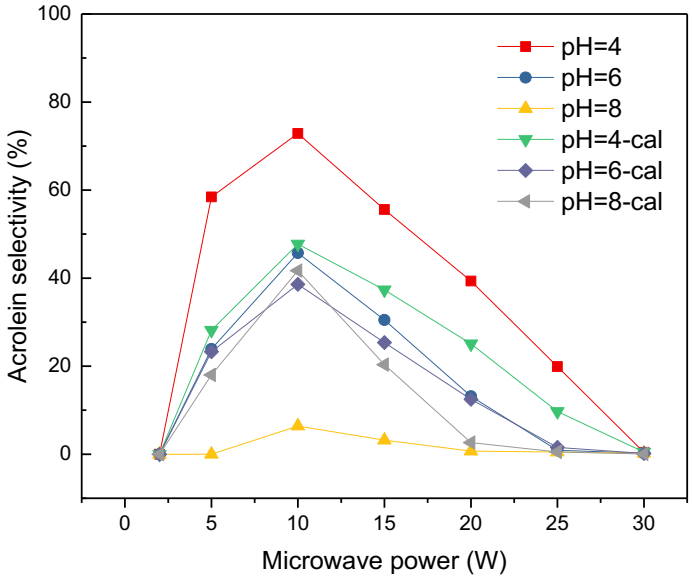

Figure 4.9 Acrolein selectivity in microwave tests (0.2 g of catalyst, propene:oxygen:nitrogen = 1:2:97, flow rate = 50 mL min^{-1})

Table 4.6 Selectivity of the main products from propene oxidation under microwave heating.

Sample	Input Power (W)	lower hydrocarbons	acetaldehyde	acrolein	other C_3 oxygenate	CO_x	higher hydrocarbons
pH=4	2	0%	0%	0%	0%	0%	0%
	5	0%	6%	59%	34%	0%	0%
	10	8%	8%	73%	10%	0%	2%
	15	8%	6%	55%	8%	21%	1%
	20	8%	6%	35%	8%	42%	1%
	25	13%	6%	19%	2%	55%	4%
	30	22%	3%	3%	1%	57%	14%
pH=4-cal	2	0%	0%	0%	0%	0%	0%
	5	0%	6%	28%	66%	0%	0%
	10	0%	8%	48%	28%	12%	4%
	15	0%	8%	37%	17%	34%	4%
	20	9%	8%	25%	16%	39%	3%
	25	23%	5%	10%	4%	41%	17%
	30	29%	3%	0%	0%	46%	22%
pH=6	2	0%	0%	0%	0%	0%	0%
	5	0%	7%	24%	68%	0%	0%
	10	6%	6%	46%	34%	7%	2%
	15	13%	6%	30%	21%	19%	12%
	20	16%	4%	13%	10%	47%	10%
	25	18%	3%	1%	12%	47%	18%
	30	24%	4%	0%	15%	35%	22%
pH=6-cal	2	0%	0%	0%	0%	0%	0%
	5	0%	6%	23%	71%	0%	0%
	10	2%	8%	39%	37%	10%	4%
	15	11%	9%	25%	31%	19%	5%
	20	34%	8%	12%	20%	21%	6%
	25	31%	5%	2%	11%	32%	19%
	30	32%	3%	0%	0%	39%	26%
pH=8	2	0%	0%	0%	0%	0%	0%
	5	16%	23%	0%	27%	0%	34%
	10	17%	6%	6%	3%	0%	67%
	15	19%	0%	3%	1%	24%	53%
	20	19%	0%	1%	1%	53%	26%
	25	20%	0%	0%	0%	48%	31%
	30	27%	0%	0%	1%	38%	33%
pH=8-cal	2	0%	0%	0%	0%	0%	0%
	5	0%	23%	18%	27%	0%	32%
	10	0%	6%	42%	3%	0%	49%
	15	11%	0%	20%	1%	24%	42%
	20	17%	0%	3%	1%	53%	26%
	25	28%	0%	1%	0%	48%	22%
	30	39%	0%	0%	1%	38%	21%

(Lower hydrocarbons include CH_4 C_2H_4 and C_2H_6, higher hydrocarbons include benzene and hexene. Other C_3 oxygenate include acetone, propanol, iso-propanol)

As introduced in Chapter 3, in the gas-solid phase microwave-assisted heterogeneous catalytic reactions, gas reactants cannot be heated by microwave, therefore the key point of initiating the microwave-assisted heterogeneous catalytic process is that the catalysts bed can reach the appropriate temperature under microwave conditions. As shown in Figure 4.8, all hydrothermally synthesized γ-Bi_2MoO_6 samples showed activity under microwave conditions. The trend of the propene conversion at different microwave powers is similar with the catalyst bed temperature shown in the Figure 4.5. As the uncalcined samples can reach higher temperature under microwave heating, the three uncalcined samples give higher conversion than the corresponding calcined samples, especially in the lower input power range.

However, if the conversion of the same samples in microwave tests (Figure 4.8) and conventional tests (Figure 4.6) is compared, a much higher enhancement on the propene conversion by the microwave was observed for the samples which are made at higher pH, and calcined. The best conversion increase was made by pH=8-calcine sample, over which the propene conversion under conventional condition is less than 10%, while reaches nearly 80% under microwave condition.

According to the results of conventional test shown in the Figure 4.6, under the conventional heating conditions, different samples showed very different performance under the same temperature. For example, when looking at the preopen conversion, and there was a large difference between the best performing and worst performing catalysts even at the same temperature. However, under the microwave condition, the situation was not same. When combining the results in Figure 4.8 with the corresponding catalyst bed temperature shown in Figure 4.5, similar propene conversions were achieved by all the samples with the almost same temperature under microwave conditions.

By this result, we can say the enhanced performances are not only caused by temperature. The propene conversions of sample pH=4 and pH=8-cal in conventional testing at 500 °C were 82%

and 20% respectively. According to the data in Figure 4.5, both of these two samples reached nearly 500 °C under 25 W input power, and there is no obvious difference in temperature of the two samples at this specific microwave condition. However, the microwave testing show a different result from the conventional testing. The two samples showed similar activity under microwave heating, and both convert nearly 90% propene. Therefore, the catalyst bed temperature is not the only factor which affects the propene conversion under microwave heating.

In terms of the acrolein selectivity, different samples performed quite differently. The order of acrolein selectivity is sample pH=4 > sample pH=6 > sample pH=8, with the uncalcined samples giving higher selectivity their calcined counterparts. As shown in Figure 4.10, sample pH=4 showed the best acrolein selectivity of 76% under 10 W input microwave power, while the sample pH=8 only led to less than 10% acrolein selectivity under the same condition.

4.3.4 Comparison - Performance in Conventional heating and Microwave heating

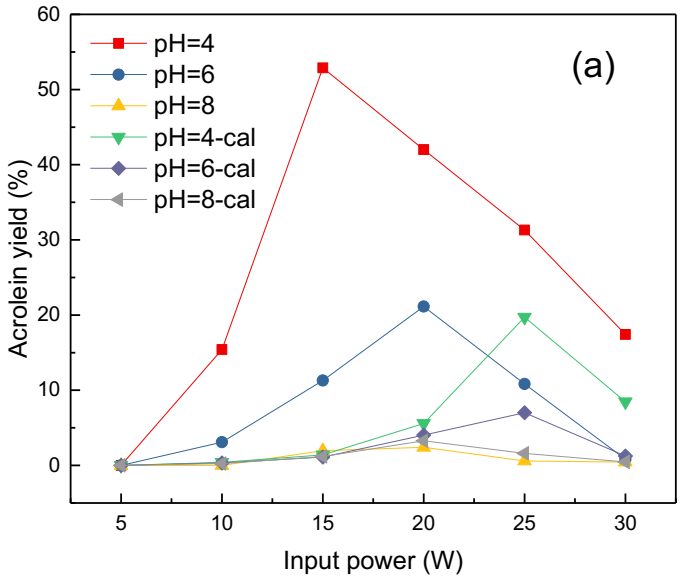

Figure 4.10 Acrolein yield under microwave heating (0.2 g of catalyst, propene:oxygen:nitrogen = 1:2:97, flow rate = 50 mL min^{-1})

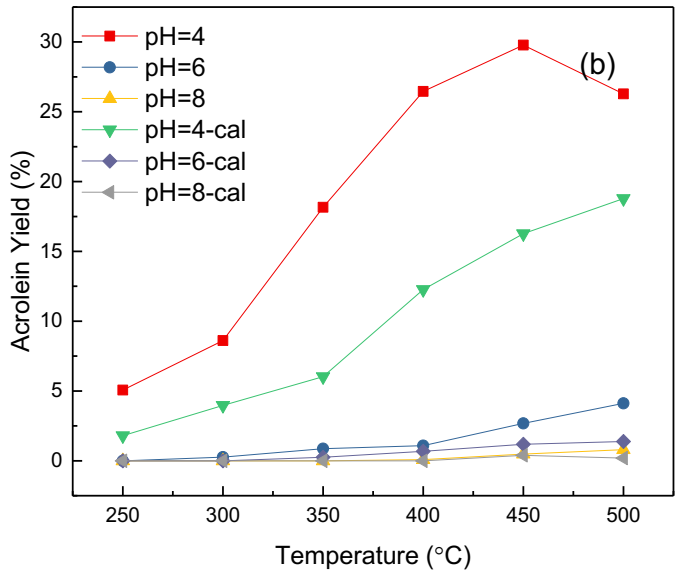

Figure 4.11 Acrolein yield under conventional heating (0.2 g of catalyst, propene:oxygen:nitrogen = 1:2:97, flow rate = 50 mL min^{-1})

Acrolein yield in both series of tests is shown in Figure 4.10 and Figure 4.11. For samples pH=4 and pH=6, great enhancements in acrolein yield (20% and 16% respectively) were made by using microwave heating. The best acrolein yield of greater than 50% was observed over sample pH=4 under 15 W microwave power, while the best acrolein yield in the conventional tests, over the same catalyst (sample pH=4), was only 30%. For calcined samples, although an increase in activity was observed under microwave heating, there was no obvious enhancement in selectivity to acrolein, and CO_2 became the main product instead.

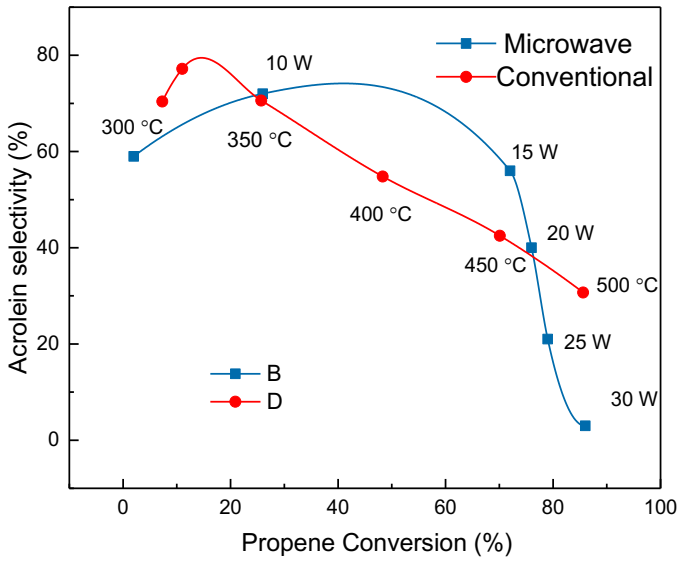

Figure 4.12 Acrolein selectivity under microwave heating and conventional heating for sample pH=4 (0.2 g of catalyst, propene:oxygen:nitrogen = 1:2:97, flow rate = 50 mL min^{-1})

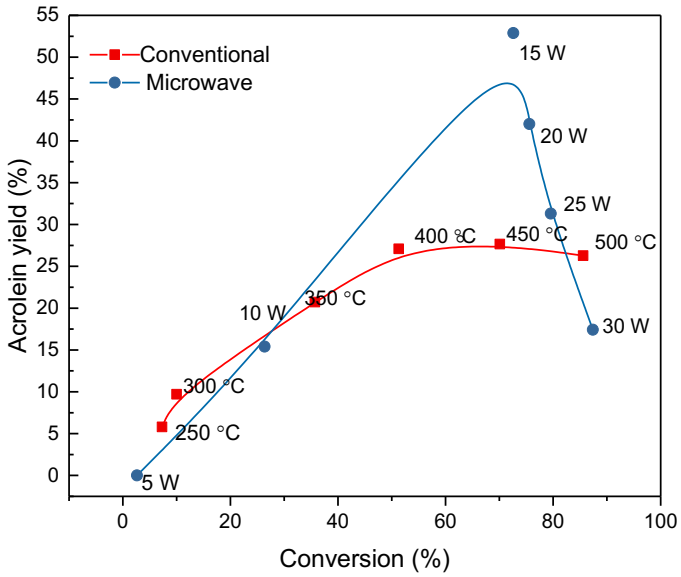

Figure 4.13 Acrolein yield under microwave heating and conventional heating for sample pH=4 (0.2 g of catalyst, propene:oxygen:nitrogen = 1:2:97, flow rate = 50 mL min^{-1})

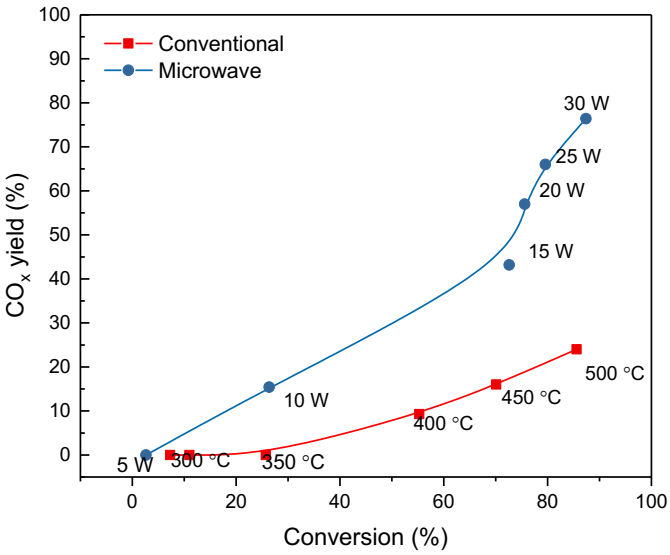

Figure 4.14 CO_x yield under microwave heating and conventional heating for sample pH=4 (0.2 g of catalyst, propene:oxygen:nitrogen = 1:2:97, flow rate = 50 mL min^{-1})

A comparison between the performance of the best sample, pH=4, in the microwave and conventional conditions gives a clearer insight into the enhanced effect of microwave heating (Figure 4.12 and Figure 4.13). As can be seen from Figure 4.12, when the microwave input power led between 10 W and 20W, with comparable propene conversion, the acrolein selectivity over the sample pH=4 in the microwave was better than the conventional test. As can be seen from the figure 4.13, the best acrolein yield in the microwave test was 53% under 15 W microwave input power, while the best yield in the conventional test was only 27% over the same sample at the temperature of 450 °C.

Apart from looking at the acrolein production, there was also another interesting phenomenon. By comparing Figure 4.13 and Figure 4.14 together, we can see that when the input power reaches 15 W, the catalytic effect of the microwave-assisted process changes greatly. The production of acrolein began to decline rapidly, and carbon dioxide began to replace it as the main product. This can indicate that, under this condition, the dominant reaction taking place on the catalyst surface has switched from propene selective oxidation to total oxidation.

As previously shown in Figure 4.5, the temperature of sample pH=4 catalyst reached 420 °C with 15 W input microwave power. The catalyst bed temperatures in these two situations are similar but the catalyst bed temperature in the microwave testing is less precise. As described in Chapter 1, accurate measurement of catalyst bed temperature has proved to be difficult in microwave-heated reactions, and the debate over whether microwaves only induce thermal effects has been going on for decades. Many researchers have attempted to definitively address this issue, but the nature of microwave effects is still not understood. Unlike conventional heating, where reaction temperature can be easily measured with a thermocouple, the interaction of electric fields with the metal probe common on contact-type thermocouples means dielectric heating in a microwave cavity cannot be measured accurately using traditional methods[28]. However, some problems associated with using non-contact infrared temperature

measurement devices have been identified. Some researchers have pointed out that the non-contact infrared camera, which can only measure the surface temperature, cannot tell the accurate temperature of the entire reaction vessel[29]. Optical fiber thermometers are a contact temperature measurement device that were specially developed for dielectric heating and similar applications. Unlike the infrared camera which measures the temperature by detecting infrared light emitted by a material, optical fiber thermometers can be put into the reaction vessel or catalyst bed during the microwave irradiation [28], and more accurate measurements can be obtained.

With the continuous improvement of temperature measurement methods, scientists have more accurately measured the temperature of the catalyst bed in microwave-assisted reactions, and many researchers had concluded that the lower apparent temperature of the catalyst bed in the microwave-assisted reaction was due to the existence of 'hot spots', or large temperature gradients, within the catalyst bed subject to microwave heating. 'Hot spots' can occur in microwave heating when the heated materials have different microwave absorbing properties, resulting in a non-uniform temperature distribution[30]. 'Hot spot' effect had been widely recognized by many researchers for microwave-assisted chemical processes[31–35].

A significant change in the observed acrolein selectivity was also observed. Under both conventional and microwave heating, the best yield of acrolein was observed at around 70% propene conversion (Figure 4.13), however, nearly twice the amount of acrolein was produced under the microwave heating. Most recent explanations for the change in products selectivity in the microwave-assisted process is due to the temperature difference inside the catalysts bed[32]. Due to the selective heating property of microwaves, in a microwave-assisted process, the catalyst particle temperature is different from the gas temperature, and the temperature of the spatial hot spot within the catalyst bed is different from the average temperature of the catalyst bed. It is possible that in the process of propene oxidation over the bismuth molybdate, the

active site on the bismuth molybdate surface was well heated by microwave, but the surrounding parts remained at a lower temperature, which effectively suppresses the further oxidation of the acrolein. In addition to the pure thermal effects, some researchers also suggested that the 'microwave-induced discharge effect' plays a role in microwave heating processes and chemical reactions [36]. When some solid inorganic materials like transition metal oxides or zeolites interact with the microwave radiation, the kinetic energy of some outer electrons may increase, enabling them to jump out of the material, resulting in the ionization of the surrounding atmosphere. The plasma usually contains highly active species such as electrons, ions, and radicals, which can change the equilibrium of the reaction, significantly enhance the reaction rate and alter the product selectivity. Some examples of microwave discharge-assisted catalysis had been reported in recent years, for example in the decomposition of NO[37] and utilization of CO_2[38]. As the temperature of the microwave plasma is usually high (600-1000 °C), a combustion or cracking reaction is usually preferred[39,40]. This could explain the formation of CH_4 and enhancement of CO_x yield under higher power conditions (see Table 4.6).

Apart from the changes observed in conversion and selectivity, a much faster catalyst deactivation was observed when microwave heating was used compared to conventional heating. In conventional testing, the samples achieve a steady state of more than 80% conversion after 10 hours heating, while in microwave testing, the samples usually became inactive within a much shorter time. For example, when running under 15 W input power, the sample pH=4, started to deactivate after 2 hours, and at 30 W only remained active for around 30 mins. The propene conversion dropped dramatically, and more CO_2 rather than acrolein was formed. The large change of selectivity also indicates that the active site of the catalyst has changed. BET and TGA tests were carried out on the used pH=4 sample after both microwave and conventional testing to investigate this process.

Table 4.7 BET specific surface area of target samples

Sample ID	15 W (microwave) 30 mins	15 W (microwave) 120 mins	30 W (microwave) 30 mins	450 °C (Conventional) 600 mins
specific surface area (m^2/g)	6	1	<1	9

A significant loss of surface area was seen for the used sample after the microwave testing. The original specific area of sample pH=4 is 16 m^2 g^{-1}, and after heating in the conventional reactor for 10 hours, the specific area dropped to 9 m^2 g^{-1}. However, after interacting with a 15 W power microwave field, under the reaction conditions, for 60 mins, the specific area dropped to 6 m^2 g^{-1} and was only 1 m^2 g^{-1} after 2 hours online. If the input power was increased to 30 W, the specific area dropped to < 1 m^2 g^{-1} after 60 mins. This phenomenon was also reported by Zhang and co-workers when using microwave heating in a gas phase heterogeneous catalytic reaction[35]. In their opinion, the much greater loss of a specific area of catalysts than the conventional process indicated that microwave heating caused a considerable reorganization of the catalyst structure.

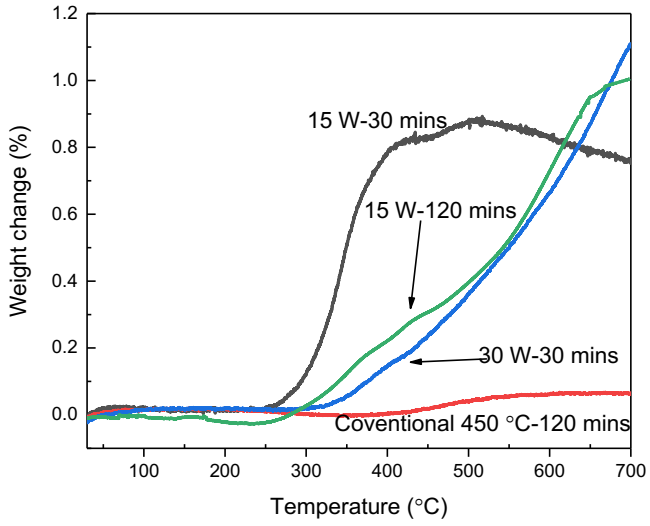

Figure 4.15 TGA for used sample pH=4 in different conditions

The Figure 4.15 shows the results of TGA analysis on the used sample pH=4 after microwave heating under different conditions. All used samples gained weight when heated in air, which indicated that the catalysts were reduced under the reaction conditions. For the TGA result of the pH=4 sample running at 15 W for 30 mins, during the period of the temperature rising from 250 °C to 500 °C, there was a weight gain during the process, indicating that the sample was reoxidized by air. For the sample heated at 15 W for 120 mins, there was a much longer process of weight gain, and the final weight change was larger than the sample heated for 30 mins, which indicated that in the 15 W condition reaction, the catalyst continuously lost oxygen during the reaction period. Which means that under microwave condition, the oxygen reinserting is limited. The sample heated at 30 W for 30 mins showed a continuous weight gain until 700 ˚C, hence a deeper reduction than which under the 15 W condition was happened on the sample by this reaction condition. This result indicated that the higher microwave input power will further limiting the insert of gas phase oxygen.

The slower rate of weight gain of the samples heated at 15 W for 120 mins and 30 W for 30 mins may be due to the smaller surface area of those two samples compared to the one heated at 15 W for 30 minutes, and caused a harder process to be reorganized. According to the molecular weight of the Bi_2MoO_6, the amount of oxygen atoms lost relative to the total amount of oxygen atoms in the sample is shown in the table below:

Table 4.8 Calculated oxygen loss of each sample

Sample ID	15 W (microwave) 30 mins	15 W (microwave) 120 mins	30 W (microwave) 30 mins	450 °C (Conventional) 120 mins
Calculated Oxygen loss	5.0%	6.4%	7.0%	<1%

As introduced in Chapter 1, the reaction of propene selective oxidation is via a Mars and Van Krevelen mechanism in which propene adsorbs reversibly and then reacts with an oxygen atom of the catalyst, therefore participation of the lattice oxide ion into the reaction is quite prominent in this catalyst system[41]. Looking at the result in Table 4.8, overall, samples are more likely to be reduced and form oxygen vacancies in the microwave-assisted process than in the conventional process, which indicated that the surface reaction in the microwave-assisted process is much quicker, and the lattice oxygen transfer cannot keep up with reduction of catalyst surface sites. This may be another reason for the quicker catalyst deactivated in the microwave-assisted process. Therefore, in order to eliminate the deactivation of the catalysts, an short "off-period" should be add in the microwave-assisted process. At the beginning of the "off-period", no microwaves react with the catalyst bed, but the temperature of the active site is still high enough. By this chance, the gas-phase oxygen can reoxidise the catalyst surface and generate new lattice oxygen.

4.4 Conclusion

In this chapter, hydrothermal synthesis has been used to prepare bismuth molybdate catalysts for the selective oxidation of propene to acrolein in a microwave-assisted heterogeneous catalytic process.

The pH of the precursor solution was found to be a strong influence on the catalyst formed. The γ-Bi_2MoO_6 phase only catalyst was formed when pH=6, and mixed phases samples was formed in both higher and lower pH values. In lower pH solution (pH=4), a small amount of molybdenum rich phase $Bi_2Mo_3O_{12}$ was formed, and in higher pH solution (pH=8) the impurity phase was the bismuth rich phase Bi_4MoO_9. Calcination at 500 °C does not change the composition of catalyst, but increases the crystallite size of the sample, and results in the decreasing of specific surface area. All samples have similar dielectric constant, but the

dielectric loss is different. The calcination process greatly reduced the dielectric loss of the samples.

In microwave-assisted tests, all samples could be heated by microwave radiation and reached a desirable and showed activity, which indicated that hydrothermally synthesised γ-Bi_2MoO_6 is a good candidate for microwave-assisted heterogeneous catalysis. When comparing the acrolein selectivity and yield in microwave tests with the results in conventional heating, the potential of using microwave heating was shown. The best acrolein yield was found to be greater than 50% under 15 W microwave power, while the best result in the conventional tests, was only 30%. This enhancement is due to the temperature difference and existence of 'hot spots' inside the catalysts bed, which are caused by the selective heating property of microwaves, and uneven thermal conductivity inside the catalyst bed.

Although a remarkable enhancement on acrolein yield was observed using microwave heating, there were disadvantages to this process. The catalysts were much more likely to be deactivated by microwave heating. The catalyst deactivation could be caused by the catalyst sintering and or reducing at the extremely high temperature produced by the 'Thermal runaway' effect at higher power.

References

1. Banavatu, L., Rao, D. S. & Basavaiah, K. Synthesis of γ-Bi_2MoO_6 by co-precipitation method and evaluation for photocatalytic degradation of rhodamine B, crystal violet and orange II dyes under visible light irradiation. *Asian Journal of Chemistry* **30**, 97–102 (2018).

2. Liang, D. *et al.* Solid-state reaction synthesis for mixed-phase Eu^{3+}-doped bismuth molybdate and its luminescence properties. *Modern Physics Letters B* **31**, 1750241 (2017).

3. Le, M. T., Do, V. H., Truong, D. D. & Pham, N. N. Sol-Gel Synthesis of Bismuth Molybdate Catalysts for the Selective Oxidation of Propylene to Acrolein: Influence of pH Value and Theoretical Molar Atomic Ratio. *Journal of the Chinese Chemical Society* **64**, 1326–1332 (2017).

4. Li, H. *et al*, Hydrothermal synthesis and photocatalytic properties of bismuth molybdate materials, *Materials Chemistry and Physics* **116**, 134-142 (2009).

5. Schuh, K. *et al.* Selective oxidation of propylene to acrolein by hydrothermally synthesized bismuth molybdates. *Applied Catalysis A: General* **482**, 145–156 (2014).

6. Schuh, K. *et al.* Bismuth molybdate catalysts prepared by mild hydrothermal synthesis: Influence of pH on the selective oxidation of propylene. *Catalysts* **5**, 1554–1573 (2015).

7. Phuruangrat, A. *et al.* Hydrothermal synthesis and characterization of Bi_2MoO_6 nanoplates and their photocatalytic activities. *Journal of Nanomaterials* **2013**, 789705 (2013).

8. Gruar, R., Tighe, C. J., Reilly, L. M., Sankar, G. & Darr, J. A. Tunable and rapid crystallisation of phase pure Bi_2MoO_6 (koechlinite) and $Bi_2Mo_3O_{12}$ via continuous hydrothermal synthesis. *Solid State Sciences* **12**, 1683–1686 (2010).

9. Bakiro, M., Hussein Ahmed, S. & Alzamly, A. Effect of pH, Surfactant, and Temperature on Mixed-Phase Structure and Band Gap Properties of $BiNbO_4$ Nanoparticles Prepared Using Different Routes. *Chemistry (Easton)* **1**, 89–110 (2019).

10. Mączka, M. *et al.* Pressure-induced phase transitions in ferroelectric Bi_2MoO_6—a Raman scattering study. *Journal of Physics: Condensed Matter* **22**, 015901 (2009).

11. Li, H., Liu, C., Li, K. & Wang, H. Preparation, characterization, and photocatalytic properties of nanoplate Bi_2MoO_6 catalysts. *Journal of Materials Science 2008 43:22* **43**, 7026–7034 (2008).

12. Kulkarni, A. K. *et al.* Bismuth molybdate (α-$Bi_2Mo_3O_{12}$) nanoplates via facile hydrothermal and its gas sensing study. *Journal of Solid State Chemistry* **281**, 121043 (2020).

13. Dai, Z. *et al.* Time-dependent evolution of the $Bi_{3.64}Mo_{0.36}O_{6.55}/Bi_2MoO_6$ heterostructure for enhanced photocatalytic activity via the interfacial hole migration. *Nanoscale* **7**, 11991–11999 (2015).

14. Matsuura, I., Schut, R. & Hirakawa, K. The surface structure of the active bismuth molybdate catalyst. *Journal of Catalysis* **63**, 152–166 (1980).

15. Ravikumar Naik, T. R. & Bhojya Naik, H. S. An efficient $Bi(NO_3)_3{\cdot}5H_2O$ catalyzed multi component one-pot synthesis of novel Naphthyridines. *Molecular Diversity* **12**, 139–142 (2008).

16. Bandyopadhyay, D., Chavez, A. & Banik, B. K. Microwave-induced Bismuth Salts-mediated Synthesis of Molecules of Medicinal Interests. *Current Medicinal Chemistry* **24**, (2017).

17. Bandyopadhyay, D., Maldonado, S. & Banik, B. K. A microwave-assisted bismuth nitrate-catalyzed unique route toward 1,4-dihydropyridines. *Molecules* **17**, 2643–2662 (2012).

18. Zhang, X., Hayward, D. O. & Mingos, D. M. P. Dielectric Properties of MoS_2 and Pt Catalysts: Effects of Temperature and Microwave Frequency. *Catalysis Letters 2002 84:3* **84**, 225–233 (2002).

19. Liu, C. *et al.* Temperature and moisture dependence of the dielectric properties of silica sand. *J Microw Power Electromagn Energy* **47**, 199–209 (2013).

20. Rayssi, C., el Kossi, S., Dhahri, J. & Khirouni, K. Frequency and temperature-dependence of dielectric permittivity and electric modulus studies of the solid solution $Ca_{0.85}$ $Er_{0.1}Ti_{1-x}Co_{4x/3}$ O_3 ($0 \leq x \leq 0.1$). *RSC Advances* **8**, 17139–17150 (2018).

21. Keulks, G. W., Rosynek, M. P. & Daniel, C. Bismuth Molybdate Catalysts Kinetics and Mechanism of Propylene Oxidation. *Industrial and Engineering Chemistry Product Research and Development* **10**, 138–142 (1971).

22. Batist, P. A., Bouwens, J. F. H. & Schuit, G. C. A. Bismuth molybdate catalysts. Preparation, characterization and activity of different compounds in the BiMoO system. *Journal of Catalysis* **25**, 1–11 (1972).

23. Peacock, J. M., Parker, A. J., Ashmore, P. G. & Hockey, J. A. The oxidation of propene over bismuth oxide, molybdenum oxide, and bismuth molybdate catalysts. IV. The selective oxidation of propene. *Journal of Catalysis* **15**, 398–406 (1969).

24. Thang, L. M. & van Driessche, I. Catalytic activities of α, β, γ - bismuth molybdates for selective oxidation of propylene to arcrolein. in *Materials Science* **804**, 225–228 (2015).

25. Bing, Z., Pei, S., Shishan, S. & Xiexian, G. Cooperation between the α and γ phases of bismuth molybdate in the selective oxidation of propene. *Journal of the Chemical Society, Faraday Transactions* **86**, 3145–3150 (1990).

26. Tonelli, M. *et al.* Cooperation between redox couples at the surface of molybdates based catalysts used for the selective oxidation of propene. *Journal of Catalysis* **370**, 412–423 (2019).

27. Martir, W. & Lunsford, J. H. The Formation of Gas-Phase π-Allyl Radicals from Propylene over Bismuth Oxide and γ-Bismuth Molybdate Catalysts. *J Am Chem Soc* **103**, 3728–3732 (1981).

28. Leonelli, C. 3. Microwave generators, transmission, and interaction with different materials. *Microwave Chemistry,* 31–52 (2017)

29. Herrero, M. A., Kremsner, J. M. & Kappe, C. O. Nonthermal microwave effects revisited: On the importance of internal temperature monitoring and agitation in microwave chemistry. *Journal of Organic Chemistry* **73**, 36–47 (2008).

30. Wang, W. *et al.* Numerical simulation of hot-spot effects in microwave heating due to the existence of strong microwave-absorbing media. *RSC Advances* **6**, 52974–52981 (2016).

31. Jie, X. *et al.* Microwave-initiated catalytic deconstruction of plastic waste into hydrogen and high-value carbons. *Nature Catalysis* **3**, 902–912 (2020).

32. Stankiewicz, A., Sarabi, F. E., Baubaid, A., Yan, P. & Nigar, H. Perspectives of Microwaves-Enhanced Heterogeneous Catalytic Gas-Phase Processes in Flow Systems. *The Chemical Record* **19**, 40–50 (2019).

33. Chemat-Djenni, Z., Hamada, B. & Chemat, F. Atmospheric pressure microwave assisted heterogeneous catalytic reactions. *Molecules* **12**, 1399–1409 (2007).

34. Bag, S., Dasgupta, S. & Torok, B. Microwave-Assisted Heterogeneous Catalysis: An Environmentally Benign Tool for Contemporary Organic Synthesis. *Current Organic Synthesis* **8**, 237–261 (2011).

35. Zhang, X. & Hayward, D. O. Applications of microwave dielectric heating in environment-related heterogeneous gas-phase catalytic systems. *Inorganica Chimica Acta* **359**, 3421-3433 (2006)

36. Sun, J., Wang, W. & Yue, Q. Review on microwave-matter interaction fundamentals and efficient microwave-associated heating strategies. *Materials* **9**, 231 (2016).

37. Tang, J. *et al.* Microwave discharge-assisted catalytic conversion of NO to N_2. *Chemical Communications,* 1861–1862 (2000)

38. Chen, G. *et al.* An overview of CO_2 conversion in a microwave discharge: the role of plasma-catalysis. *Journal of Physics D: Applied Physics* **50**, 084001 (2017).

39. Plasma Catalysis of Methane Decomposition in Pulse Microwave Discharge - NASA/ADS. https://ui.adsabs.harvard.edu/abs/1997APS..GEC.AM205P/abstract.

40. Babaritskiĭ, A. I. *et al.* The repetitive microwave discharge as a catalyst for a chemical reaction. *Technical Physics 2000 45:11* **45**, 1411–1416 (2000).

41. Le, M. T. Bismuth Molybdate-Based Catalysts for Selective Oxidation of Hydrocarbons. in *Bismuth - Advanced Applications and Defects Characterization* (InTech, 2018). doi: 10.5772/intechopen.75105

42. Ohsato, H., Varghese, J. & Jantunen, H. Dielectric Losses of Microwave Ceramics Based on Crystal Structure. *Electromagnetic Materials and Devices* (InTech, 2018)

doi: 10.5772/intechopen.82483

43. Tamura, H. Microwave dielectric losses caused by lattice defects. *J Eur Ceram Soc* **26**, 1775–1780 (2006).

5 Microwave-assisted Catalysis: Propene Selective Oxidation by Bismuth Molybdate and Bismuth Vanadate

5.1 introduction

5.1.1 Aims

The main aim of this chapter is to investigate the sol-gel synthesized bismuth molybdate catalysts. In Chapter 4, hydrothermally synthesized γ-Bi_2MoO_6 was thoroughly investigated under microwave heating. The non-calcined hydrothermally synthesized samples gave an excellent acrolein yield under microwave conditions, but the stability was poor, while the calcined samples performed worse in terms of acrolein yield but showed better stability. This indicates that a calcination step is crucial to form a stable catalyst for microwave heating.

The process of synthesizing γ-Bi_2MoO_6 by the sol-gel method includes a calcination step. According to the results shown in Chapter 3, sol-gel synthesized γ-Bi_2MoO_6 is also activate under microwave heating and showed good acrolein selectivity. Therefore, γ-Bi_2MoO_6 synthesized by the sol-gel method is a good candidate material to give both activity and stability under microwave heating. Sol-gel synthesized γ-Bi_2MoO_6 will be one of the key catalysts to be investigated in this chapter.

Chapter 3 also showed that, although $BiVO_4$ did not perform as well as γ-Bi_2MoO_6, it was still very active under microwave conditions and can be regarded as a potential catalyst for the microwave-assisted selective oxidation of propene. Therefore, we will investigate mixed

bismuth molybdate and vanadate materials by exchanging molybdenum for an equal amount of vanadium to investigate if there is any enhanced performance.

5.1.2 An Overview of Relevant Research

The sol-gel method was considered as an effective pathway to afford pure phases of these catalysts. Bismuth molybdate had been successfully synthesized by sol-gel methods previously. Godard and co-workers prepared bismuth molybdates by a citrate-based method from aqueous solutions of Bi^{3+} and Mo^{6+} and citric acid in equivalent amounts[1], whereas Wildberger and co-workers used an alkoxide method to prepare bismuth molybdates supported on titania[2]. The gelation occurs at low temperatures and results in amorphous materials with unique morphology and high dispersion of the active compound. Bismuth molybdates are obtained by calcining these materials at around 500 °C.

The studies of propene selective oxidation to acrolein over sol-gel synthesized bismuth molybdate catalysts has been reported by Le's group. In 2017, Le and co-workers reported a comprehensive study of the sol-gel synthesis of bismuth molybdates at different pH values and theoretical molar Bi/Mo/citric acid atomic ratios[3]. They attempted to synthesize bismuth molybdate at different pH values and concluded that pH=5 was the best condition for making bismuth molybdate used in propene to acrolein, and at neutral and basic pH, it was difficult to obtain the pure phases of bismuth molybdates. Later in 2018, Le summarized recent research on the development of bismuth molybdate-based catalysts with new achievements in the catalysis field[4].

Adding vanadium into bismuth molybdate catalysts for the selective oxidation of propene to produce acrolein was reported by Alexis' group in 2013.[5] They carried out a systematic investigation of the kinetics of propene oxidation to acrolein over $Bi_{1-x/3}V_{1-x}Mo_xO_4$. The

activity and selectivity of $Bi_{1-x/3}V_{1-x}Mo_xO_4$ for the oxidation of propene to acrolein changes in a systematic manner with the value of x = Mo/(Mo + V). The best activity for acrolein formation occurs when x = 0.45, whereas the maximum in the selectivity to acrolein occurs at x = 0.15. They also use XANES spectra to establish which elements in the catalysts are reduced during the propene oxidation. They concluded that for all compositions of $Bi_{1-x/3}V_{1-x}Mo_xO_4$, bismuth is not reduced after exposure to propene. However, under the reaction conditions molybdenum was reduced from Mo^{6+} to Mo^{4+}, and vanadium was reduced from V^{5+} to V^{4+}. They also indicated that at temperatures above 370 °C, the rate of acrolein formation is first order in the partial pressure of propene and zero-order in the partial pressure of oxygen for all values of x between 0 and 1, suggesting that the catalyst is fully oxidized and that the formation of acrolein does not involve gas-phase O_2.

Another two papers based on propene oxidation over bismuth molybdate vanadate mixed metal oxide catalysts were published by Alexis and coworkers in 2014 and 2015. In these papers, they investigated how the band energy[6] and crystal structure[7] influence the selective oxidation of propene to acrolein. They studied propene oxidation over Bi, Mo, V oxides having the aurivillius structure with the composition $Bi_4V_{2-x}Mo_xO_{11+x/2}$ (x = 0−1) and compared them with scheelite structured $Bi_{2-x/3}Mo_xV_{1-x}O_{12}$ (x = 0−1). They explained that catalysts with bandgaps greater than 2.1 eV can usually achieve more than 75% acrolein selectivity for the conditions used and independent of the propene conversion, while for catalysts with bandgaps lower than 2.1 eV, the intrinsic selectivity to acrolein decrease rapidly, they suggested that this is due to the lower bandgap material's lattice oxygen mobility. Later, they studied the bismuth vanadium molybdenum oxide catalysts into the oxidative dehydrogenation of propane to propene and defined the effects of catalyst and reactant composition on the reaction kinetics[8].

5.2 Characterization

5.2.1 XRD

Bismuth molybdate vanadate samples were prepared by sol-gel method with different V amount, the samples are labelled as S1-S7 with V content from low to high. The XRD patterns of the materials with different Mo/V ratios, which were made by the sol-gel method are shown in Figure 5.1.

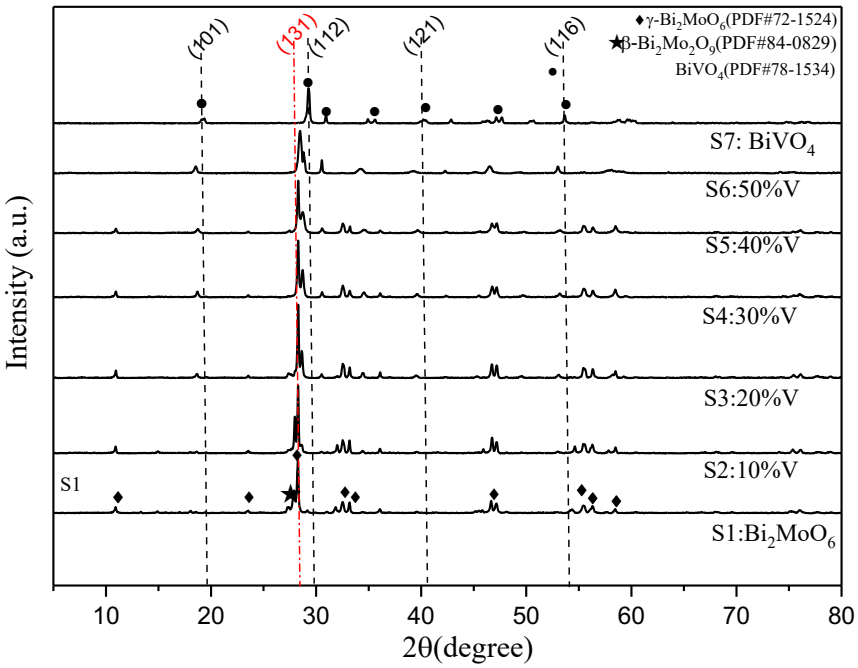

Figure 5.1 The XRD patterns of the bismuth molybdate vanadate samples prepared with different V amount

The XRD patterns revealed that S1 is mainly the orthorhombic structure Bi_2MoO_6 combined with a small amount of $Bi_2Mo_2O_9$. S2 is still the orthorhombic structure but splitting of the

peak at $2\theta = 28°$ is observed. This is due to V^{5+} cations replace an equivalent number of Mo^{6+} cations at the orthorhombic sites which creates O vacancies.

The patterns of S3-S5 show two structures are present, orthorhombic structured Bi_2MoO_6 which is noted by X-ray powder diffraction peak marked (131); and tetragonal structured $Bi_{1-X/3}V_{1-x}Mo_XO_4$ which is identified by the X-ray powder diffraction peaks marked (101) (112) (121) and (116). A similar structure has been reported previously which was described as a $Bi_{1-X/3}V_{1-x}Mo_XO_4$ solid solution[5,9,10]. In $Bi_{1-X/3}V_{1-x}Mo_XO_4$ solid solutions, Mo^{6+} cations replace an equivalent number of V^{5+} cations at the tetrahedral sites, leaving vacancies evidenced by the splitting of the peaks at $2\theta = 19°$, 29°,47°, and 53°[10]. S6 contains only tetragonal structured $Bi_{1-X/3}V_{1-x}Mo_XO_4$ with x = 0.4 and S7 is indexed to $BiVO_4$ with tetragonal structure.

Using the reference intensity ratios (RIR) from the International Centre for Diffraction Data reference patterns, based on the intensity of the reflections in the powder pattern compared to corundum (I/Ic), the relative amounts of each phase could be estimated, and these are shown in Table 5.1.

Although the use of RIR can only be considered semi-quantitative, some general observations can be made from the analysis. The relative amount of $BiVO_4$ tetrahedral phases is seen to increase with increasing vanadium content. The stoichiometry indicates that excess bismuth will be present when the $Bi_{1-X/3}V_{1-x}Mo_XO_4$ tetrahedral phase is formed, so that X-ray amorphous Bi_2O_3 should be formed in high vanadium ratio samples.

Table 5.1 Relative amounts of phases present in bismuth molybdate vanadate materials prepared with different Mo:V ratios

Sample	**Composition from powder XRD patterns (%)**		
	Bi_2MoO_6/ orthorhombic	$BiVO_4$/ tetrahedral	$Bi_2Mo_2O_9$/ Monoclinic
Bi_2MoO_6	92.63	0	7.37
10%V	87.63	0	12.37
20%V	79.46	21.54	0
30%V	63.86	35.14	0
40%V	56.76	43.24	0
60%V	0	100	0
$BiVO_4$	0	100	0

Table 5.2 Crystallite Size and Lattice Constants for bismuth molybdate vanadate samples prepared with different V amounts(O for Orthorhmobic, T for Tetrahedral, and M for Monoclinic)

Samples	Crystallite Size (Å)		Lattice Parameters						
			a	*b*	*c*	*α*	*β*	*γ*	Volume
Bi_2MoO_6	607	O	5.50	16.20	5.49	90	90	90	490
	394	M	11.94	10.82	10.87	90	89.81	90	1534
Replacing 10% Mo by V	599	O	5.50	16.20	5.48	90	90	90	489
	665	M	11.90	10.79	11.85	90	90.62	90	1521
Replacing 20% Mo by V	588	O	5.50	16.20	5.48	90	90	90	489
	442	T	5.21	5.21	11.69	90	90	90	317
Replacing 30% Mo by V	580	O	5.50	16.20	5.48	90	90	90	489
	352	T	5.19	5.19	11.69	90	90	90	315
Replacing 40% Mo by V	536	O	5.51	16.18	5.48	90	90	90	488
	289	T	5.17	5.17	11.82	90	90	90	317
Replacing 60% Mo by V	270	T	5.21	5.21	11.72	90	90	90	317
$BiVO_4$	381	T	5.10	5.10	11.58	90	90	90	301

Crystallite size and lattice constants for bismuth molybdate vanadate samples are shown in Table 5.2. the crystallite size of orthorhombic structured Bi_2MoO_6 is found to decrease with increasing vanadium content. Also, the crystallite size of tetragonal structured

$Bi_{1-X/3}V_{1-x}Mo_xO_4$ (vanadium content less than 60%) and $BiVO_4$ (vanadium content higher than 60%) are found to decrease with increasing vanadium content.

5.2.2 Raman

Raman spectra of the bismuth molybdate vanadate materials were obtained using a Renishaw Ramascope, Raman and spectra are shown in Figure 5.2.

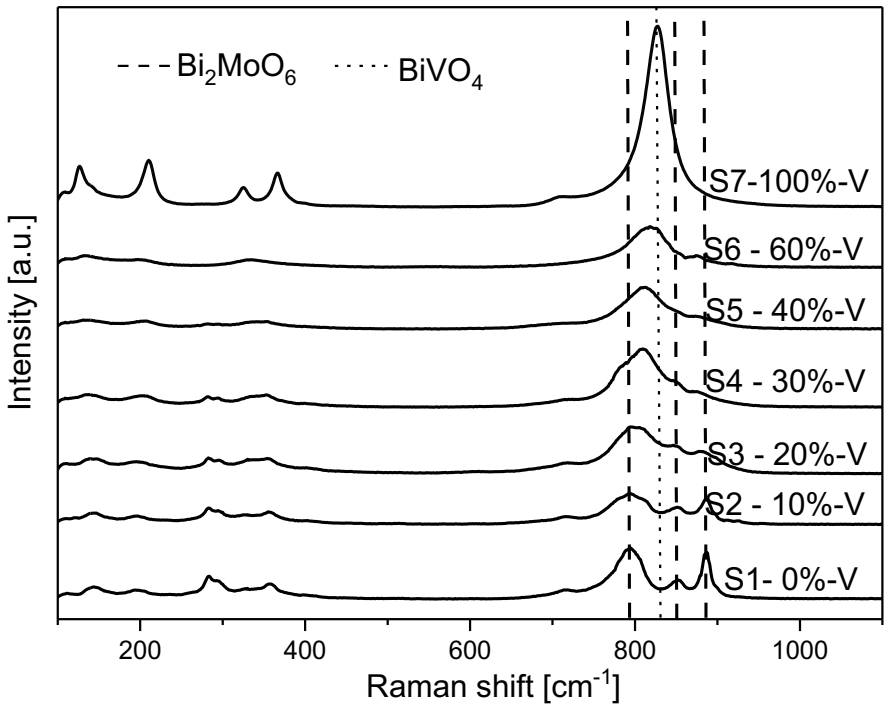

Figure 5.2 Raman spectroscopy

The spectra of the material without vanadium (S1) contains most of the characteristic bands of γ-Bi_2MoO_6 at around 144, 198, 288, 360, 720, 795, 849 and 898 cm^{-1}. The peaks in the 180–500 cm^{-1} range originated from bending modes of the MoO_6 octahedrons coupled with stretching and bending modes of the bismuth-oxygen polyhedrons. The Raman modes near 290

cm^{-1} are from the E_g bending vibrations. Those at 325, 340, and 401 cm^{-1} corresponded to the E_u symmetric bending. The mode at 712 cm^{-1}, exhibiting no evident shift or broadness, was specified as the asymmetric stretching vibration (E_u mode) of the MoO_6 octahedrons involving the motion of equatorial oxygen atoms joining the MoO_6 octahedrons within the layers. The Raman vibrations at 795 cm^{-1} (A_{1g} mode) and 849 cm^{-1} (A_{2u} mode) were, respectively, assigned to the symmetric and asymmetric stretching vibrations of the MoO_6 octahedrons involving the motion of apical oxygen atoms, normally directed to the $(Bi_2O_2)^{2+}$.[11–16].

The spectra of S7 that does not contain molybdenum contains most of the characteristic bands of $BiVO_4$ at around 129, 210, 330, 370, 710, and 826 cm^{-1}. The Raman band at 826 cm^{-1} is assigned to v_s(V–O), and the weak shoulder at about 710 cm^{-1} is assigned to v_{as}(V–O). Bands near 370 and 330 cm^{-1}, are the symmetric A_g bending mode of vanadate anion δ_s (VO_4^{3-}) and the antisymmetric B_g bending mode of vanadate anion δ_{as} (VO_4^{3-}) modes, respectively. and external modes (rotation/translation) occur near 210 cm^{-1} and 129 cm^{-1}, respectively[17].

For the spectra of sample S2-S6 content different amounts of vanadium, Raman vibrations band at around 795 cm^{-1}, 849 and 898 cm^{-1} became weaker with increasing vanadium content and disappear when 60% vanadium is used. A shoulder peak assigned to the V-O vibration appears in the spectra of S2 -S6, at the range of 810-820 cm^{-1} and this gradually shifts right and become larger with the increasing of vanadium content and can be the evidence of the formation of the tetrahedral phase $Bi_{1-X/3}V_{1-x}Mo_XO_4$. According to the XRD result shown in Section 5.2.2, no diffraction pattern of tetrahedral phase $Bi_{1-X/3}V_{1-x}Mo_XO_4$ can be seen in S2 and S3, which means it does not have long range order and cannot show up in the XRD partern. This indicated that the Raman spectroscopy is more sensitive than XRD. When the vanadium content reaches 30%, its intensity surpasses the peak of Mo-O stretching and become the main peak.

5.2.3 BET

BET surface areas were determined by N_2 adsorption at -196 °C using a Quantachrome Quadrasorbevo instrument. The results are shown in Table 5.3.

Table.5.3 Specific surface area for bismuth molybdate vanadate samples

Sample	BET surface area (m^2/g)
Bi_2MoO_6	8
10%V	9
20%V	10
30%V	10
40%V	10
60%V	14
$BiVO_4$	17

Replacing molybdate with vanadium was shown to slightly increase the specific surface area of the catalyst. The increase in the specific surface area is due to the addition of vanadium decreasing the particle size as shown in Table 5.2).

5.2.4 Dielectric experiment

The dielectric properties were measured using a cyl-ε cavity operating at 2.5 GHz in the TM_{010} mode. Details of the cyl-ε cavity and method for calculating the dilectric properties were introduced in Section 2.3.4.

Table 5.4 Dielectric parameter of samples

Samples	Dielectric constant (ε')	Dielectric loss (ε'')
Bi_2MoO_6	1.0013	0.04738
10%V	1.0012	0.04927
20%V	1.0010	0.05364
30%V	1.0010	0.05776
40%V	1.0009	0.05833
60%V	1.0010	0.04289
$BiVO_4$	1.0013	0.02828

The dielectric constant (ε') does not show significant change for the materials with different V:Mo ratios, while replacing Mo with V leads to changes in the dielectric loss (ε''). The dielectric loss firstly increases with vanadium addition and reaches the maximum value at 40% vanadium. The dielectric loss starts to decrease at higher vanadium content and is considerably lower for the pure $BiVO_4$ phase.

As previously mentioned in Section 3.1, in microwave heating systems, it is understood that the interaction of materials with microwaves and the heating behaviour of materials by microwave irradiation is strongly dependent on their dielectric properties. The most important property related to the heating processes is the complex permittivity (ε^*), and the ratio of the dielectric loss and the dielectric constant is commonly used to measure the ability of a material to convert electromagnetic energy into heat energy, which is referred to as the loss tangent ($\tan\delta$). The loss tangent of bismuth molybdate vanadate catalysts is shown in Figure 5.3.

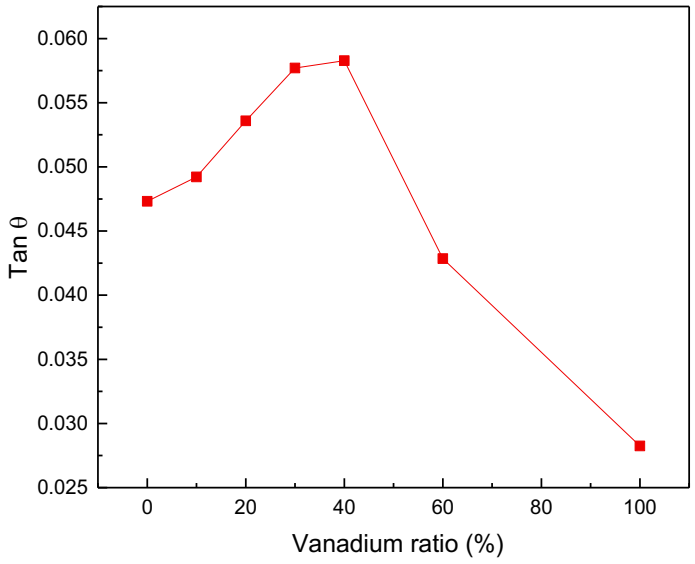

Figure 5.3 Loss tangent of bismuth molybdate vanadate catalysts synthesised with different V amount

With increasing vanadium content, the loss tangent of the samples rises to a maximum when the vanadium content is 40%. When the vanadium content is greater than 40%, the sample's loss tangent started to drop sharply with the increase of the vanadium content.

Samples with lower than 40% vanadium have a much larger loss tangent than the samples with a higher vanadium content. The main difference between samples with less vanadium and more vanadium is in their structure. According to the XRD data shown in section 5.2.1, within the vanadium range of 0-40%, all catalysts contain a certain amount of orthorhombic structured Bi_2MoO_6, and when the vanadium increased to more than 40%, the orthorhombic structure starts to disappear. This suggests that the orthorhombic structured Bi_2MoO_6 has a larger loss tangent (which was confirmed in section 3.5.2), and it is crucial for the catalyst to convert the energy in the microwave into heat. Also, in this range, the value of $\tan\delta$ increases with the

increased vanadium. The increase in the loss tangent may also be caused by an increasing number of defects in the sample. According to the XRD patterns shown in Figure 5.1, $Bi_{1-X/3}V_{1-x}Mo_XO_4$ solid solutions are present, where V^{5+} cations replace an equivalent number of Mo^{6+} cations at the orthorhombic sites, leaving a high concentration of vacancy in the catalyst structure. It has previously been reported that introducing defects in a dielectric material will increase the loss tangent[18,19]. This is because the dielectric loss tangent increases when the ions are non-uniformly distributed so that they break the periodic arrangement of charges in the crystal.

5.3 Catalyst Testing

5.3.1 Influence of Vanadium Content

To find investigate the influence of the V amount, the initial tests under microwave and conventional heating were carried out in a mixed flow of propene, oxygen, and nitrogen at 15 W microwave power or 400 °C respectively. Figure 5.4 shows the propene conversion over the bismuth molybdate vanadate catalysts with different vanadium content under microwave heating. The catalyst bed temperature under the microwave condition is also given in Figure 5.4.

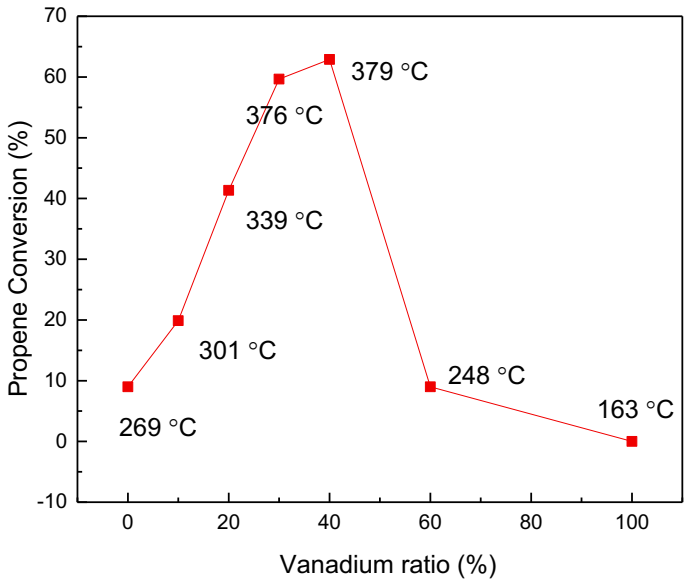

Figure 5.4 Propene conversion to vanadium ratio under microwave condition (15 W input power, 0.2 g of catalyst, propene:oxygen:nitrogen = 1:2:97, flow rate = 50 mL min^{-1})

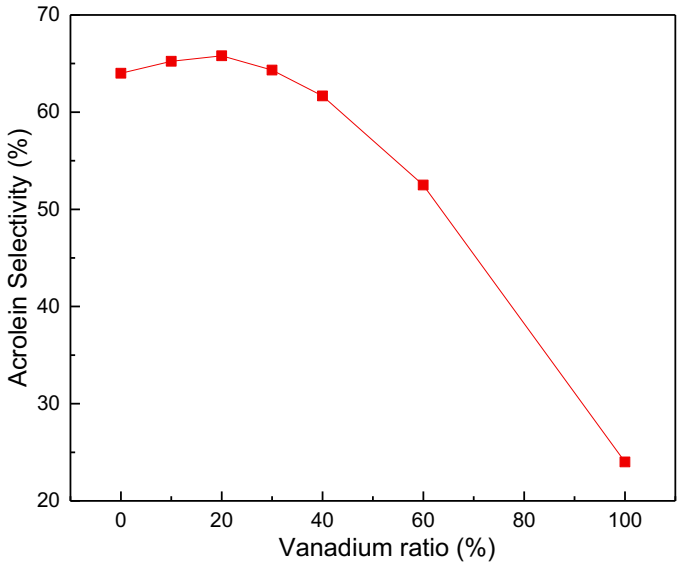

Figure 5.5 Acrolein selectivity to vanadium ratio under microwave condition (15 W input power, 0.2 g of catalyst, propene:oxygen:nitrogen = 1:2:97, flow rate = 50 mL min^{-1})

As the results show in Figure 5.4, replacing appropriate amounts of molybdenum with vanadium in the bismuth molybdate can improve the activity of catalysts under microwave heating, and the catalyst with 40% vanadium was found to give a 6 fold enhancement over the bismuth molybdate, which leads to the propene conversion increasing from 10% to 64%. When the vanadium content increases to 60%, the catalyst starts to become difficult to heat as the loss tangent reduces, and catalysts perform worse than the original Bi_2MoO_6. The propene conversion shows a positive correlation with the temperature of the catalyst bed. According to the dielectric parameters shown in Section 5.2.4, the 40% V sample has the largest loss tangent among the samples, which means that sample can convert the microwave energy into heat more effectively than other materials and reaches a higher temperature.

Figure 5.5 shows the acrolein selectivity over different catalysts at 15 W microwave power. Catalysts with vanadium content from 0-40% all display a good acrolein selectivity of more than 60%, with the best acrolein selectivity of 65% achieved by the material containg 20% V. However, it is hard to compare the selectivity between different samples, because there is more than one factor that can affect the selectivity, for example, the structure of the catalyst and the temperature the catalyst bed can achieve. To have a clearer understanding of the influence of vanadium substitution, conventional tests was also done at a fixed temperature of 400 °C.

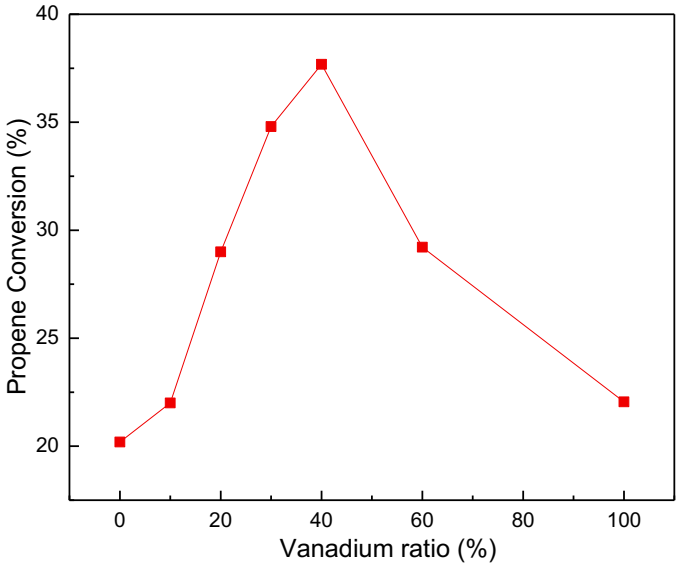

Figure 5.6 Propene conversion to vanadium ratio in conventional heating (400 °C, 0.2 g of catalyst, propene:oxygen:nitrogen = 1:2: 97, flow rate = 50 mL min^{-1})

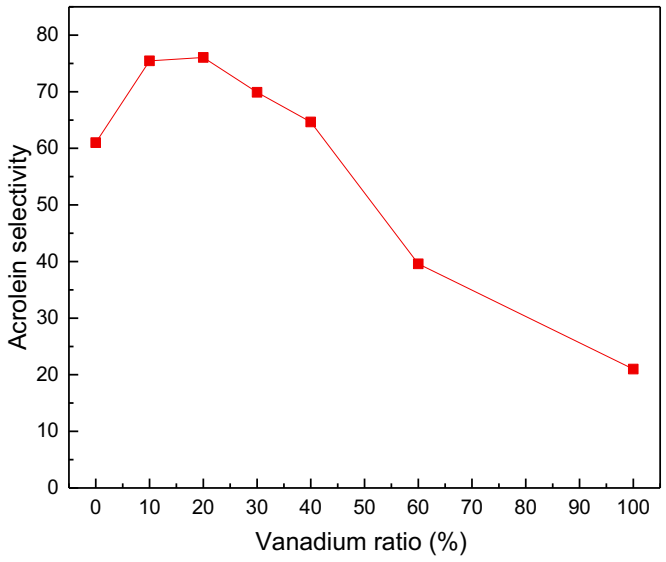

Figure 5.7 Acrolein selectivity to vanadium ratio in conventional heating (400 °C, 0.2 g of catalyst, propene:oxygen:nitrogen = 1:2:97, flow rate = 50 mL min^{-1})

Apart from explaining the influence of the dielectric properties, probing the active catalytic site is also important for an understanding of the performance under microwave heating. As the results show in Figure 5.6 and Figure 5.7, in conventional heating, replacing molybdenum with vanadium also improves samples' catalytic activity and acrolein selectivity. The trend is very similar to the microwave tests, with the 40%V sample giving the highest conversion under conventional testing, and when the vanadium ratio increases, the activity begins to drop. The acrolein selectivity also shows a similar trend with the microwave test results, with high selectivity at low vanadium content which drops when it goes above 20% V.

The results of conventional tests with fixed temperature revealed that temperature is not the only factor for the performance of bismuth vanadate molybdate samples, and the composition and structure of catalysts also play an important role. Replacing 40% molybdenum with vanadium in the bismuth molybdate can improve the propene conversion from 20% to 38%. This result is consistent with previous research investigating the influence of vanadium content on catalyst activity[5,20]. In addition, replacing 20% molybdenum with vanadium in the bismuth molybdate can improve the acrolein selectivity from 60% to 80%. This observation is similar to the results reported by Alexis' group[5]. They investigated the kinetics of propene oxidation over bismuth molybdate vanadate mixed metal oxide catalysts and found that, with the increasing of the vanadium content, the formation of tetragonal structure $Bi_{1-X/3}V_{1-x}Mo_xO_4$ will facilitate the production of CO and CO_2, and thus leads to the drop in acrolein selectivity.

5.3.2 Microwave heating: Influence of Input Power

As discussed in Section 5.3.1, sample containing 40% V is the most efficient catalyst to absorb energy in the microwave and so this material was tested in the microwave cavity at different

powers from 2.5 W to 25 W. The temperature of the catalyst bed was measured by an infrared camera and the results shown in Figure 5.8.

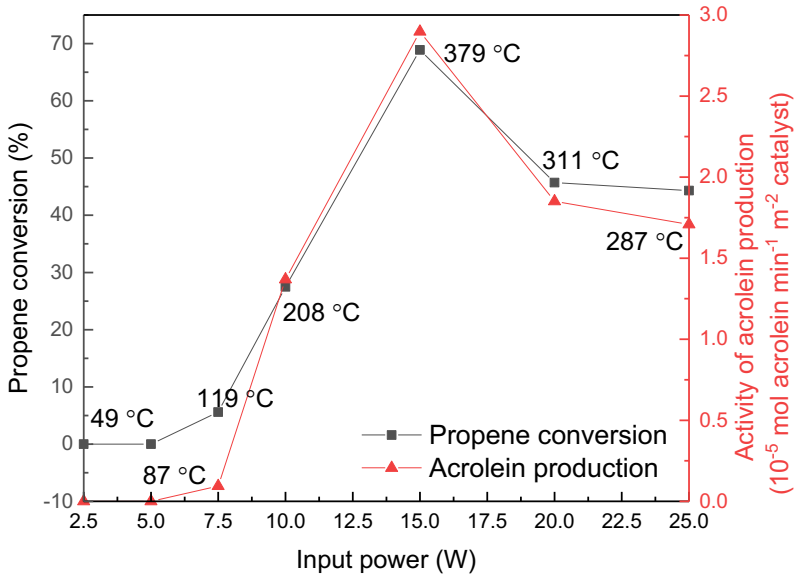

Figure 5.8 Propene conversion and rate of acrolein production from sample 40% V in different power input power (0.2 g of catalyst, propene:oxygen:nitrogen = 1:2:97, flow rate = 50 mL min^{-1})

Figure 5.8 illustrates how the propene conversion and acrolein production rate change with increasing microwave power. The acrolein production initially increases as the input power increases and then decreases at higher power input. The best acrolein production rate is 2.7×10^{-5} mol acrolein min^{-1} m^{-2} catalyst.

As mentioned in section 5.2.4, sample 40% V has a good ability to convert the electromagnetic energy into heat and the temperature of the catalyst bed increases rapidly with increasing input power. In the low power range (<7.5 W), the catalyst bed temperature is relatively low, and no

propene was converted and no acrolein was produced. This is because the catalyst did not absorb enough energy from the microwave to reach the reaction temperature. When the input power increases to 7.5 W, the catalyst starts to show activity, and then the highest activity is achieved by 15 W input power. In the input power region ranges between 7.5 W and 15 W, the propene conversion and acrolein production both experienced sharp rises. The good performance of the 40% V sample demonstrate that this is a good candidate as a catalyst for microwave-assisted propene selective oxidation.

In the higher power region (> 15 W), the propene conversion and acrolein production showed a decreasing trend. In this region, the temperature of the catalyst bed increases sharply at first and reaches a very high temperature which is higher than 600 °C in a very short time, and then decreases dramatically and cannot successfully reach a steady state. The uncontrollable temperature is a sign of the 'thermal runaway' effect that can occur at high power under microwave heating [21]. Zhang and Hayward reported this phenomenon in their review of the applications of microwave-assisted heating in the field of environmental-related heterogeneous catalysis and concluded that there is a critical power value. When the input power is less than the critical power, the sample will heat up to a steady temperature, but for input powers above critical power, the temperature will continue to rise uncontrollably (Thermal runaway). In the 'thermal runaway' situation, the sample temperature will keep on rising until the sample melts, decomposes or electrical breakdown occurs.

However, there is an interesting phenomenon observed following the 'thermal runaway'. If the microwave irradiation is stopped and the catalyst bed allowed to cool down, a steady catalyst bed temperature will be reached in the next run. As shown in Figure 5.8, the steady temperature for 20 W and 25 W is lower than the temperature reached in the 15 W input. This may be because the uncontrolled high temperature that happened in the first run has caused the

sintering or phase change of the catalyst that led to a change in the dielectric properties of the sample. Further dielectric measurements should be taken to investigate this hypothesis.

5.3.3 Comparision between Microwave-assisted and Conventional Heating

Observing the results from the microwave-assisted process alone is not enough to thoroughly evaluate the performance. To understand the effect of the microwave, parallel conventional testing and a comparison between the two processes was carried out.

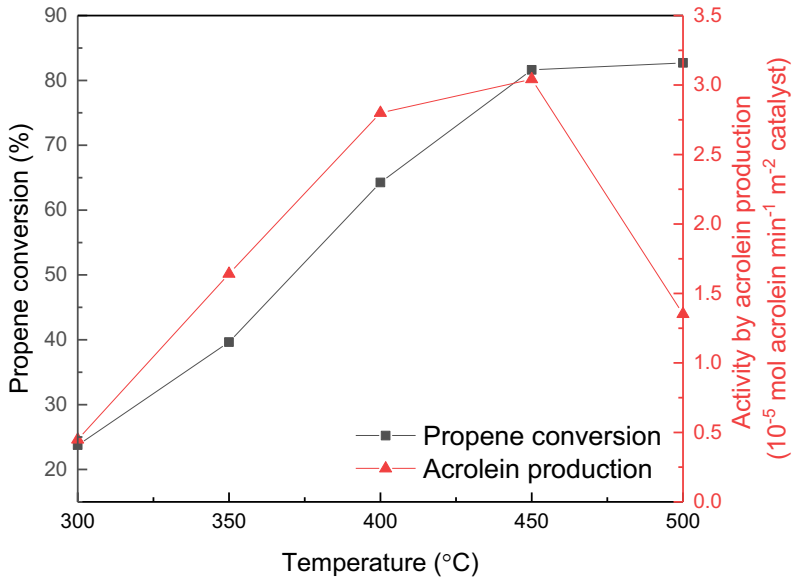

Figure 5.9 Propene conversion and activity of acrolein production from sample 40% V under conventional heating (0.2 g of catalyst, propene:oxygen:nitrogen = 1:2:97, flow rate = 50 mL min^{-1})

The most promising catalyst from the microwave-assisted process, containing 40% V, was tested under conventional heating conditions. Figure 5.9 illustrates how the propene conversion and acrolein production rate change with increasing catalyst bed temperature. As can be seen,

the propene conversion increases with increasing temperature, while the highest acrolein production rate was achieved at 450 °C, not at the higher temperature. This is because, in a higher temperature region (greater than 450 °C), the selectivity of CO and CO_2 starts to increase over the tetrahedral phase bismuth molybdate vanadate mixed metal oxide catalysts. Similar results have been reported previously[5,20,22], with the Zheng suggesting a correlation between the acrolein selectivity and the bandgap of the catalyst [20] having observed that when the catalyst's bandgap falls below 2.1 eV, the intrinsic selectivity to acrolein decreases rapidly and then decreases further with increasing propene conversion. They explained that when the activity of oxygen atoms at the catalyst surface becomes very high, two processes become more rapid – the oxidation of the intermediate from which acrolein is formed and the sequential combustion of acrolein to CO_2. They investigated the scheelite structured $Bi_{2-x/3}Mo_xV_{1-x}O_{12}$ (x = 0-1) catalyst for the propene selective oxidation and found that the bandgap of this catalyst decreases with the increasing of V content.

Looking at Figure 5.8, the best acrolein production rate in microwave testing was achieved at 15 W input power and reached the best acrolein production rate at around 2.9×10^{-5} mol acrolein min^{-1} m^{-2} catalyst with catalyst bed temperature at 379 °C. As shown in Figure 5.9, a similar acrolein production rate at 3.0×10^{-5} mol acrolein min^{-1} m^{-2} catalyst is achieved at 450 °C in the conventional test. By comparing the acrolein production rate of conventional processes and microwave-assisted processes, a conclusion can be drawn that the catalyst performance is largely related to the temperature of the catalyst bed. Analysing the catalyst bed temperature from the best performance in both processes, a much lower catalyst bed temperature can be found. Although the catalyst bed temperature of the best point in the microwave test is much lower than the temperature in the conventional test, we still cannot say that the microwave has any non-thermal effects, as the temperature measured is the overall

temperature of the whole catalyst bed. The 'hotspot' effect should be responsible for the observed temperature decreases, and this hypothesis had been suggested previously and had been introduced in detail in Chapter 4.

In catalytic terms, the bismuth molybdate vanadate catalyst can actively produce acrolein in both processes. Although no rate enhancement has been made by the microwave-assisted catalytic process, it is still meaningful to use the microwave as an energy supplement. As explained in Chapter 2, the microwave cavity used in this project can deliver the microwave directly to the sample packing in the middle of the cavity, and it is energy efficient. The oven used in conventional heating tests is operated by an electrical heater. Unlike the microwave passes through the surrounding gases and quartz tube and directly interact with the catalyst bed, the conventional electrical heater heats the catalysts bed by conduction and convection, and it needs to heat the surrounding stuff first. A much larger amount of energy is consumed by heating the devices and surrounding gases.

5.4 Conclusion

The original bismuth molybdate made in this part of the work is a mixture phase of γ-Bi_2MoO_6 with orthorhombic structure and a small amount of β-$Bi_2Mo_2O_9$ with monoclinic structure. Replacing Mo in the γ-Bi_2MoO_6 into V can cause changes in both crystallite size and structure. When the V content is smaller than 20%, the catalyst remains mixture of orthorhombic and monoclinic structures, and the crystallite size decreases. When the V content gets larger, the β-$Bi_2Mo_2O_9$ starts to disappear, and a tetrahedral phase $Bi_{1-X/3}V_{1-x}Mo_XO_4$ is formed. Both the crystallite size of orthorhombic γ-Bi_2MoO_6 and tetrahedral phase $Bi_{1-X/3}V_{1-x}Mo_XO_4$ decrease with increasing vanadium content up to 60%.

Replacing appropriate amounts of molybdenum with vanadium can increase the samples' ability to convert the electromagnetic microwave energy into heat and enhances the propene conversion and the acrolein production rate. The investigation of the performance of bismuth molybdate vanadate with different V ratios in both the microwave cavity and conventional reactor reveals that, in terms of acrolein production, 40% V sample is the best in both processes. Changing the input power of the microwave can affect the performance. By investigating the performance of 40% V sample when heated by the microwave field at different powers, a non-monotonic relationship between input power and propene conversion and acrolein production rate is found. In the lower power region the propene conversion and acrolein production have both experienced exponential rises with increased power. However, in the higher power region, the propene conversion and acrolein production did not continuously increase with input power increase and showed a declining trend which could be caused by the catalyst sintering and or reducing at the extremely high temperature produced by the 'Thermal runaway' effect at higher power.

Compared with using conventional heating techniques, a comparable acrolein production rate can be achieved by using a microwave and two main advantages were found. Firstly the reaction temperature can be largely reduced and the 'hotspot' effects could be responsible for the observed temperature decreases. Secondly, the microwave process is more energy efficient. Microwave can pass through the surrounding gases and quartz tube and directly interact with the catalyst bed, which makes it a much more efficient process than conventional heating.

Reference

1. Godard, E., Gaigneaux, E. M., Ruiz, P. & Delmon, B. New insights in the understanding of the behaviour and performances of bismuth molybdate catalysts in the oxygen-assisted dehydration of 2-butanol. *Catalysis Today* **61**, 279–285 (2000).
2. Wildberger, M. D., Grunwaldt, J. D., Maciejewski, M., Mallat, T. & Baiker, A. Sol-gel bismuth-molybdenum-titanium mixed oxides I. Preparation and structural properties. *Applied Catalysis A: General* **175**, 11–19 (1998).
3. Le, M. T., Do, V. H., Truong, D. D. & Pham, N. N. Sol-Gel Synthesis of Bismuth Molybdate Catalysts for the Selective Oxidation of Propylene to Acrolein: Influence of pH Value and Theoretical Molar Atomic Ratio. *Journal of the Chinese Chemical Society* **64**, 1326–1332 (2017).
4. Le, M. T. Bismuth Molybdate-Based Catalysts for Selective Oxidation of Hydrocarbons. in *Bismuth - Advanced Applications and Defects Characterization* (InTech, 2018). doi:10.5772/intechopen.75105
5. Zhai, Z., Getsoian, A. B. & Bell, A. T. The kinetics of selective oxidation of propene on bismuth vanadium molybdenum oxide catalysts. *Journal of Catalysis* **308**, 25–36 (2013).
6. Getsoian, A., Zhai, Z. & Bell, A. T. Band-gap energy as a descriptor of catalytic activity for propene oxidation over mixed metal oxide catalysts. *Journal of the American Chemical Society* **136**, 13684–13697 (2014).
7. Zhai, Z., Wütschert, M., Licht, R. B. & Bell, A. T. Effects of catalyst crystal structure on the oxidation of propene to acrolein. *Catalysis Today* **261**, 146–153 (2016).
8. Zhai, Z., Wang, X., Licht, R. & Bell, A. T. Selective oxidation and oxidative dehydrogenation of hydrocarbons on bismuth vanadium molybdenum oxide. *Journal of Catalysis* **325**, 87–100 (2015).

9. Zhou, D. *et al.* Phase evolution and microwave dielectric properties of xBi $_{2/3}MoO_4$-(1-x)$BiVO_4$ ($0.0 \leq x \leq 1.0$) low temperature firing ceramics. *Dalton Transactions* **43**, 7290–7297 (2014).

10. Nell, A., Getsoian, A. Q., Werner, S., Kiwi-Minsker, L. & Bell, A. T. Preparation and characterization of high-surface-area $Bi_{(1-x)/3}V_{1-x}Mo_xO_4$ catalysts. *Langmuir* **30**, 873–880 (2014).

11. Matsuura, I., Schut, R. & Hirakawa, K. The surface structure of the active bismuth molybdate catalyst. *Journal of Catalysis* **63**, 152–166 (1980).

12. Schuh, K. *et al.* Bismuth molybdate catalysts prepared by mild hydrothermal synthesis: Influence of pH on the selective oxidation of propylene. *Catalysts* **5**, 1554–1573 (2015).

13. Gruar, R., Tighe, C. J., Reilly, L. M., Sankar, G. & Darr, J. A. Tunable and rapid crystallisation of phase pure Bi_2MoO_6 (koechlinite) and $Bi_2Mo_3O_{12}$ via continuous hydrothermal synthesis. *Solid State Sciences* **12**, 1683–1686 (2010).

14. Mączka, M. *et al.* Pressure-induced phase transitions in ferroelectric Bi_2MoO_6—a Raman scattering study. *Journal of Physics: Condensed Matter* **22**, 015901 (2009).

15. Li, H., Liu, C., Li, K. & Wang, H. Preparation, characterization and photocatalytic properties of nanoplate Bi_2MoO_6 catalysts. *Journal of Materials Science 2008 43:22* **43**, 7026–7034 (2008).

16. Phuruangrat, A. *et al.* Hydrothermal synthesis and characterization of Bi_2MoO_6 nanoplates and their photocatalytic activities. *Journal of Nanomaterials* **2013**, (2013).

17. Pang, L. X. *et al.* Structure–property relationships of low sintering temperature scheelite-structured $(1 - x)BiVO_4$–$xLaNbO_4$ microwave dielectric ceramics. *Journal of Materials Chemistry C* **5**, 2695–2701 (2017).

18. Ohsato, H., Varghese, J. & Jantunen, H. Dielectric Losses of Microwave Ceramics Based on Crystal Structure. *Electromagnetic Materials and Devices* (InTech, 2018)

19. Tamura, H. Microwave dielectric losses caused by lattice defects. *Journal of the European Ceramic Society* **26**, 1775–1780 (2006).

20. Ikawa, T. Catalytic Properties of Tricomponent Metal Oxides Scheelite Structure Having the Scheelite Structure. *Journal of Catalysis* **368**, 360–368 (1986).

21. Zhang, X. & Hayward, D. O. Applications of microwave dielectric heating in environment-related heterogeneous gas-phase catalytic systems. *Inorganica Chimica Acta* (2006).

22. Zhai, Z., Wütschert, M., Licht, R. B. & Bell, A. T. Effects of catalyst crystal structure on the oxidation of propene to acrolein. *Catalysis Today* **261**, 146–153 (2016).

6 Microwave-assisted Catalysis: Propene Selective Oxidation by Silicon Carbide Promoted Bismuth Molybdate

6.1 Introduction

6.1.1 Aims

In Chapter 3, a nickel catalyst supported by silicon carbide (SiC) was proved to be effectively heated under microwave conditions, which suggests that SiC could be a good promoter in microwave-assisted processes if in close contact to a catalytically active material. In this chapter, two groups of silicon carbide supported bismuth molybdate catalysts were tested under both microwave and conventional conditions, and the effect of bismuth and molybdenum ratio in the catalyst synthesis procedure and the influence of bismuth molybdate loading amount were investigated.

6.1.2 Review of Relevant Research

SiC has been established as a novel support for heterogeneous catalysis reactions, because of its several appealing properties like high heat conductivity, superior mechanical strength and thermal stability[1]. Porous SiC materials have been demonstrated as ideal alternative supports in several industrial catalytic processes like Fischer–Tropsch synthesis[2] and H_2S selective oxidation and Friedel–Crafts benzoylation[3]. For most of the applications, SiC's excellent stability and thermal conductivity allow it to maintain good and stable performance[4,5].

In recent years, with the development of microwave-assisted applications in chemical reactions, SiC has once again emerged as a promising support material. The excellent dielectric and physical properties of SiC make it a popular choice in microwave-assisted chemistry. SiC is an excellent microwave absorbent which makes it a good support candidate for microwave-assisted catalysis, it can efficiently convert the microwave energy into heat and then activate the active component on its surface to initiate the chemical reaction[6,7]. At the same time, the high thermal conductivity of SiC significantly improves the heat transfer in catalytic processes by reducing the formation of local hot spots as well as gradient temperature across the catalyst bed[3]. Therefore, SiC can potentially enable easy and precise temperature control of the catalyst bed when incorporated into a microwave-assisted catalytic system.

Recently, SiC has been widely used in microwave-assisted catalysis research and has demonstrated many promising results. In 2015, Guo and co-workers prepared a novel Cu-Mn-Ce oxide/SiC monolithic catalyst by a sol-gel method and tested it for microwave-assisted catalytic toluene oxidation, and they compared the performance of microwave-assisted reaction with the conventional heating. They concluded that the monolithic catalyst showed much better catalytic activity for toluene oxidation under microwave heating in the low-temperature range. At 350 °C, 90% of toluene conversion was obtained under microwave heating, while only 40% under conventional heating[8]. A similar catalyst system was used by Bo and Sun in 2019 for the same reaction under microwave conditions[9]. In 2018, Zhang and co-workers used Fe/SiC catalyst for the CH_4-CO_2 reforming reaction under microwave irradiation. They illustrated that the microwave dry reforming reaction can be divided into a rapid reaction stage, slow reaction stage, and reaction equilibrium stage. The conversion of reactants and selectivity of products in the slow reaction stage were both higher than 95% under the power density of 90 W/g. They also carried out a stability test for 50 hours, in which the catalyst activity did not reduce

significantly, and the amount of carbon formed on the catalyst surface was also negligible. These results indicate that the cheap Fe-based catalyst has good catalytic activity and stability under microwave irradiation and hence is a promising material for this application[10]. In 2020, Wang and co-workers reported the microwave-assisted catalytic cracking strategy for 5-5′ C(phenyl)–C(phenyl) bonds cleavage. In their research, SiC was modified as the catalyst support for the carbide-derived carbon (CDC) layer to form CDC-SiC, and then the Pt/CDC-SiC catalyst was prepared to use in the microwave-assisted reation[11]. Pt/CDC-SiC exhibited a high selectivity to monomers with total mass yields of 49.3 wt %. The conversion rate increased from 17.1% to 85% with Pt/CDC-SiC under the dynamic vapour flow reaction system.

6.2 Characterization

6.2.1 XRD

The SiC supported materials were synthesised by the sol-gel method described in full in Chapter 2, a physical mixed sample made with 0.2 g and 1 g SiC were also made and sign as 20% $Bi_2Mo_3O_{12}$&SiC. The XRD patterns of the two groups of materials made with different ratios of Bi:Mo are shown in Figure 6.1 and Figure 6.2.

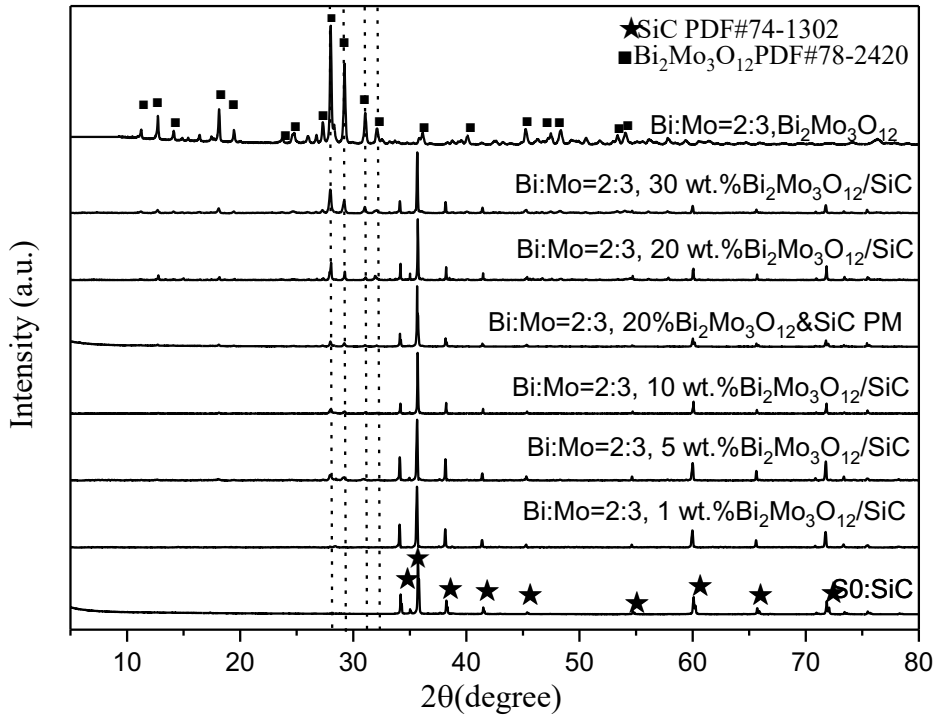

Figure 6.1 XRD patterns of the bismuth molybdate catalysts supported on SiC made with Bi:Mo = 2:3

Figure 6.1 shows the XRD patterns of catalysts made from solution with Bi:Mo = 2:3. After the loading of bismuth molybdate onto the SiC support, the characteristic XRD peaks corresponding to $Bi_2Mo_3O_{12}$ at 2θ = 27.9°, 29.2°, 31.0° and 32.0° were found in catalyst samples with loadings above 5wt.%.

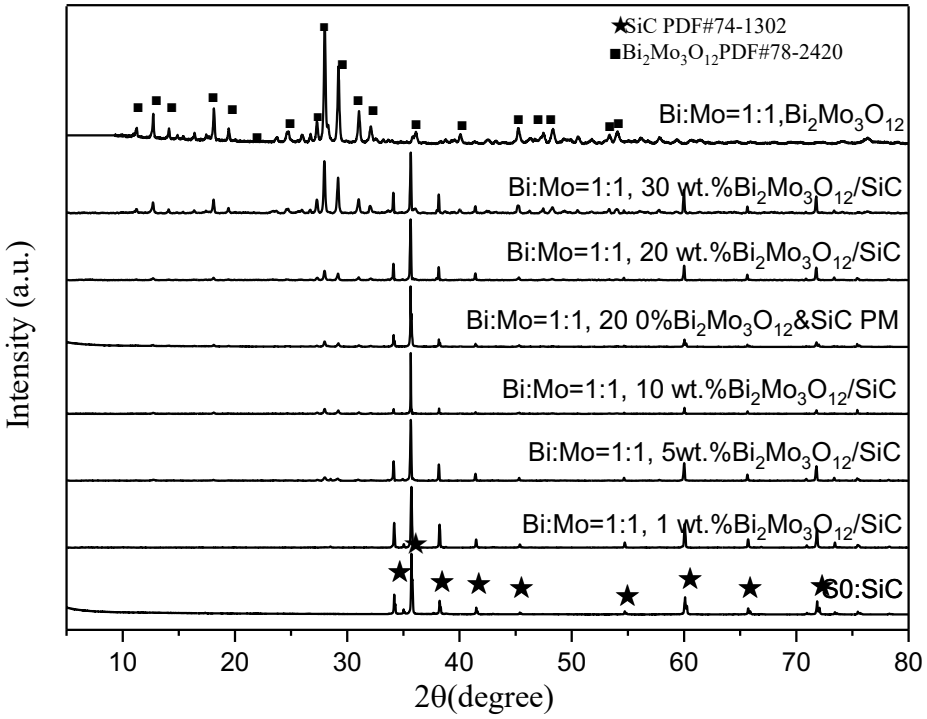

Figure 6.2 XRD patterns of the bismuth molybdate catalysts supported on SiC made with Bi:Mo = 1:1

Figure 6.2 shows the XRD patterns of catalysts made from solution with Bi:Mo = 1:1. Similar to the samples made with a lower Bi:Mo ratio, the characteristic XRD peaks corresponding to $Bi_2Mo_3O_{12}$ at 2θ = 27.9°, 29.2°, 31.0° and 32.0° were found in catalyst samples with loading larger than 5 wt.%. By comparing XRD patterns in Figure 6.1 and Figure 6.2, there is no obvious difference between two group of samples made by precursors solutions with different Bi:Mo ratios. For the Bi:Mo=1:1 group, the excessive bismuth in should form amorphous Bi_2O_3, which would be further conformed by other characterization method in the later Sections.

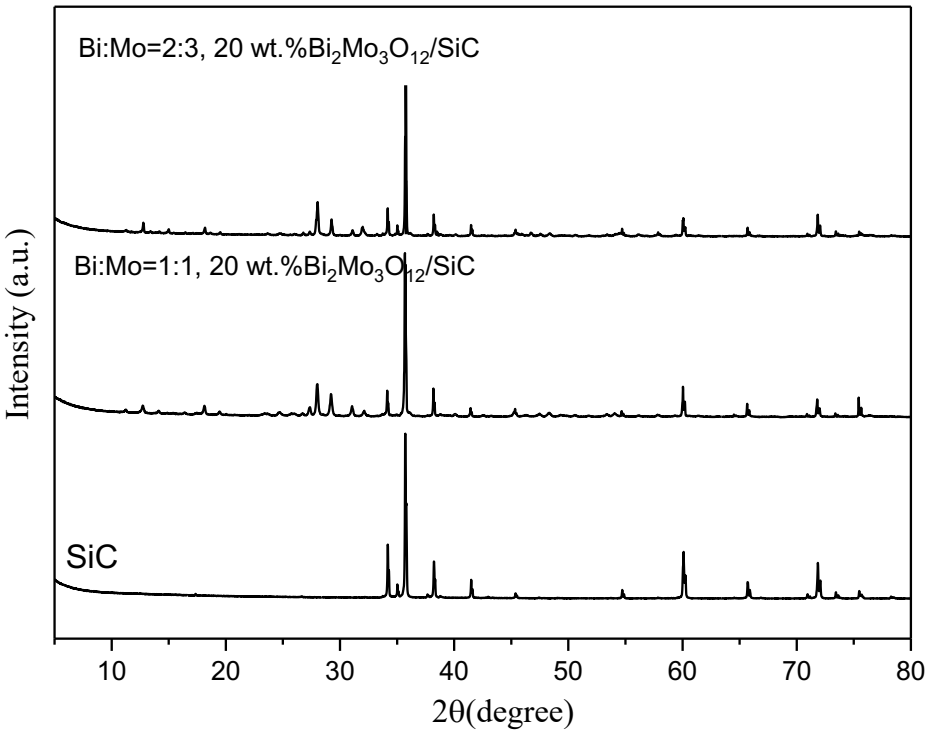

Figure 6.3 XRD patterns of 20 wt.% $Bi_2Mo_3O_{12}$/SiC, Bi:Mo =2:3 and 20 wt.% $Bi_2Mo_3O_{12}$ /SiC, Mo:Bi =1:1

To have a clearer insight into the difference between the supported sample made with different Bi:Mo ratios, XRD patterns of two 20% $Bi_2Mo_3O_{12}$/SiC samples were compared. It can be seen from Figure 6.3, in the pattern of the two samples, there are some differences in the relative heights of the $Bi_2Mo_3O_{12}$ and SiC characteristic peaks. The details are shown in Table 6.1.

Table 6.1 Relative intensities (%) for reflections of $Bi_2Mo_3O_{12}$, and crystallite size of $Bi_2Mo_3O_{12}$

Sample	SiC (006)	$Bi_2Mo_3O_{12}$ (-221)	$Bi_2Mo_3O_{12}$ (023)	$Bi_2Mo_3O_{12}$ (040)	$Bi_2Mo_3O_{12}$ (-123)	crystallite size (Å)
20% $Bi_2Mo_3O_{12}$-Bi:Mo=2:3	100	7.9	5.6	2.5	2.0	426
20% $Bi_2Mo_3O_{12}$-Bi:Mo=1:1	100	7.0	6.3	3.1	2.9	339

($Bi_2Mo_3O_{12}$' s (-221) peak was used to calculate the $Bi_2Mo_3O_{12}$ crystallite size)

The XRD patterns also show differences in the relative intensities of the $Bi_2Mo_3O_{12}$ reflections in the different samples based on the (-221), (023), (040), (-123) peaks, indicating the possibility of different preferential orientation growth when synthesized using different Bi:Mo ratios. The average crystallite size was calculated using Debye–Scherrer equation considering the broadening of the main peak of $Bi_2Mo_3O_{12}$, (-221), at each case, the sample made with the solution with Bi:Mo = 1:1 has a smaller crystalline size than the sample made with the solution with Bi:Mo = 2:3.

Table 6.2 Relative intensities (%) for reflections of SiC, and crystalline size of SiC

Sample	SiC (006)	SiC (101)	SiC (103)	SiC (040)	SiC (110)	SiC (116)	crystalline size (Å)
SiC	100	41.2	43.6	17.4	44.1	34.3	>1000
20% $Bi_2Mo_3O_{12}$-Bi:Mo=2:3	100	37.8	31.1	12.5	28.8	24.6	>1000
20% $Bi_2Mo_3O_{12}$-Bi:Mo=1:1	100	35.3	30.1	11.1	20.4	28.9	>1000

XRD patterns also show that there were differences in the relative intensities based on the (101), (103), (103), (-123), (110), (116) peaks for the SiC, indicating the possibility of the microstructure change. The synthesis method of these SiC supported $Bi_2Mo_3O_{12}$ samples which had been introduced in Section 2.5.3, involves the addition of HNO_3 to the $Bi(NO_3)_3$ solution. Acid pre-treatment has been previously shown to change the microstructure of the SiC[12].

6.2.2 Raman Spectroscopy

To gain a better understanding of the differences between the samples synthesized with different Bi:Mo ratios, Raman spectroscopy was used to gain detailed insight into the molybdenum–oxygen coordination geometries for the samples.

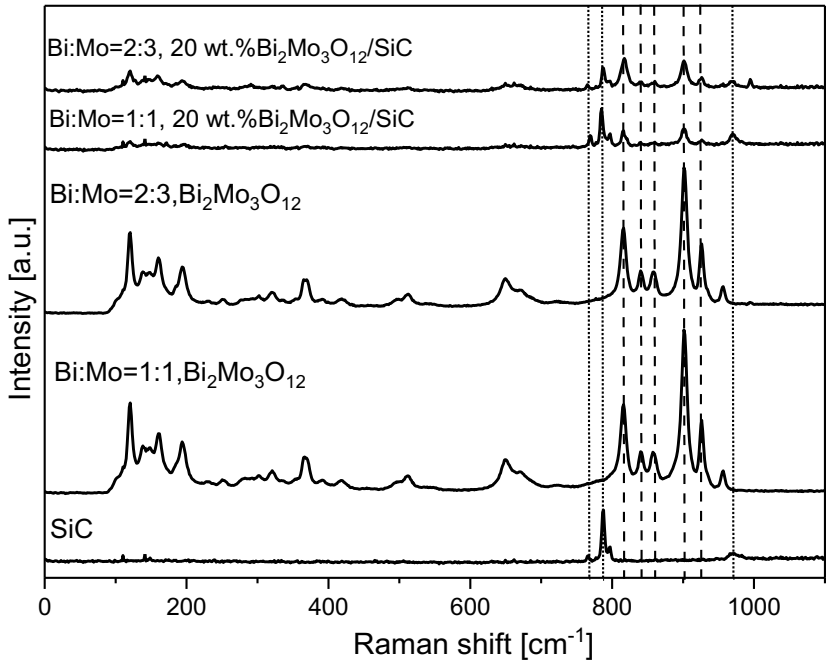

Figure 6.4 Raman spectra of 20 wt.% $Bi_2Mo_3O_{12}$/SiC, Bi:Mo=2:3 and 20 wt.% $Bi_2Mo_3O_{12}$ /SiC, Mo:Bi =1:1

Wachs and co-workers examined the Bi_2O_3-MoO_3 system with Raman spectroscopy and identified seven different phases of bismuth molybdates[13]. According to Wachs' work, the Raman spectrum obtained for the non-supported $Bi_2Mo_3O_{12}$ confirmed the coordination environment around molybdenum in these samples was identical to that of crystalline $Bi_2Mo_3O_{12}$. The Mo–O bond stretches were assigned based on the observed Raman stretching

frequencies at 957,928, 904, 861, 843 and 817 cm^{-1}. The band at 992 cm^{-1} was not observed, some other researchers[14] also have not reported the band at 992 cm^{-1} for the $Bi_2Mo_3O_{12}$ phase.

As shown in Figure 6.4, although there are differences in the intensity of peaks in the spectrum, the Raman spectrum of two supported samples both contain the characteristic bands of $Bi_2Mo_3O_{12}$ at 928, 904, 861, 843 and 817 cm^{-1}, while the band at 957 cm^{-1} was not observed in the spectrum of both supported samples. A weak peak at 992 cm^{-1} appeared in the spectrum of the supported sample made from solution with Bi:Mo = 2:3. The band at 992 cm^{-1} is assigned to the Raman stretches of the shortest Mo-O bond of 1.68 Å. Generally, the Raman intensity is very strong for crystalline compounds and not for dispersed and non-crystalline compounds. As the loading amount of the two samples is the same, the weaker Raman response of the $Bi_2Mo_3O_{12}$ of the sample made from solution with Mo:Bi = 1:1 could be due to the $Bi_2Mo_3O_{12}$ being more dispersed on the SiC surface.

6.2.3 BET Surface Area

The BET specific surface areas of all samples were determined using a Quantachrome Quadrasorb-Evo instrument before and after the microwave testing.

According to the results in Table 6.2, for both series, the specific surface area of the supported samples was getting larger with the increase of the bismuth molybdate loading. Samples loaded with Bi:Mo = 1:1 solutions have a larger specific area than the sample loaded under Bi:Mo = 2:3 conditions. According to the results of the after-reaction analysis, all the supported samples experienced a specific surface area loss during the microwave-assisted processes. The surface area loss of samples loaded under Bi:Mo = 1:1 condition is larger than its counterparts, which represents the severe sintering of $Bi_2Mo_3O_{12}$.

Table 6.3 Characterization data for nitrogen physisorption measurements (BET)

Sample name	Specific surface area before reaction (m^2/g)	Specific surface area after reaction (m^2/g)	Sample name	Specific surface area before reaction (m^2/g)	Specific surface area after reaction(m^2/g)
S0: pure SiC	2	2		2	2
1 wt.% $Bi_2Mo_3O_{12}$/SiC, Bi:Mo=2:3	3	2	1 wt.% $Bi_2Mo_3O_{12}$/SiC, Bi:Mo=1:1	3	2
5 wt.% $Bi_2Mo_3O_{12}$/SiC, Bi:Mo=2:3	4	3	5 wt.% $Bi_2Mo_3O_{12}$/SiC, Bi:Mo=1:1	5	3
10 wt.% $Bi_2Mo_3O_{12}$/SiC, Bi:Mo=2:3	5	4	10 wt.% $Bi_2Mo_3O_{12}$/SiC, Bi:Mo=1:1	6	4
20 wt.% $Bi_2Mo_3O_{12}$/SiC, Bi:Mo=2:3	5	5	20 wt.% $Bi_2Mo_3O_{12}$/SiC, Bi:Mo=1:1	7	4
30 wt.% $Bi_2Mo_3O_{12}$/SiC, Bi:Mo=2:3	7	5	30 wt.% $Bi_2Mo_3O_{12}$/SiC, Bi:Mo=1:1	9	4
20% $Bi_2Mo_3O_{12}$&SiC Bi:Mo=2:3	4	2	20% $Bi_2Mo_3O_{12}$&SiC Bi:Mo=1:1	4	2
$Bi_2Mo_3O_{12}$, Bi:Mo=2:3	8	8	$Bi_2Mo_3O_{12}$, Bi:Mo=1:1	12	11

(The specific surface area of these two groups of catalysts is relatively small, because the main body of these catalyst is SiC, and the specific surface area of SiC support used is only 2 m^2/g)

6.2.4 ICP-MS and XPS

To further investigate the differences between the samples synthesised with different Bi:Mo ratio solutions, the bismuth and molybdate composition were analysed. The surface bismuth and molybdate composition was determined using a Thermo Scientific Kα X-ray photoelectron spectrometer (XPS). The bulk composition of the catalysts was determined by optical emission spectrometry with inductively coupled plasma (ICP-MS).

Table 6.4 Bi:Mo ratios of the bulk and surface determined by ICP-MS and XPS respectively

Sample name	Mo:Bi ratio of the bulk	Mo:Bi ratio of the surface
20 wt.% $Bi_2Mo_3O_{12}$/SiC, Bi:Mo=2:3	1.54	1.74
20 wt.% $Bi_2Mo_3O_{12}$/SiC, Bi:Mo=1:1	1.21	1.39

As shown in Table 6.4, the sample synthesized in the solution with a higher Mo:Bi ratio contains a larger amount of Mo both in the bulk and on the surface, and for both samples, the Mo ratio was larger on the surface than the bulk. For the sample made from solution with Bi:Mo ratio of 1:1, the Mo:Bi ratio of the bulk sample was only 1.21, which is much less than the stoichiometric ratio, which approved the former hypothesis in 6.2.1 that some amorphous Bi_2O_3 existed. The proportion of silicon and carbon on the surface for the supported materials are shown in Table 6.5.

Table 6.5 XPS analysis of the SiC support ratios for the 20% $Bi_2Mo_3O_{12}$/SiC materials prepared with differing Mo:Bi ratios

Sample name	Si (Carbide)	Si(Oxide)	C
SiC	20%	7%	45%
20 wt.% $Bi_2Mo_3O_{12}$/SiC, Bi:Mo=2:3	14%	6%	29%
20 wt.% $Bi_2Mo_3O_{12}$/SiC, Bi:Mo=1:1	3%	2%	27%

As discussed in previous sections, samples made from solution with Mo:Bi = 1:1 have more dispersed $Bi_2Mo_3O_{12}$ on the SiC surface. The XPS results of surface Si and C proportion provide evidence for this conclusion. Compared with the reference SiC, the surface Si and C concentration of both supported samples is lower, as the loading of $Bi_2Mo_3O_{12}$ will cover the SiC surface. The sample made from solution with Mo:Bi =1:1 has lower Si and C concentration on the surface, which suggests that the $Bi_2Mo_3O_{12}$ is more dispersed for this sample.

6.2.5 Dielectric Properties

The dielectric properties were measured by a cyl-ε cavity operating at 2.5 GHz with TM_{010} mode. The detailed instruction of the cyl-ε cavity and calculating method were introduced in Section 2.3.4.

Table 6.6 Dielectric parameters of the bismuth molybdate catalysts supported on SiC made with Bi:Mo = 2:3

Sample name	Dielectric constant (ε')	Dielectric loss (ε'')
SiC	1.005622	0.194784
$Bi_2Mo_3O_{12}$	1.000989234	0.00195059
1 wt.% $Bi_2Mo_3O_{12}$/SiC, Bi:Mo=2:3	1.003821974	0.197563792
5 wt.% $Bi_2Mo_3O_{12}$/SiC, Bi:Mo=2:3	1.003659568	0.191450981
10 wt.% $Bi_2Mo_3O_{12}$/SiC, Bi:Mo=2:3	1.003656587	0.181813751
20 wt.% $Bi_2Mo_3O_{12}$/SiC, Bi:Mo=2:3	1.003369064	0.1641300618
30 wt.% $Bi_2Mo_3O_{12}$/SiC, Bi:Mo=2:3	1.0032554713	0.157196529
20% $Bi_2Mo_3O_{12}$&SiC Bi:Mo=2:3 (physical mixture)	1.003071475	0.133491009

Table 6.7 Dielectric parameters of the bismuth molybdate catalysts supported on SiC made with Bi:Mo = 1:1

Sample name	Dielectric constant (ε')	Dielectric loss (ε'')
SiC	1.005622	0.194784
$Bi_2Mo_3O_{12}$	1.000889	0.001506
1 wt.% $Bi_2Mo_3O_{12}$/SiC, Bi:Mo=1:1	1.004007	0.196508
5 wt.% $Bi_2Mo_3O_{12}$/SiC, Bi:Mo=1:1	1.003545	0.183189
10 wt.% $Bi_2Mo_3O_{12}$/SiC, Bi:Mo=1:1	1.002593	0.128394
20 wt.% $Bi_2Mo_3O_{12}$/SiC, Bi:Mo=1:1	1.001814	0.091451
30 wt.% $Bi_2Mo_3O_{12}$/SiC, Bi:Mo=1:1	1.001682	0.068964
20% $Bi_2Mo_3O_{12}$&SiC Bi:Mo=1:1 (physical mixture)	1.002942	0.122645

The dielectric constant (ε') does not show a significant change in different bismuth molybdate samples, while there are many differences between the dielectric loss (ε'') of the materials. SiC

has a relatively large dielectric loss of 0.195 and the $Bi_2Mo_3O_{12}$ samples made using different Bi:Mo ratios both have a much lower dielectric loss.

As had been mentioned in Section 3.1.2, in microwave heating systems, it is understood that the interaction of materials with microwaves and the heating behaviour of materials by microwave irradiation is strongly dependent on their dielectric properties. The most important property of heating processes is the complex permittivity (ε^*), and the ratio of the dielectric loss and the dielectric constant is commonly used to measure the ability of a material to convert electromagnetic energy into heat energy, which is referred to as the loss tangent ($\tan\delta$). The loss tangent of SiC, pure $Bi_2Mo_3O_{12}$, and supported bismuth molybdate catalysts are shown in Figure 6.5 and Figure 6.6.

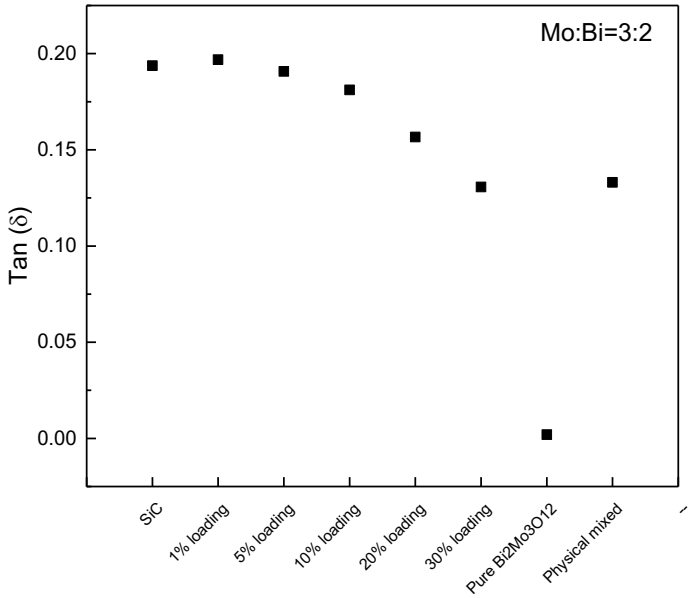

Figure 6.5 Loss tangent of the bismuth molybdate catalysts supported on SiC made with Bi:Mo = 2:3

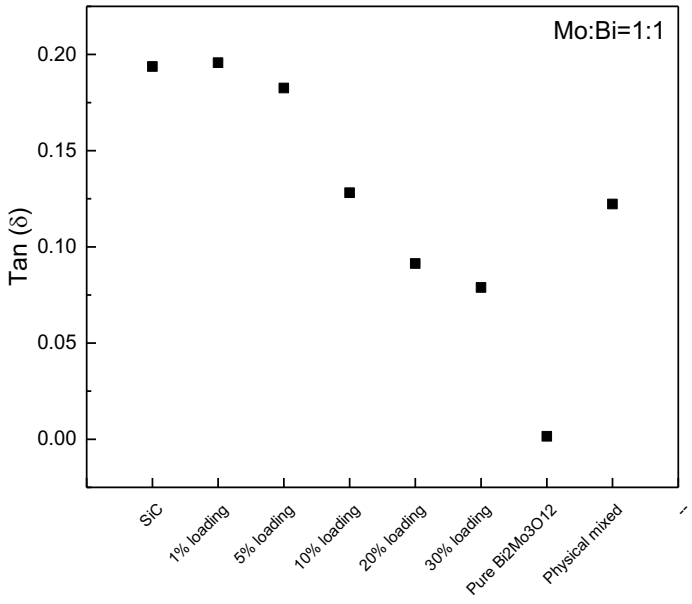

Figure 6.6 Loss tangent of the bismuth molybdate catalysts supported on SiC made with Bi:Mo = 1:1

Pure $Bi_2Mo_3O_{12}$ samples made with both Bi:Mo ratios have low loss factors, and the support material SiC has a very large loss factor of greater than 0.19. When the $Bi_2Mo_3O_{12}$ was supported by SiC, the catalysts' loss tangents are highly enhanced, which indicated that the samples have the ability to convert the energy in the microwave into heat to initiate the chemical reaction. As can be seen in Figure 6.5 and Figure 6.6, the value of the loss tangent decreases with the increase of the amounts of $Bi_2Mo_3O_{12}$ loading. This is because the dielectric property testing is based on volume. Specifically, when the $Bi_2Mo_3O_{12}$ loading is higher, the partial volume of non-lossy $Bi_2Mo_3O_{12}$ is a higher proportion of the total volume which causes the decrease in the sample's loss tangent. It is interesting to see that, when the loading is 1%, the loss tangent is slightly higher than the pure SiC. This may be due to the loading process (which need to be heated in dilute nitric acid for 24 hours) having introduced some defects on the SiC surface, or lowered the particle size of the SiC. As discussed in Section 6.2.1, according

to the XRD data, there are the same changes in the microstructure and previous research had suggested that surface defects are playing an important role in the dielectric properties[15].

6.3 Catalyst Testing

6.3.1 Effect of SiC

In Chapter 3, sol-gel synthesized $Bi_2Mo_3O_{12}$ was tested under 25 W microwave power and showed low activity (less than 5%) due to its low dielectric loss tangent. In this section, $Bi_2Mo_3O_{12}$ was supported on a more lossy material SiC. To check the effects of SiC support, pure $Bi_2Mo_3O_{12}$, SiC supported $Bi_2Mo_3O_{12}$, and SiC were tested in the microwave with different input power respectively. The propane conversion and acrolein yield are shown in Figure 6.7 and Figure 6.8 below.

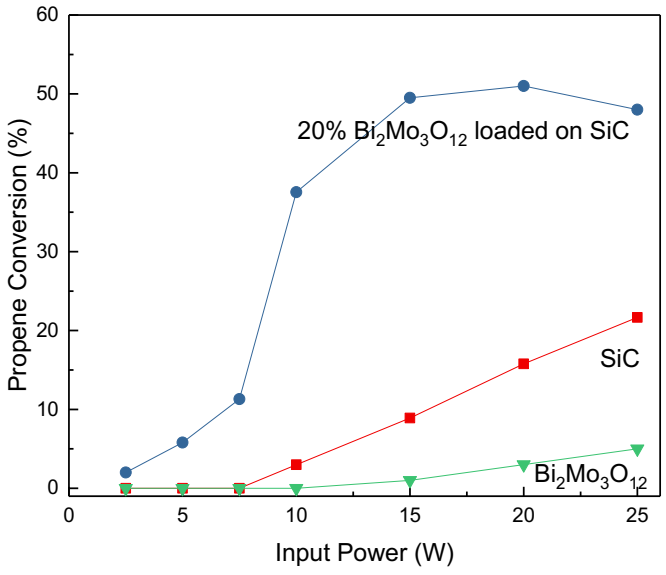

Figure 6.7 Microwave tests: Propene conversion over pure $Bi_2Mo_3O_{12}$, 20% $Bi_2Mo_3O_{12}$/SiC and SiC (0.2 g of catalyst, propane:oxygen:nitrogen = 1:2:97, flow rate = 50 mL min^{-1})

Under microwave conditions, there was a very large difference in the catalyst performance between the non-supported $Bi_2Mo_3O_{12}$ sample and SiC supported $Bi_2Mo_3O_{12}$ sample. Pure $Bi_2Mo_3O_{12}$ did not perform well in microwave conditions, with the low propene conversion (5%) due to the low temperature achieved of 218 °C at 25 W.

When the SiC supported sample was tested, the temperature of the catalyst bed increased gradually at the lower temperature region, and the propene conversion also increased slowly with the temperature rising. When the input power becomes higher than 7.5W, the catalyst bed became hot rapidly and could reach 500 °C, and more than 50% propene was converted when the microwave power was only 20 W.

Pure SiC also converted the propene as it can be heated to high temperatures under microwave conditions, reaching over 600 °C at 25 W power input giving 23% propene conversion in the gas flow, but only CO_x and lower hydrocarbons are formed.

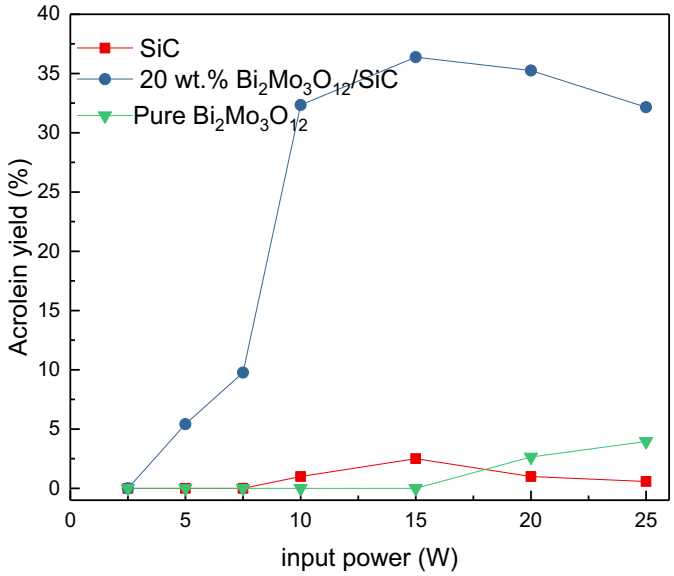

Figure 6.8 Microwave tests: Acrolein yield over pure $Bi_2Mo_3O_{12}$, 20% $Bi_2Mo_3O_{12}$/SiC and SiC (0.2 g of catalyst, propane:oxygen:nitrogen = 1:2:97, flow rate = 50 mL min^{-1})

Apart from the propene conversion, another very important indicator to evaluate the performance of the catalyst is the product yield. As the result shown in Figure 6.8, pure $Bi_2Mo_3O_{12}$ did not perform well in the microwave and only yielded less than 5% acrolein, due to the low conversion. This is because of the lower loss factor of pure $Bi_2Mo_3O_{12}$ (see Section 6.2.5), which indicated that this material cannot convert the microwave energy into heat efficiently. SiC can reach more than 500 °C when the input power is above 15 W, although at these temperatures CO_x is the main product observed. It is noticeable that the performance of $Bi_2Mo_3O_{12}$ was greatly enhanced by support. The supported $Bi_2Mo_3O_{12}$ sample could yield 37% acrolein with 15 W input power, which was more than 6 times higher than the pure $Bi_2Mo_3O_{12}$. This result indicated that support material SiC can effectively provide the heat to the $Bi_2Mo_3O_{12}$ on its surface to carry out the reaction.

6.3.2 Loading or Mixing

The effect of using SiC as a support was confirmed in the last section. In this section, two different methods of combining $Bi_2Mo_3O_{12}$ and SiC were used, and the performances of the two samples were compared.

The supported sample and physical mixed sample were tested under the same conditions, and the propene conversion over these two samples is shown in Figure 6.9. At low power (< 15 W), the two samples can covert similar amounts of propene, while at higher power (≥ 15 W), the physically mixed sample shows a higher propene conversion than the supported material.

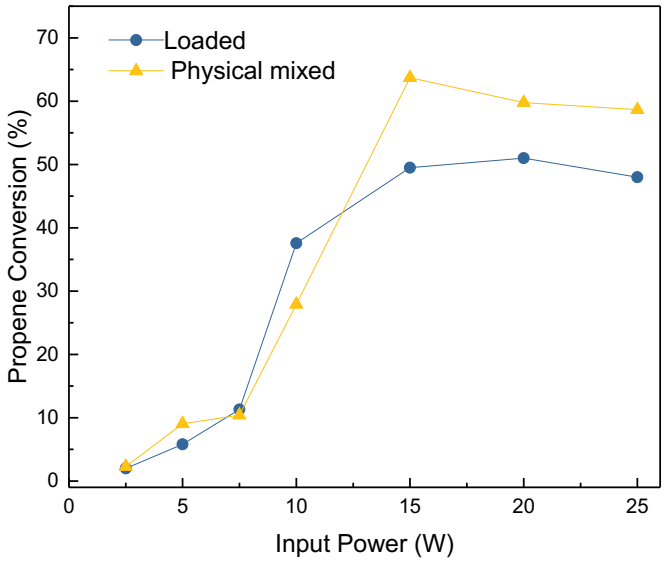

Figure 6.9 Microwave tests: Propene conversion over the supported $Bi_2Mo_3O_{12}$/SiC catalyst and a physical mixture of $Bi_2Mo_3O_{12}$ and SiC (0.2 g of catalyst, propane:oxygen:nitrogen = 1:2:97, flow rate = 50 mL min^{-1})

As the dielectric parameters shown in Table 6.6 and Table 6.7, physical mixed samples have larger dielectric loss factors than their loaded counterparts, and the dielectric loss factor represents the ability of the sample to convert the absorbed microwave energy into heat.

When the input power was 15 W, the supported and physical mixed samples reached temperatures of 341 °C and 395 °C respectively, and when the input power increased to 25 W, the samples reached a high temperature at 530 °C and 590 °C, respectively. The higher temperature reached is the reason for the mixed sample giving higher propene conversion.

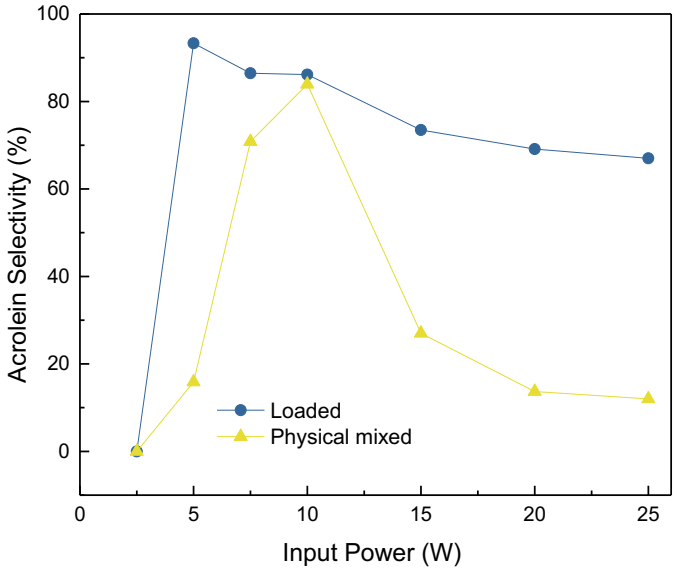

Figure 6.10 Microwave tests: Acrolein selectivity over the supported 20 wt.%$Bi_2Mo_3O_{12}$/SiC catalyst and a physical mixture of $Bi_2Mo_3O_{12}$ and SiC (0.2 g of catalyst, propane:oxygen:nitrogen = 1:2:97, flow rate = 50 mL min^{-1})

Another important indicator for evaluating how well a catalyst performed is the selectivity to the desired product. In this project, acrolein is the target product for the selective oxidation of propene, and Figure 6.10 shows how the selectivity to acrolein over the different catalysts. Although the best acrolein selectivity observed for the two catalysts were similar at around 90%, the supported sample performed much better than the physical-mixed sample, especially at higher power. The supported catalyst can maintain a relatively high selectivity in a larger power range and at the same time gives a good conversion of propene (see in Figure 6.9).

When the input power was lower, both samples produced isopropanol. When input power was higher than 10 W, the physical-mixed sample started to be more selective to CO_x rather than acrolein. For this phenomenon, one possible explanation would be the change of the dominant reaction site at high temperatures. Under lower power, the catalyst bed only reaches a relatively low temperature, which can only activate the reaction on the $Bi_2Mo_3O_{12}$ surface, while under higher input power, the temperature can be enough to activate the reaction on the SiC surface, and it becomes the dominant reaction site. As discussed in the last section, $Bi_2Mo_3O_{12}$ was not active under microwave conditions, and SiC was the heat source for both samples. For the supported sample, the SiC surface was largely covered by $Bi_2Mo_3O_{12}$, and the heat was more easily delivered to the active phase. In the physical mixture, the $Bi_2Mo_3O_{12}$ and SiC were separate phases, the heat transfer between the SiC and $Bi_2Mo_3O_{12}$ is not as sufficient as the heat transfer on the support catalysts. In addition to the heat transfer, both $Bi_2Mo_3O_{12}$ and SiC surfaces are clean and propene can adsorbed onto the surface of both $Bi_2Mo_3O_{12}$ and SiC. In the last section, SiC had been proved to be able to be activated by the microwave greater than 10 W and yield CO_x. Therefore, when the input power was lower than 10 W, the SiC cannot reach the activated temperature, and propene was only oxidized by the $Bi_2Mo_3O_{12}$ and mainly yield acrolein, and when the input power became larger, the SiC had gained enough heat to be

activated, it started to convert the propene into CO_x. Another possible reason for the decline of acrolein selectivity would be the further oxidation of the acrolein on the SiC surface. In this case, at the beginning propene reacts simultaneously on both active sites on physical-mixed samples. Acrolein was produced on the surface of $Bi_2Mo_3O_{12}$, and CO_x was produced on the surface of SiC. Next, since acrolein is more easily to be oxidized than propene, acrolein will continue to be oxidized on the SiC surface to form CO_x.

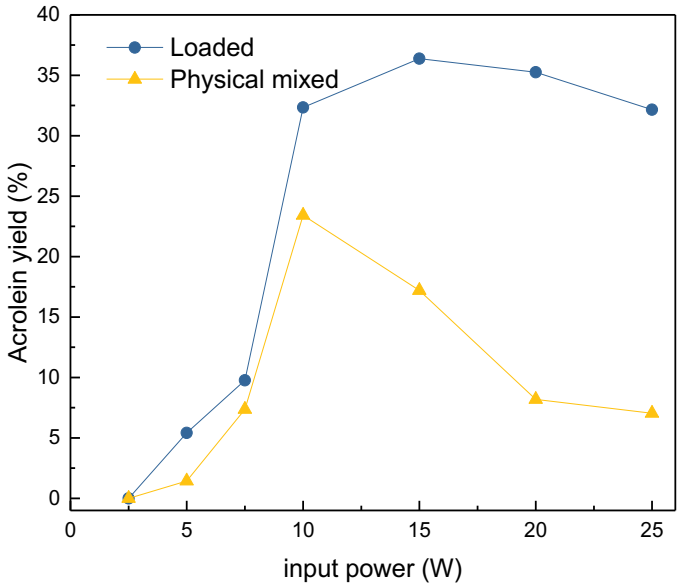

Figure 6.11 Microwave tests: Acrolein yield over the supported $Bi_2Mo_3O_{12}$/SiC catalyst and a physical mixture of $Bi_2Mo_3O_{12}$ and SiC (0.2 g of catalyst, propane:oxygen:nitrogen = 1:2:97, flow rate = 50 mL min^{-1})

The results of acrolein yield over the supported catalyst and physical mixture are shown in Figure 6.11. For both samples, when the input power was lower than 10 W, the acrolein yield increased with increasing input power, although the supported sample has a higher acrolein

yield. When the input power was greater than 10 W, the two samples showed different performance. For the supported sample, the acrolein selectivity remained fairly constant with increased input power, while for the loaded sample, the acrolein yield dropped dramatically. As discussed above, at a higher power range, an increase in the CO_x production at higher power over the physical mixture leads to a decrease in the acrolein yield. The highest yield of acrolein produced by the supported sample was around 37% which is 60% higher than the best acrolein yield produced by the physically mixed sample at around 23%. These result indicate that the intimate contact between phases in the supported materials gives better catalysts than simply mixing the two components in the catalyst bed.

6.3.4 Influence of Bi:Mo Ratio

In the last section, the benefit of supporting $Bi_2Mo_3O_{12}$ on SiC was demonstrated. In this section, the influence of using different Bi:Mo ratios in the synthesis of SiC supported $Bi_2Mo_3O_{12}$ samples was investigated.

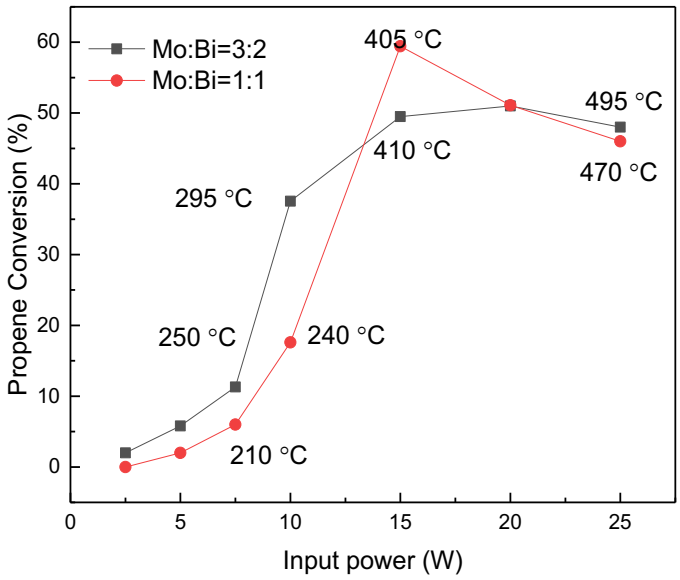

Figure 6.12 Microwave tests: Propene conversion over bismuth molybdate catalysts supported on SiC synthesized from solution with either Bi:Mo = 2:3 or Bi:Mo = 1:1 (0.2 g of catalyst, propane:oxygen:nitrogen = 1:2:97, flow rate = 50 mL min^{-1})

The temperature of the catalyst bed under different microwave input power and the corresponding propene conversion for the two catalysts are shown in Figure 6.12. Both performed well under microwave conditions giving good conversions of propene, with the best propene conversion of 60% observed for the material made with Bi:Mo = 1:1 at 15 W input power.

When the input power is ≤10 W, the propene conversion over the sample made with Bi:Mo = 1:1 was lower than the propene conversion over the sample made with Bi:Mo = 2:3 ratio. The dielectric parameters shown in Section 6.2.5, indicate the sample made with the Bi:Mo = 2:3 solution has a larger dielectric loss factor than the material made using the Bi:Mo = 1:1 solution,

which means it can convert the microwave energy into heat more efficiently. This explains why the catalyst bed for the material synthesised with the Bi:Mo ratio of 2:3 reached a higher overall temperature under the same microwave power, and hence, led to a higher propene conversion.

When the input power was 15 W, higher propene conversion was obtained over the sample made with a Bi:Mo ratio of 1:1 at almost the same catalyst bed temperature as the other sample. This may be because of the higher dispersion of $Bi_2Mo_3O_{12}$ on the SiC surface in the sample made with Bi:Mo ratio of 1:1. Many previous studies have shown that for supported catalysts, better dispersion and smaller active component size are beneficial to the catalytic reaction, as there are more active sites on the catalyst surface[16,17]. According to the information from the XRD analysis (see Section 6.2.1) $Bi_2Mo_3O_{12}$ made from solution with Bi:Mo = 1:1 has lower crystallite size, and both Raman (see Section 6.2.2) and XPS (see Section 6.2.4) results had demonstrated that, for the sample made from solution with Bi:Mo = 1:1, $Bi_2Mo_3O_{12}$ is more dispersed on the SiC surface. Similar results were reported by Wang and co-workers in their work of microwave-assisted NH_3 synthesis using a variable frequency microwave reactor. In their work, they studied Ru catalysts with MgO and CeO_2 supports, and found the Ru/CeO_2 performed much better than the MgO supported material. They explained that this advantage was because of the stronger interaction between Ru and CeO_2 support, meaning Ru particle size was smaller with higher dispersion, creating more active sites for NH_3 synthesis[7].

When the input power is greater than 20 W, the propene conversion over the sample made with Bi:Mo ratio of 1:1 started to decrease, while the performance of the other sample was more stable. The conversion decline over the sample made from the solution with Bi:Mo = 1:1 could be caused by the sintering of the $Bi_2Mo_3O_{12}$. According to the BET result in Section 6.2.3, the

specific surface area had experienced a severe loss after the reaction, which indicated that the sample was sintered under the reaction conditions.

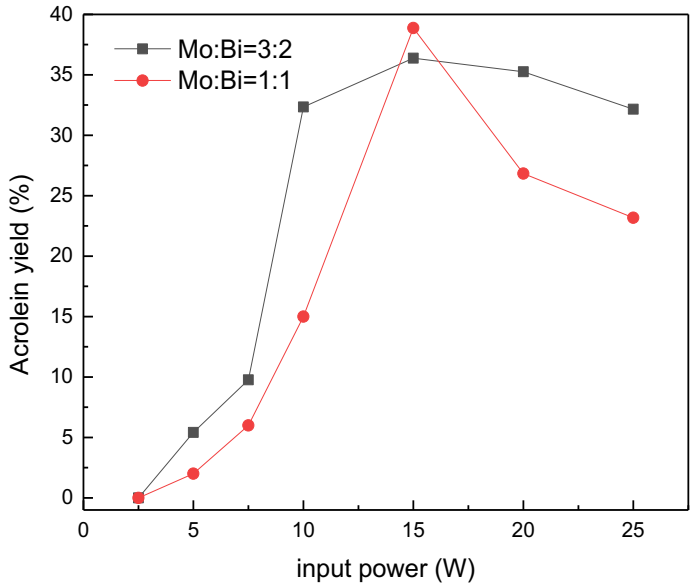

Figure 6.13 Microwave tests: Acrolein yield over bismuth molybdate catalysts supported on SiC synthesized from solution with either Bi:Mo = 2:3 or Bi:Mo = 1:1 (0.2 g of catalyst, propane:oxygen:nitrogen = 1:2:97, flow rate = 50 mL min^{-1})

The acrolein yield over the two samples is shown in Figure 6.13. The sample made from solution with Bi:Mo = 2:3 showed a more stable performance while the best acrolein yield was acheived with the sample made from solution with Bi:Mo ratio of 1:1. As mentioned in the propene coversion discussion, sintering of $Bi_2Mo_3O_{12}$ caused a decline of the propene conversion and hence yield. Additionally, the sintering of $Bi_2Mo_3O_{12}$ also results in the exposure of more of the SiC surface, which is more selective to the CO_x. Therefore, the acrolein yield was even badly affected by the sintering of $Bi_2Mo_3O_{12}$.

6.3.3 Influence of amount of loading

In the previous section, two different Bi:Mo ratios were chosen for the synthesis the SiC supported $Bi_2Mo_3O_{12}$ samples, and the performances of the two samples were compared. In this section, SiC supported $Bi_2Mo_3O_{12}$ samples with different loadings of $Bi_2Mo_3O_{12}$ were tested under a fixed condition (15 W input power). The acrolein yield obtained over the SiC supported $Bi_2Mo_3O_{12}$ catalysts synthesized from solution with Bi:Mo = 2:3 and Bi:Mo = 1:1 were shown in Figures 6.14 and Figure 6.15, respectively. This section aims to find the optimimum loading of the $Bi_2Mo_3O_{12}$ for propene oxidation under the microwave-assisted catalytic process. For both Bi:Mo ratios, the results showed that 20 wt.% would be the best amount of loading for microwave-assisted processes.

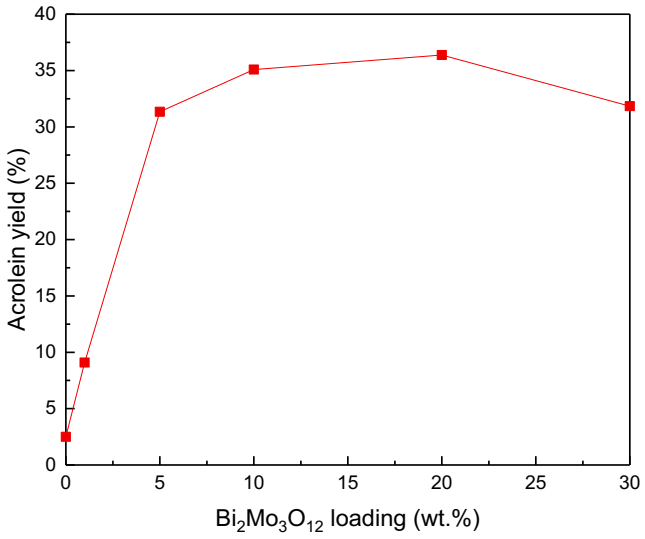

Figure 6.14 Microwave tests at 15 W: Acrolein yield over bismuth molybdate catalysts supported on SiC with different loading of $Bi_2Mo_3O_{12}$ synthesized from solution with Bi:Mo = 2:3 (0.2 g of catalyst, propane:oxygen:nitrogen = 1:2:97, flow rate = 50 mL min^{-1})

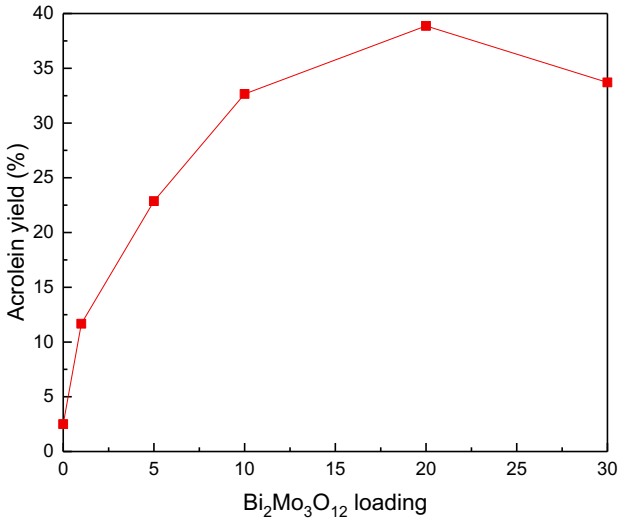

Figure 6.15 Microwave tests at 15 W: Acrolein yield over bismuth molybdate catalysts supported on SiC with different loading of $Bi_2Mo_3O_{12}$ synthesized from solution with Bi:Mo = 1:1 (0.2 g of catalyst, propane:oxygen:nitrogen = 1:2:97, flow rate = 50 mL min^{-1})

As can be seen from Figure 6.14 and Figure 6.15, the relationship between loading and yield showed a volcano curve, which is because SiC and $Bi_2Mo_3O_{12}$ play different roles in the microwave-assisted process. On the one hand, when the loading is low, the dielectric loss tangent (see Section 6.2.5) of the catalyst sample is high, and the catalyst bed has a strong ability to convert microwaves into heat, which is beneficial to the thermal activation of the catalyst. On the other hand, when the loading is higher, there is less SiC in the material and t dialectric loss tangent will decrease accordingly, resulting in a decrease in the overall ability of the catalyst to convert microwaves into heat. However, higher loading also brings an increase in active sites on $Bi_2Mo_3O_{12}$, so the selectivity of the target product is also higher. The results illustrate that, for the two groups of catalysts synthesized with different precursor concentration solutions, 20% is the best loading for both.

6.3.5 Compare with Conventional Tests

In the last few sections, the effect of SiC support, catalyst structure, Bi:Mo ratio and loading amount were investigated, and 20% $Bi_2Mo_3O_{12}$ loaded samples were foundd to be the most efficient catalysts. In this section, the two 20% $Bi_2Mo_3O_{12}$/SiC supported samples, two 20% $Bi_2Mo_3O_{12}$-SiC physically mixed samples, pure SiC and bulk $Bi_2Mo_3O_{12}$ were tested under both microwave and conventional heating conditions.

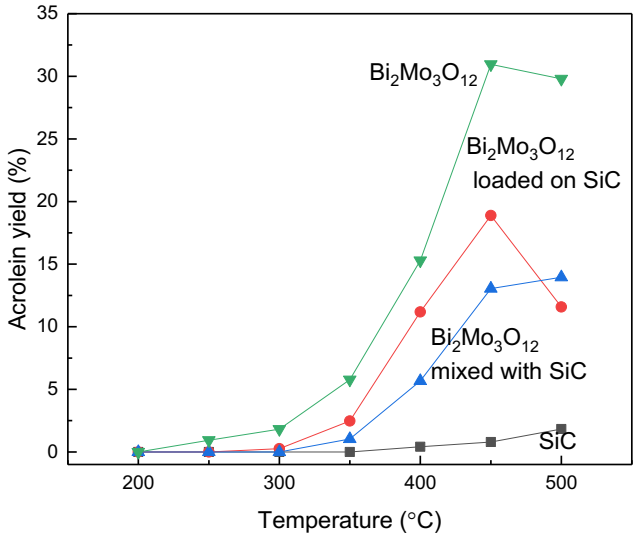

Figure 6.16 Conventional test: Acrolein yield over pure $Bi_2Mo_3O_{12}$, supported 20% $Bi_2Mo_3O_{12}$/SiC, physically mixed $Bi_2Mo_3O_{12}$-SiC synthesized from solution with Bi:Mo = 2:3 and SiC (0.2 g of catalyst, propane:oxygen:nitrogen = 1:2:97, flow rate = 50 mL min^{-1})

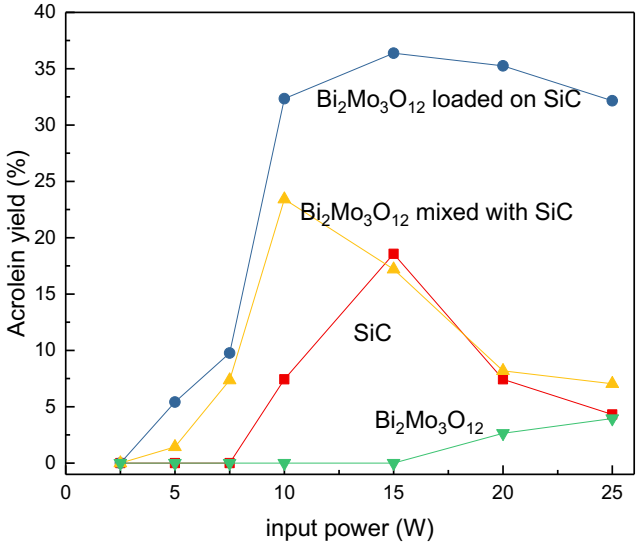

Figure 6.17 Microwave test: Acrolein yield over pure $Bi_2Mo_3O_{12}$, supported 20% $Bi_2Mo_3O_{12}$/SiC, physically mixed $Bi_2Mo_3O_{12}$-SiC synthesized from solution with Bi:Mo = 2:3 and SiC (0.2 g of catalyst, propane:oxygen:nitrogen = 1:2:97, flow rate = 50 mL min^{-1})

To give a clearer insight into the enhanced effect of the microwave on acrolein yield, a comparison of the performance of the SiC, and SiC supported $Bi_2Mo_3O_{12}$, SiC physically mixed with $Bi_2Mo_3O_{12}$ and bulk $Bi_2Mo_3O_{12}$ synthesized from solution with Bi:Mo = 2:3 under both the microwave and conventional conditions was made. The results are shown in Figure 6.16 and Figure 6.17.

Under conventional heating, the best acrolein yield was 33%, which was over the bulk $Bi_2Mo_3O_{12}$ catalyst at 450 °C. The SiC support material alone only showed very low acrolein production (< 3%), whereas the supported and physically mixed materials showed a reasonable performance, although lower than the pure phase, at 14% and 18% respectively. In microwave tests, the supported sample is found to be the best catalyst, with a yield of acrolein of 37% over,

which was 54% higher than the best performance of the physically mixed sample. The bulk $Bi_2Mo_3O_{12}$ catalyst only yield less than 5% acrolein as it cannot be well heated by microwave radiation and conversion is low.

When comparing the performance of the supported sample under both conditions, it is clear that the acrolein yield was enhanced by microwave heating. In the conventional heating test, the best acrolein yield was 18%, which was made at 450 °C, while in the microwave test, the best acrolein yield was 37% under 15 W input power, which is more than twice the best yield under the conventional conditions. This indicates that the microwave has a huge effect on the catalytic performance of the supported sample. This is because the microwave-assisted catalytic process provides a form of heat transfer for the reaction that is different from traditional catalysis.

In the conventional catalytic process, heat is transferred from the outside to the inside. Initially, the reactor tube wall will be heated by thermal radiation, and then the gas and catalyst bed will be heated successively by thermal conduction. This can lead to temperature differences in the gas and catalyst beds, as well as within the bed itself. The gas temperature is higher than the bed temperature, and there is also a temperature gradient from the outside to the inside of the bed. Under microwave heating, SiC absorbs microwaves and is thus heated first, then it acts as a heat source, heating the reactants on its surface. The high thermal conductivity of SiC enables it to uniformly transfer heat to the active components on the surface, effectively eliminating temperature gradients and preventing the generation of local hot spots inside the $Bi_2Mo_3O_{12}$[4], which is beneficial to the temperature control and to maintain good selectivity to the target products. Due to the advantages of thermal transfer, under microwave heating, the supported sample can maintain high propene conversion and selectivity (see section 6.3.2), and hence delivered a good acrolein yield.

Moreover, if comparing the microwave-assisted performance of the loaded sample with the performance of the bulk $Bi_2Mo_3O_{12}$ catalyst in the conventional test, the performance of the loaded sample still shows an advantage. The loaded sample can yield 37% acrolein while the bulk $Bi_2Mo_3O_{12}$ catalyst can only yield around 33% acrolein in the conventional test. In the microwave-assisted process, the loaded sample, as a diluted catalyst, can gain a 9% higher acrolein yield than the bulk catalyst in conventional test, which indicates that the efficiency of the catalyst had been largely enhanced by the microwave-assisted process.

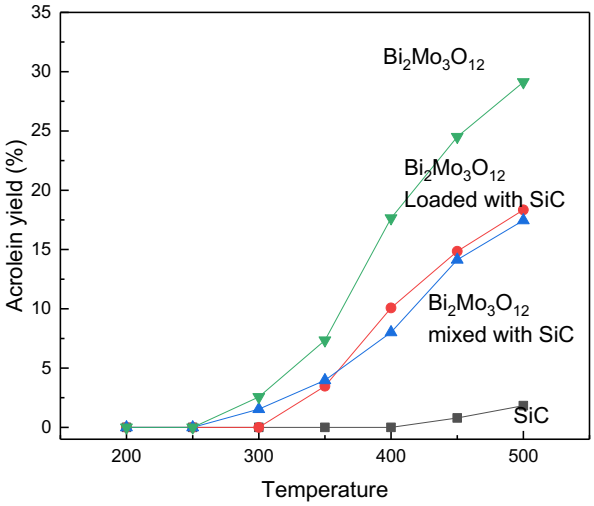

Figure 6.18 Conventional test: Acrolein yield over pure $Bi_2Mo_3O_{12}$, supported 20% $Bi_2Mo_3O_{12}$/SiC, physically mixed $Bi_2Mo_3O_{12}$-SiC synthesized from solution with Bi:Mo = 1:1 and SiC (0.2 g of catalyst, propane:oxygen:nitrogen = 1:2:97, flow rate = 50 mL min^{-1})

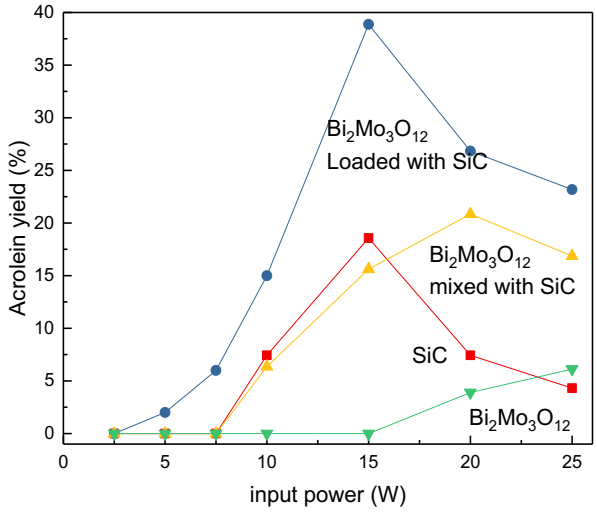

Figure 6.6.19 Microwave test: Acrolein yield over over pure $Bi_2Mo_3O_{12}$, supported 20% $Bi_2Mo_3O_{12}$/SiC, physically mixed $Bi_2Mo_3O_{12}$-SiC synthesized from solution with Bi:Mo = 1:1 and SiC (0.2 g of catalyst, propane:oxygen:nitrogen = 1:2:97, flow rate = 50 mL min^{-1})

The comparison results of the materials prepared with a Bi:Mo ratio of 1:1 is shown in Figures 6.18 and 6.19. In the conventional test, the best acrolein yield was 30%, over the bulk $Bi_2Mo_3O_{12}$ catalyst. The supported and physically mixed samples performed similarly, and the best acrolein yield observed was 16% and 17% respectively. Similar to the result of the tests on Bi:Mo = 2:3 catalysts, under microwave heating, the supported sample shows the best performance, with a yield of acrolein of 39%, which was 85% higher than the best performance of the physically mixed sample. The bulk $Bi_2Mo_3O_{12}$ catalyst only yield 8 % acrolein as it cannot be well heated.

In the conventional heating test, the best acrolein yield for the loaded sample was 17%, which was made at 500 °C, while in the microwave test, the best acrolein yield was 40% under 15 W input power, which is around 2.4 times of its best yield under the conventional condition.

Similar to the results for the Bi:Mo = 2:3 catalysts, the microwave-assisted performance of the supported material performance (39% acrolein yield) was higher than over the bulk $Bi_2Mo_3O_{12}$ catalyst in conventional testing (30% acrolein yield). If the efficiency of the catalyst is evaluated in terms of the amount of the active $Bi_2Mo_3O_{12}$ phase, the microwave-assisted process is 6.5 times more efficient than the conventional catalysis process. The main reason for this phenomenon is the difference in the process of heat transfer, which had been detailed explained in the former part.

6.4 Conclusion

In this chapter, two groups of silicon carbide supported bismuth molybdate catalysts were tested under both microwave and conventional conditions, the effect of SiC support, synthesis method, Bi:Mo ratio in the catalyst synthesis procedure and loading amount of $Bi_2Mo_3O_{12}$ was investigated. XRD, Raman, BET, XPS, ICP-OES were used to investigate the samples' microstructure and monitor the structural changes of samples. The dielectric parameters were also measured to understand the dielectric properties of the samples.

Loading small amounts of $Bi_2Mo_3O_{12}$ can enhance the loss factor of the SiC. The introduction of nitric acid during the synthesis process caused a change in the SiC's microstructure and potentially change the particles' shape and reduced its size, which led to the change in the dielectric properties.

Combining $Bi_2Mo_3O_{12}$ with SiC can largely enhance the catalyst's performance in microwave tests. Bulk $Bi_2Mo_3O_{12}$ cannot be heated in the microwave test, but when combined with SiC, the $Bi_2Mo_3O_{12}$ started to convert the propene and produce a promising yield of acrolein under microwave conditions. The method used to combine the SiC and $Bi_2Mo_3O_{12}$ also influences

the performance. Two methods of the combination were used and the corresponding made samples were tested under the same conditions. Both samples performed well in converting the propene, but the loaded sample had much better results on yielding acrolein. The Bi:Mo ratio of the precursor solution also affects the microstructure of the sample and hence, influences the performance. The sample prepared using a solution with a Bi:Mo ratio of 2:3 showed a larger loss tangent and can be better heated under the microwave conditions than the material synthesised using a solution with a Bi:Mo ratio of 1:1. The material synthesised using a solution with a Bi:Mo ratio of 1:1. has a smaller $Bi_2Mo_3O_{12}$ crystalline size and is more dispersed on the SiC surface.

In the microwave-assisted process of propene selective oxidation, SiC and $Bi_2Mo_3O_{12}$ play different roles in the microwave conditions. SiC supports the ability of heat generation, and $Bi_2Mo_3O_{12}$ is the effective active component of producing the acrolein to achieve the best acrolein yield, the loading should balance the function of the catalyst and dielectric material. For the two groups of catalysts synthesized with different precursor concentration solutions, 20% is the best loading for both, and produce the optimum acrolein yield.

Due to the good thermal conductivity and microwave absorbing ability of SiC support, the efficiency of the supported catalysts was largely enhanced in the microwave-assisted process. Compared with the results in the conventional test, more than twice the acrolein yields observed in the microwave test for both supported samples.

References

1. Ledoux, M. J. & Pham-Huu, C. Silicon carbide a novel catalyst support for heterogeneous catalysis. *CATTECH* **5**, 226–246 (2001).

2. Liu, Y., Ersen, O., Meny, C., Luck, F. & Pham-Huu, C. Fischer–Tropsch Reaction on a Thermally Conductive and Reusable Silicon Carbide Support. *ChemSusChem* **7**, 1218–1239 (2014).

3. Duong-Viet, C. *et al.* Silicon carbide foam as a porous support platform for catalytic applications. *New Journal of Chemistry* **40**, 4285–4299 (2016).

4. Sun, J. *et al.* An Al_2O_3-Coated SiC-Supported Ni Catalyst with Enhanced Activity and Improved Stability for Production of Synthetic Natural Gas. *Industrial and Engineering Chemistry Research* **57**, 14899–14909 (2018).

5. Kulkarni, S. R. *et al.* Silicon carbide in catalysis: from inert bed filler to catalytic support and multifunctional material. *https://doi-org.abc.cardiff.ac.uk/10.1080/01614940.2022.2025670* (2022).

6. Sun, J. *et al.* Experimental Study on Microwave–SiC-Assisted Catalytic Hydrogenation of Phenol. *Energy & Fuels* **33**, 11092–11100 (2019).

7. Wang, Y. *et al.* Effects of support and promoter on Ru catalyst activity in microwave-assisted ammonia synthesis. *Chemical Engineering Journal* **425**, 130546 (2021).

8. Guo, B., Hu, X., Wang, X. & Zhang, S. Catalytic performances of Cu-Mn-Ce oxide/SiC monolithic catalyst for oxidation of toluene under microwave irradiation. 593–597 (2015).

9. Bo, L. & Sun, S. Microwave-assisted catalytic oxidation of gaseous toluene with a Cu-Mn-Ce/cordierite honeycomb catalyst. *Frontiers of Chemical Science and Engineering* **13**, 385–392 (2019).

10. Zhang, F. *et al.* Process of CH_4-CO_2 reforming over Fe/SiC catalyst under microwave irradiation. *Science of the Total Environment* **639**, 1148–1155 (2018).

11. Wang, W. *et al.* Microwave-Assisted Catalytic Cleavage of C-C Bond in Lignin Models by Bifunctional Pt/CDC-SiC. *ACS Sustainable Chemistry and Engineering* **8**, 38–43 (2020).

12. Min, L., Aiqin, W., Jingpei, X., Pengfei, Z. & Yali, S. Influence of pretreatment of SiC on microstructure and properties of SiC p/A390. *Emerging Materials Research* **5**, 81–87 (2016).

13. Hardcastle, F. D. & Wachs, I. E. Molecular structure of molybdenum oxide in bismuth molybdates by Raman spectroscopy. *Journal of Physical Chemistry* **95**, 10763–10772 (1991).

14. Ono, T. & Ogata, N. Raman band shifts of γ-Bi_2MoO_6 and α-$Bi_2Mo_3O_{12}$ exchanged with ^{18}O tracer at active sites for reoxidation. *Journal of the Chemical Society, Faraday Transactions* **90**, 2113–2118 (1994).

15. Duan, W. J., Lu, S. H., Wu, Z. L. & Wang, Y. S. Size Effects on Properties of NiO Nanoparticles Grown in Alkalisalts. *Journal of Physical Chemistry C* **116**, 26043–26051 (2012).

16. Liu, L. & Corma, A. Metal Catalysts for Heterogeneous Catalysis: From Single Atoms to Nanoclusters and Nanoparticles. *Chemical Reviews* **118**, 4981–5079 (2018).

17. Chen, J., Zhang, Q., Wang, Y. & Wan, H. Size-Dependent Catalytic Activity of Supported Palladium Nanoparticles for Aerobic Oxidation of Alcohols. *Advanced Synthesis & Catalysis* **350**, 453–464 (2008).

7 Conclusions and Future Plan

7.1 Conclusions

The overall objective of this thesis was to explore the feasibility and potential of using the designed microwave cavity in the gas-phase heterogeneous catalytic process. Propene selective oxidation was chosen as the target reaction. Various catalysts made using different routes were tested under microwave conditions. Conventional tests were also carried out for comparison.

7.1.1 Chapter 3 A Feasibility Study on Propene Selective Oxidation

Chapter 3 focused on introducing the feasibility of microwave-assisted heterogeneous catalysis and screening potential catalysts for the selective oxidation of propene in a microwave-assisted heterogeneous catalytic process. In this part, two groups of catalysts were screened, which included a group of bismuth-based Bi–Me–O oxides, where the Me is V, Mo, Ti, Fe, and a group of supported nickel catalysts.

Among the bismuth-based Bi–Me–O oxides materials, $BiVO_4$ and γ-Bi_2MoO_6 are two of the most promising samples for investigating microwave-assisted selective oxidation. Compared with the catalyst made by the sol-gel method, the hydrothermally synthesized catalysts uaually has larger dielectric loss factor and showed a better ability to utilize microwave power. This may be due to the fact that there is no calcination process in the hydrothermal synthesis, impurities like NO_3^- and water may remain in the lattice of the material and cause the larger dielectric loss of the sample.

Several interesting points were also found based on the tests over the supported nickel catalysts. Firstly, loading metallic nickel on a common microwave-inert support material can improve the overall microwave usage capability of the sample, and it is possible to conduct gas-phase catalytic reactions assisted by microwaves. Secondly, the absorbing supports materials like SiC and $BaTiO_3$ showed a very good heating effect under microwave conditions. Therefore, combining the advantaged catalysts in

traditional catalytic processes with these materials that can be heated well in microwaves may yield good results in microwave-assisted catalysis.

7.1.2 Chapter 4 Propene Selective Oxidation by Hydrothermally Synthesized Bismuth Molybdate

In Chapter 4, hydrothermal synthesis has been used to prepare bismuth molybdate catalysts for the selective oxidation of propene to acrolein in a microwave-assisted heterogeneous catalytic process. Compared with the results of conventional catalytic processes, great potential for using microwave heating was shown. The best acrolein yield in the microwave tests was found to be 66% higher than in the conventional tests.

The pH of the precursor solution was found to be a strong influence on the catalyst formed. The γ-Bi_2MoO_6 phase only catalyst was formed when pH=6, and mixed phases samples were formed in both higher and lower pH values. In the lower pH solution (pH=4), a small amount of molybdenum rich phase $Bi_2Mo_3O_{12}$ was formed, which had facilitated the formation of acrolein, and in a higher pH solution (pH=8) the impurity phase was the bismuth rich phase Bi_4MoO_9, which was more selective to CO_x.

Calcination also affected the performance of the catalyst. Calcination at 500 °C does not change the composition of the catalyst, but increases the crystallite size of the sample, and results in the decrease of specific surface area. Also, the calcination process greatly reduced the dielectric loss of the samples The non-calcined materials were found to be more likely to reach higher temperatures than the calcined samples, while the calcined materials were found to have better stability under higher input power.

Although a remarkable enhancement in acrolein yield was observed using microwave heating, there were disadvantages to this process. The catalysts were much more likely to be deactivated by microwave heating. The catalyst deactivation may be due to the changes in catalyst structure, and catalyst reduction was seen under the reaction conditions.

7.1.3 Chapter 5 Propene Selective Oxidation by Bismuth Molybdate and Bismuth Vanadate

In Chapter 5, a group of bismuth vanadate molybdate catalysts were synthesized by the sol-gel method. Compared with using conventional heating techniques, no obvious enhancement was noticed by using a microwave, but a comparable acrolein production rate can be achieved.

Replacing Mo in the γ-Bi_2MoO_6 with V can cause changes in both crystallite size and structure. When the V content is smaller than 20%, the catalyst is a mixture of orthorhombic γ-Bi_2MoO_6 and monoclinic β-$Bi_2Mo_2O_9$, and when the V content gets larger, the monoclinic phase starts to disappear, and a tetrahedral phase $Bi_{1-X/3}V_{1-x}Mo_XO_4$ is formed. Both the crystalline size of orthorhombic γ-Bi_2MoO_6 and tetrahedral phase $Bi_{1-X/3}V_{1-x}Mo_XO_4$ is reducing with the increase of V content up to 60%.

Orthorhombic γ-Bi_2MoO_6 was found to be crucial for this catalyst to be effective in the microwave-assisted reaction, as it has a larger loss tangent and can effectively convert the energy in the microwave into heat. When the vanadium content increased to more than 40 %, the orthorhombic γ-Bi_2MoO_6 started to disappear, and consequently the catalysts' dielectric loss factor also dropped sharply, and the catalyst became inactive under the microwave conditions.

7.1.4 Chapter 6 Propene Selective Oxidation by Silicon Carbide Promoted Bismuth Molybdate

In Chapter 3, SiC was found to have a very good ability to utilize microwave energy, therefore, in Chapter 6, bismuth molybdate catalysts were combined with SiC, and then, the formed samples were tested under both microwave and conventional conditions. Due to the high thermal conductivity and microwave absorbing ability of SiC, the catalytic efficiency of the supported catalysts was largely enhanced in the microwave-assisted process. Compared with the results in the conventional test, more than twice the acrolein yields were observed in the microwave test for both supported samples.

Combining the well-performed catalysts $Bi_2Mo_3O_{12}$ in traditional catalytic processes with SiC that can be heated well in microwaves exactly yielded good results in microwave-assisted catalysis. Bulk $Bi_2Mo_3O_{12}$ cannot be heated in the microwave test as it has a very low dielectric loss factor. When combined with SiC, the catalyst produced a promising yield of acrolein under microwave conditions. This result indicated that the traditional catalytic reactions can be successfully transferred to microwave-assisted catalysis by combining microwave absorbing materials with the dominant catalysts in the traditional catalytic process. Well, the method used to combine the absorber and catalyst also influences the performance. In this work, the loaded sample had much better results in yielding acrolein than the physical mixed sample.

In the microwave-assisted process of propene selective oxidation, SiC and $Bi_2Mo_3O_{12}$ play different roles in microwave conditions. SiC supports the ability of heat generation, and $Bi_2Mo_3O_{12}$ is the effective active component of producing the acrolein. For the two groups of catalysts synthesized with different precursor concentration solutions, 20% is the best loading for both groups to balance the function of SiC and $Bi_2Mo_3O_{12}$, and then produce the optimum acrolein yield.

7.2 Future Plan

First of all, this work still has some problems that need to be improved. For example, in Chapter 4, the hydrothermally synthesized bismuth molybdate sample was observed to be easily reduced in the microwave-assisted process. Therefore, investigating the catalysts under a more oxidising feed to prevent reduction and deactivation may improve this, although it may also impact CO_x formation. In future work it would be interesting to investigate adding water into the gas flow in the future to see if this might to initiate discharges in the catalytic zone and form hydroxyl radicals to see if this impacted on the selectivity, which belongs to the microwave-plasma catalysis.

Some further characterization would also be insightful, such as particle size determination of bismuth molybdate by scanning electron microscopy. The catalysts after microwave-assisted reaction should

also be characterized, to further study the effect of microwaves on the catalysts. These follow-up studies will help to further understand the mechanism of the microwave-assisted catalytic process, and also help to solve the problem of catalyst instability and deactivation.

In addition to refining and improving the existing study, in the process of completing this thesis, some promising research directions have also been identified, which may be carried out in future research. Firstly, as discussed in Chapter 3, bismuth titanate and bismuth ferrite can be heated to suitable temperatures in the process of microwave-assisted heterogeneous catalysis and had shown a good ability to convert propene. Although they are not selective to acrolein, they are still good catalyst candidates for the cracking of hydrocarbons. In the future, these two catalysts could be modified and will be used in microwave-assisted catalytic cracking of hydrocarbons. Secondly, in Chapter 3, it was also proved that loading metallic nickel on a common microwave-inert support material can improve the overall microwave usage capability of the sample. Supported nickel catalysts have been widely studied and applied in traditional catalysis. It is also a promising direction to transfer it to the process of microwave-assisted catalysis, for example, applying it to the microwave-assisted dry and steam reforming of alkanes. Finally, several other possibilities are available for the design and preparation of catalysts for microwave-assisted catalytic processes. For instance, defects can be created in the catalyst by doping to increase the dielectric loss factor of the catalyst, thereby improving its usability in microwave-assisted catalysis. Also, the combination of microwave absorbing materials and effective catalysts in the traditional catalysis process, such as the production of core-shell catalysts with activated carbon as the core.

References

1. Ohsato, H., Varghese, J. & Jantunen, H. Dielectric Losses of Microwave Ceramics Based on Crystal Structure. *Electromagnetic Materials and Devices* (Intech, 2018)

2. Tamura, H. Microwave dielectric losses caused by lattice defects. *Journal of the European Ceramic Society* **26**, 1775–1780 (2006).

3. Schuh, K. *et al.* Bismuth molybdate catalysts prepared by mild hydrothermal synthesis: Influence of pH on the selective oxidation of propylene. *Catalysts* **5**, 1554–1573 (2015).